STIMULI-RESPONSIVE ELECTROSPUN FIBERS

A Dissertation

Presented to the Faculty of the Graduate School

of Cornell University

In Partial Fulfillment of the Requirements for the Degree of

Doctor of Philosophy

by

Erin Sue Hendrick

August 2011

STIMULI-RESPONSIVE ELECTROSPUN FIBERS

Erin Sue Hendrick, Ph.D.

Cornell University 2011

Stimuli-responsive fibers were created by incorporating pH-sensitive nanoparticles into electrospun cellulose acetate (CA) and poly(lactic acid) (PLA) fibers. The fluorescent silica nanoparticles, Cornell dots (C dots), have both a fluorescent core (518 nm emission), and a fluorescent pH-sensitive shell (572 nm emission). Using confocal microscopy, the signaling effectiveness of these fibers was studied by varying several parameters: fiber diameter, substrate, and surface hydrophilicity.

For the CA fibers, fiber diameter was varied by changing the feed rate during the electrospinning process to 0.03 mL/hr, 0.30 mL/hr and 0.30 mL/min, producing fibers with average diameters of 1.1 μm, 1.8 μm and 9.5 μm, respectively. It was found that fibers with larger surface area had a greater sensitivity to pH change than fibers with smaller surface area. The response of the pH-sensitive fibers also varied when both the nanoparticles and CA fibers were applied/electrospun onto the surface of four different substrates: optical glass slides, cotton, cotton/polyester, and nylon/spandex fabrics. Fibers spun onto glass slides and cotton/polyester showed an improvement in sensitivity to pH change, while the cotton and nylon/spandex samples were greatly influenced by the chemistry inherent to these substrates.

Poly(lactic acid) – b – poly(ethylene glycol) (PLA-b-PEG) copolymers with block lengths of 1000-750, 5000-1000 and 1000-5000 and bulk PEG were added to PLA electrospinning dopes to create hydrophilic but non-water soluble nanofibers. PLA-b-PEG

block lengths strongly affected the total amount of PEG that could be incorporated, spinnability and fiber morphology. Solutions containing >1% w/w of the lowest molecular weight copolymer PLA (1000) – b – PEG (750) formed an unspinnable, cloudy gel. Addition of the PLA (5000) – b – PEG (1000) to the base spinning solution influenced fiber diameters and spinnability in the same manner as simply increasing PLA concentration in the spinning dope. Addition of PLA (1000) – b – PEG (5000) resulted in decreased fiber diameters, and allowed for the highest overall copolymer loading. In final fiber formulations, maximums of 0.9, 2.9 and 9.3 wt% PEG could be added to the fibers using the PLA-b-PEG 1000-750, 5000-1000 and 1000-5000 respectively. PEG (M_W = 3350 g/mol) homopolymer was added to the spinning dopes to result in 1.0 and 5.0 wt% PEG in the final fibers. These spinning dopes were electrospun with more non-uniform and variable morphology and diameter size than occurred with the addition of PEG in block copolymer form. Water absorbance by electrospun nonwoven fabrics increased by four times over the control PLA with the addition of 1.0 wt% PEG, and by eighteen times with the addition of 9.3 wt% PEG with the block copolymers. At similar overall PEG loadings, the addition of PLA-b-PEG resulted in a two to four fold increase in water wicking over the addition of PEG homopolymer. The improvement in water wicking was mirrored in the pH-measurement data compiled for these samples on glass slides. It was found that response to pH change was influenced by PEG content, copolymer chain length, fiber geometry and water wicking.

Finally, incorporating CA and PLA/PLA-b-PEG fibers into a prototype fluidic chip created a pH-sensing device. The response of the fibers was consistent with the increases in surface area and wicking rate, just as in the glass slides experiments, and proved to be a functional method for measuring pH change.

BIOGRAPHICAL SKETCH

Erin Hendrick was born in Rochester, NY, and received her B.S. in Materials Science and Engineering from the SUNY College of Ceramics at Alfred University. She began her studies in Fiber Science at Cornell University in 2006, and completed her M.S. in 2008. Her research interests are in the creation of novel fiber systems and sensors.

Dedicated to my family and friends

ACKNOWLEDGMENTS

I would like to express my heartfelt thanks to a number of the people in Ithaca and Rochester, NY, without whom this accomplishment would not have been achieved. First of all, I would like to thank my advisor, Professor Margaret Frey, for her support, guidance, and encouragement throughout my doctoral studies. I would also like to thank my other thesis committee members, Professor Ulrich Wiesner from the Department of Materials Science and Engineering, and Professor Antje Baeumner from the department of Biological and Environmental Engineering. In addition, I'd like to thank John Hunt from the CCMR, and Carol Bayles from the NBTC, for their assistance with electron and confocal microscopy.

Next, I would like to thank the entire faculty and staff of the Department of Fiber Science and Apparel Design. Without your support and free food, this research would not have been possible. Thanks also go to the past and present members of the Frey research group. Specifically, I'd like to thank my undergraduate research assistants, Larissa Buttaro and Aditi Naik, who assisted in collecting experimental data.

Finally, I would like to give a huge thanks to my friends and family. To the Wine'o'clock crew, thank you for keeping me sane. To my parents and brother, thank you for your unwavering support, guidance, and love. To Greg Kirkpatrick, thank you for the Matlab coding, constant moral support, cups of coffee, plates of lasagna, bowls of ice cream, and for washing the dishes!

TABLE OF CONTENTS

LIST OF FIGURES

LIST OF TABLES

CHAPTER 1

STIMULI-RESPONSIVE ELECTROSPUN FIBERS: THE INFLUENCE OF FIBER DIAMETER AND SUBSTRATE

1.1 ABSTRACT

A unique pH-sensing device was created by incorporating fluorescing nanoparticles into electrospun cellulose acetate (CA) fibers. The fluorescent silica nanoparticles, Cornell dots (C dots), have both a fluorescent core (518 nm emission), and a fluorescent pH-sensitive shell (572 nm emission). Using confocal microscopy, the signaling effectiveness of these fibers was studied by varying two parameters: fiber diameter and substrate. Fiber diameter was varied by changing the feed rate during the electrospinning process to 0.03 mL/hr, 0.30 mL/hr and 0.30 mL/min, producing fibers with average diameters of 1.1 μm, 1.8 μm and 9.5 μm, respectively. It was found that fibers with smaller diameters had a greater sensitivity to pH change than fibers with larger diameters. The response of the pH-sensitive fibers also varied when both the nanoparticles and CA fibers were applied/electrospun onto the surface of four different substrates: optical glass slides, cotton, cotton/polyester, and nylon/spandex fabrics. Fibers spun onto glass slides and cotton/polyester showed an increase in sensitivity to pH change, while the cotton and nylon/spandex samples were greatly influenced by the chemistry inherent to these substrates.

1.2 INTRODUCTION

Ultra-endurance athletes (i.e. marathon runners, long-distance cyclists) engage in activities that can lead to severe, and even deadly, levels of sweat loss. In order to maximize performance, and to ensure safety, these athletes must always be conscious of their fluid intake.

Previous research has shown that the most significant change in sweat composition during exercise is in sodium ions [1-5]. Studies have even found that a direct relationship exists between sodium concentration, and the pH of sweat [3, 6]. Since sodium concentration is related to hydration, it is logical to suggest that sweat pH can be useful in monitoring fluid levels [1, 7-8]. However, dehydration is not the only problem that endurance athletes can encounter. Over-hydration, a condition known as hyponatremia, can also occur when the sodium levels in an athletes' body are too low. Therefore, it is crucial for endurance athletes to properly balance their hydration and electrolyte levels, and monitoring the pH of sweat is an excellent way of doing so [9-11]. The goal of this project is the creation of a pH-sensitive fabric that may one day be used to monitor sodium and hydration levels in sweat.

One way to create a suitable monitor is by incorporating a signal or sensor into a polymeric fiber. Many unique signals have previously been incorporated into polymeric materials, including: magnetic, electrical, thermal, chemical, radio frequency, and fluorescence signals [12-43]. Fluorescence is conventionally applied to fibers using fluorescent dyes and coatings. Small fluorescent dye molecules can be placed in solution with dry polymer and solvent, which can then be spun into fibers. However, these dyes have the potential to leak in certain environments, and to lose their fluorescent strength during exposure to certain wavelengths of light. Common fluorescent dye molecules include Alq3, 10-(3-sulfopropyl), acridinium betaine, quinacrine dihydrochloride, naphthofluorescein, fluorescein, 8-hydroxypyrene-1, and 3, 6-trisulfonic acid trisodium salt [13-14]. These dyes can easily provide fluorescence to polymer fibers, but they are not permanent, and their volatile nature within fibers can lead to certain health and environmental concerns. Figure 1.1 illustrates a confocal microscopy image of an electrospun CA fabric with 10 μL of fluorescent

tetramethylrhodamine (TRITC) dye incorporated before and after one week of light exposure. It is clear from these images that the light exposure led to a decrease in fiber fluorescence intensity.

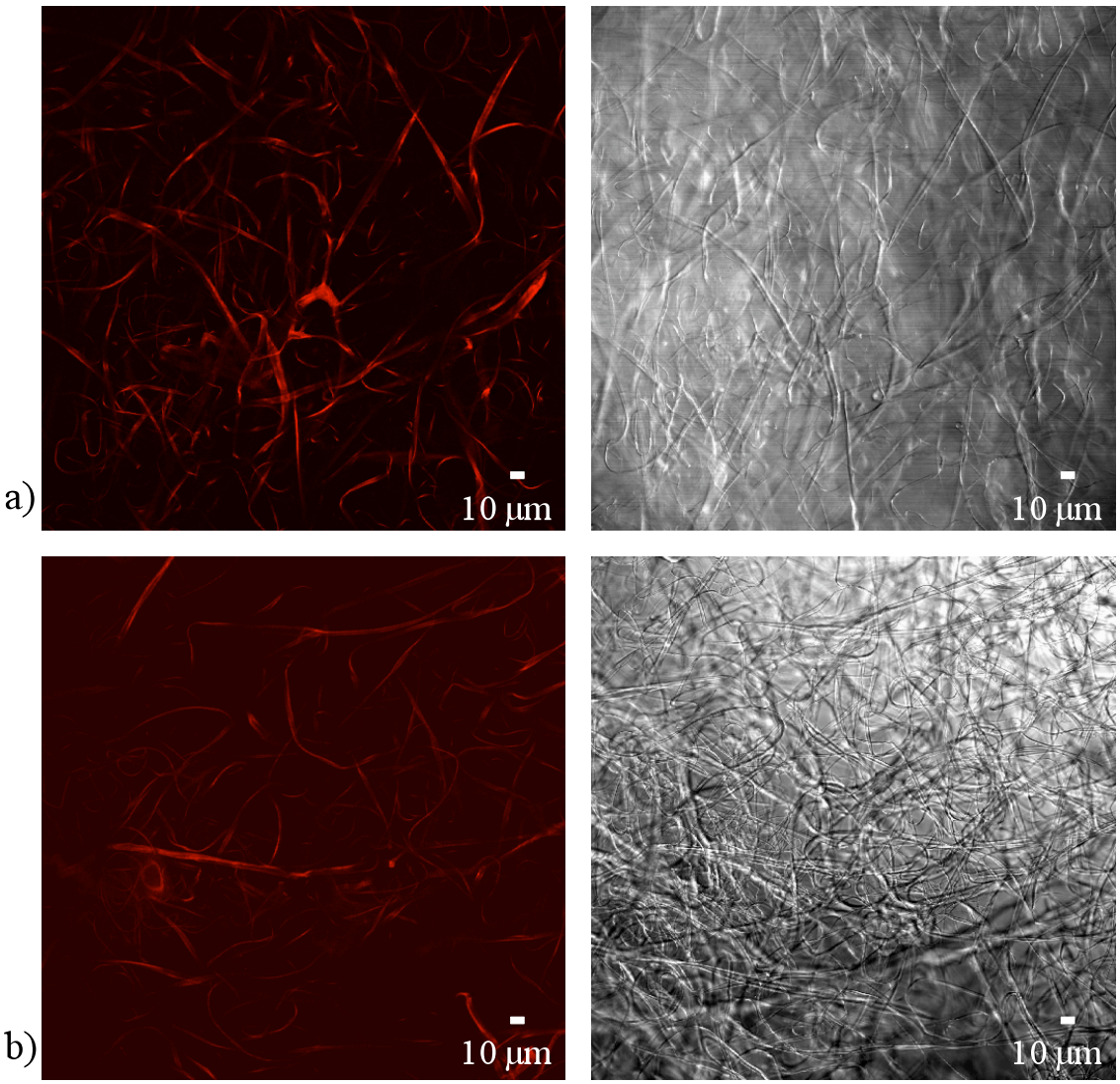

FIGURE 1.1. Fluorescence and light microscope images of electrospun CA fibers with 10 µL of TRITC dye incorporated a) before and b) after one week of light exposure.

Therefore, though it is relatively simple to create fluorescent signal in fibers with fluorescent dyes, it is advisable to use a more contained method if longer-term fluorescence is desired. One way this can be accomplished is by using nanoparticles mixed in to the matrix of,

or to coat the surface of, a polymer fiber. This research focuses on the creation of a functional fabric device using Cornell dots. These are safe, fluorescent, core-shell silica nanoparticles that can impart a unique fluorescence signal to polymeric fibers.

Cornell dots, also known as C dots, were developed in the Wiesner group in the Materials Science and Engineering department at Cornell University [44]. These nanoparticles are composed of a dye rich core surrounded by a silica shell, which exhibits fluorescent emission when excited by an external light source at a specific wavelength. The 30 nm C dots are 20-30 times brighter than single fluorescent dye molecules, resistant to quenching, and exhibit greater resistance to photo bleaching [45]. These nanoparticles can be dispersed in many different polar solvents, including water and acetone, without degradation. To disperse the C dots in a nonpolar solvent, such as benzene or diethyl ether, surface modification of the nanoparticles is required. The only solvents that the C dots cannot be dispersed in are strong acids and bases, which can damage the silica shell. Additionally, the dye encapsulated within the nanoparticles can resist degradation at temperatures up to 150°C, depending on dye structure and heat duration [45-48]. In addition to these structural benefits, the unique core–shell architecture of the C dots is ideal for the development of ratiometric nanoscale fluorescent sensors (Figure 1.2).

The nanoparticles use a TRITC dye core as an internal reference, allowing for quantitative concentration measurements. By placing a fluorescein isothiocyanate (FITC) sensor dye on the surface of the silica shell, the maximum amount of surface area can be exposed to the environment. The emission and absorption properties of FITC and TRITC are detailed in Table 1.1.

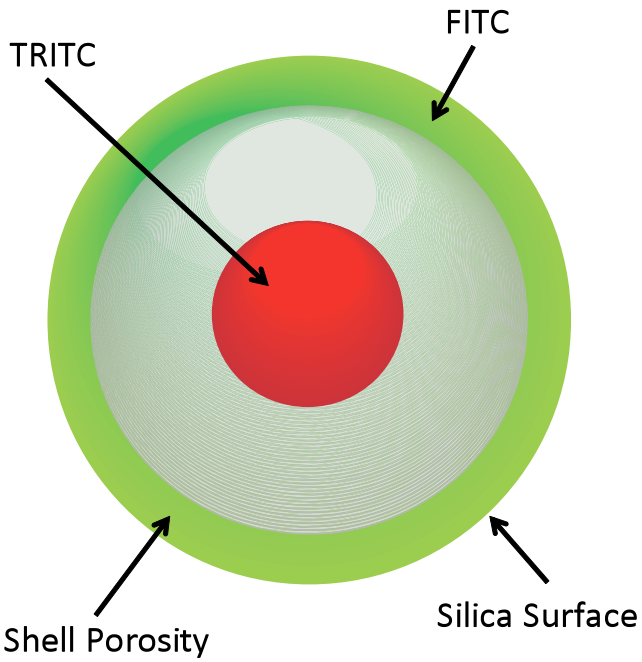

FIGURE 1.2. A schematic illustration of the dual-emission core–shell nanoparticle sensor architecture.

TABLE 1.1. Emission and absorption wavelengths for FITC and TRITC dye.

Dye	Absorption (nm)	Emission (nm)
FITC	488	518
TRITC	541	572

FITC was chosen as a pH sensor because, with a pK_a of 6.4, it is an excellent pH sensor in the biologically relevant range for human sweat from pH 5–8.5. In aqueous solutions, FITC can exist in cationic, neutral, anionic, and dianionic forms (Figure 1.3). These molecular structures have different requirements for photon absorption, making the fluorescence properties strongly dependent on pH. The anionic form of FITC has a quantum yield of 36%, while the dianionic form yields 93% [49]. This means that the intensity of the FITC dye

changes with its molecular state, which varies in the presence of aqueous buffer solutions. TRITC was chosen as the internal standard because its quantum yield of 35% is unaffected by pH changes in this range [45]. Therefore, by taking a ratio between these two dyes, a ratiometric sensor can be created.

In this study, the C dots were incorporated into cellulose acetate (CA) fibers during the fiber spinning process. The resulting fibers respond to pH change in their environment through changing fluorescent emission. CA was used because it is relatively simple to spin, and the optimal solvent, acetone, is compatible with the as-made C dots.

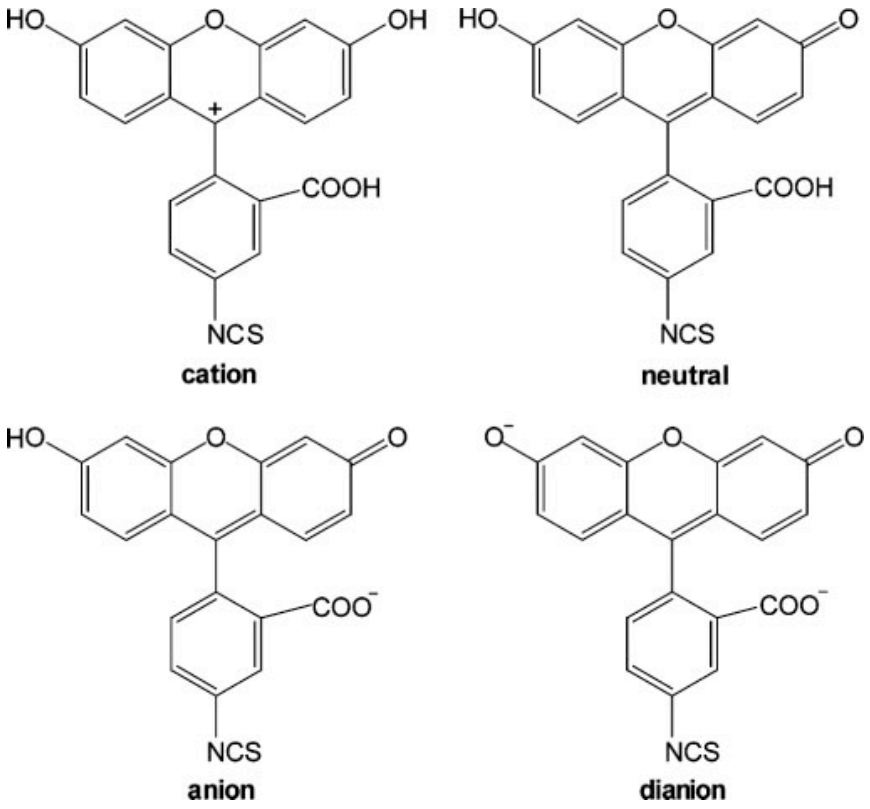

FIGURE 1.3. Four protolytic forms of FITC [50]. For the current study, the anionic to dianionic transition is most relevant.

Electrospinning was used to incorporate the C dots into CA fibers, which allowed for the C dots to be well-dispersed in the nonwoven fabric. Electrospinning is a unique method for forming fibers with submicron scale diameters using electrostatic forces. When an electrical force is applied at the interface of a liquid polymer, a charged jet is ejected. The jet initially extends in a straight line, then moves into a whipping motion caused by the electro-hydrodynamic instability at the tip. As the solvent evaporates, the polymer is collected, e.g. onto a grounded piece of aluminum foil as a nonwoven mat [51]. Previous research has shown that it is possible to successfully incorporate the C dots into CA fibers by electrospinning (Figure 1.4) [52-53]. However, this research seeks to show that it is possible to create a unique pH-sensing device using the nanoparticle-incorporated CA fibers.

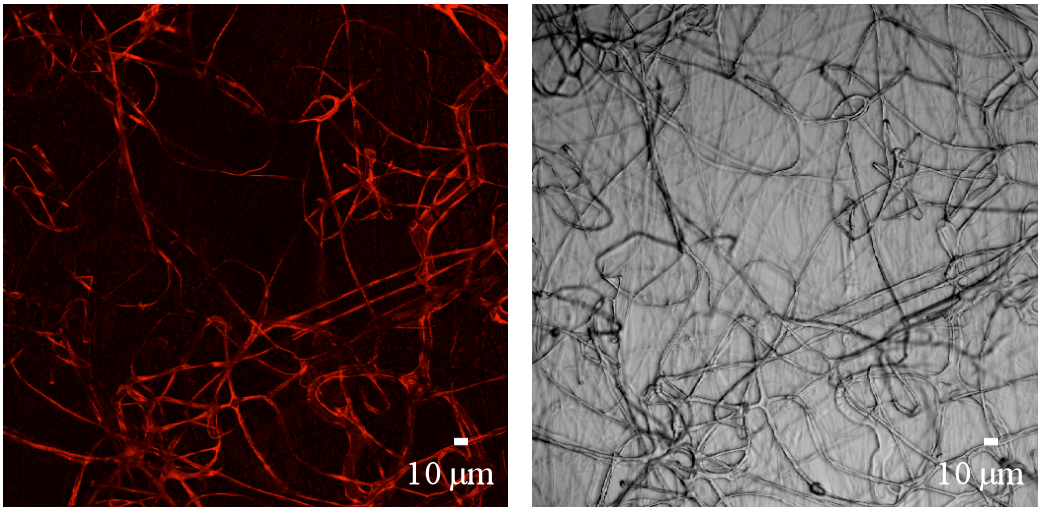

FIGURE 1.4. Fluorescence and light microscope images of CA electrospun fabrics containing core-shell silica nanoparticles.

Therefore, the focus of this study was on the signaling effectiveness of the fibers with two changing variables: fiber diameter and substrate. First, fiber diameter was varied by changing the feed rate during the electrospinning process. The responses of these differently sized pH-sensitive fibers were then observed under confocal microscopy. Image analysis was

used to compare the pixel intensities of the FITC and TRITC images, resulting in an average intensity value for each pH. Secondly, both the pH-sensitive nanoparticles, as well as the pH-sensitive fibers, were applied/electrospun onto the surface of several different substrates: glass, cotton, nylon/spandex, and cotton/polyester. By changing these parameters, this project seeks to find the optimal parameters for making these pH measurements as accurate and reproducible as possible.

1.3 MATERIALS AND METHODS

1.3.1 Materials

Cellulose acetate (M_w = 30,000 g/mol), monobasic sodium phosphate (M_w = 137.99 g/mol), dibasic sodium phosphate (M_w = 141.96 g/mol), and sodium chloride (M_w = 58.44 g/mol) were supplied by Aldrich Chemical Co Ltd (St. Louis, MO). The acetone and glass slides were purchased from VWR Scientific (West Chester, PA). The C dots were made by the Wiesner lab in the Materials Science and Engineering department at Cornell University using previously described techniques [44, 48]. The cotton, nylon/spandex, and cotton/polyester substrate materials were purchased from Joann Fabrics (Hudson, OH).

1.3.2 Preparation of electrospun solutions

The electrospun fabrics were manufactured using 17 wt% CA (M_w = 30,000 g/mol) dissolved in a 3:1 v/v acetone: water solution. The C dots were suspended in water, and added to the CA solutions in 15 vol%. The solution of cellulose acetate, acetone, water and C dots was mixed on an Innova™ 2300 platform shaker (New Brunswick Scientific Co., NJ) for twelve hours prior to fiber formation.

1.3.3 Electrospinning

The electrospinning apparatus consisted of a programmable syringe pump (Harvard Apparatus, MA) and a high-voltage supply (Gamma High Voltage Research Inc., FL). Electrospinning of the 17 wt% CA solution was carried out with a 20 G needle at 0.03 mL/hr, 0.30 ml/hr, and 0.30 mL/min, with an applied voltage of 14 kV. The nonwoven fabric was formed on grounded collection substrates 15 cm from the spinneret tip.

1.3.4 Scanning Electron Microscopy

Examination of the morphology and fiber diameters for the electrospun fabrics was performed using a Leica 440 scanning electron microscope (SEM) at 25 kV. Samples were coated for 30 seconds with 10 nm Au–Pd prior to imaging in order to prevent charging. The average fiber diameters were analyzed from the SEM images using ImageJ software.

1.3.5 Preparation of Buffer Solutions

Precise pH buffer solutions were prepared by mixing 0.15 M monobasic sodium phosphate buffer solution (0.01 M NaH_2PO_4, 0.14 M NaCl), and 0.15 M dibasic sodium phosphate buffer solution (0.01 M Na_2HPO_4, 0.14 M NaCl). Table 1.2 details the amounts of each solution used, as well as the pH produced.

TABLE 1.2. Solution recipes for pH buffer solutions.

pH	Dibasic sodium phosphate saline solution (µl)	Monobasic sodium phosphate saline solution (µl)
5	0	4200
6	630	3570
7	2100	2100
8	3360	840
8.5	4200	0

1.3.6 Confocal Microscopy

A Leica TCS SP2 laser confocal scanning microscope was used to examine the fluorescence of the C dots within the CA fibers. The pH-sensitive electrospun fabrics were imaged with a water immersion lens at 200 X with both red (460-500 nm) and green (480/40 nm) fluorescence filters. Three images were taken with each pH buffer solution, and averaged over the ten trials that were performed. A ratio of the pixel intensity in the green and red filtered images was taken, averaged for each image, and plotted against pH.

1.4 RESULTS AND DISCUSSION

1.4.1 Fiber Diameter

Electrospun fiber diameter was varied by changing the feed rate during the spinning process. Once the nonwoven samples were formed, SEM images were taken in order to examine the morphology of the CA fibers, as well as to measure average fiber diameter. The average diameters for the electrospun samples spun at 0.03 mL/hr, 0.3 mL/hr, and 0.3 mL/min were compiled using ImageJ software, and are given in Table 1.3. The SEM images show the electrospun CA fibers to be smooth, with a ribbon shaped cross-section (Figure 1.5).

TABLE 1.3. Average fiber diameters for fabric samples electrospun at varying feed rates.

Feed Rate	Average Fiber Diameter (μm)
0.03 mL/hr	1.1 ± 0.3
0.30 mL/hr	1.8 ± 0.7
0.30 mL/min	9.5 ± 1.1

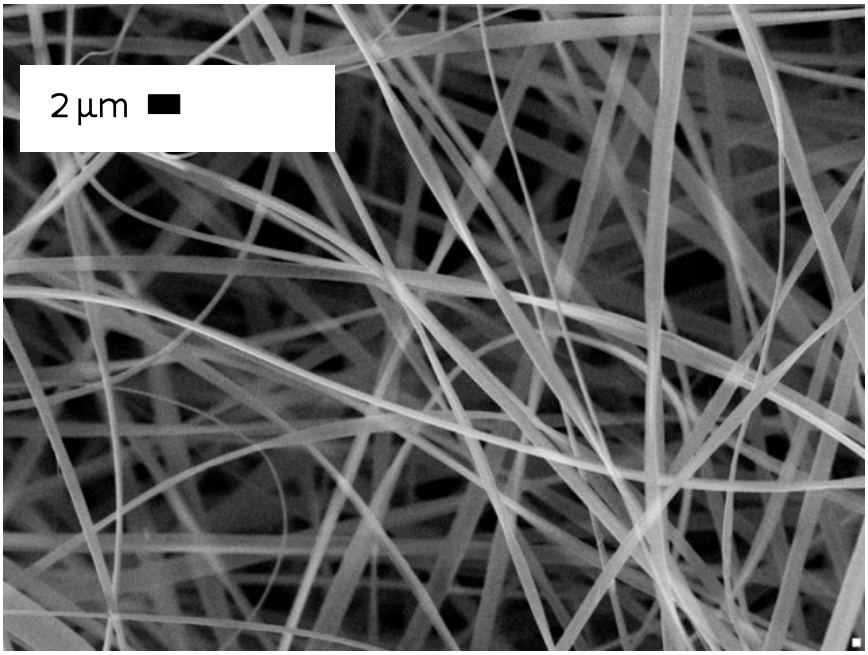

FIGURE 1.5. Representative SEM image of electrospun CA fibers spun at 0.30 mL/hr at 3500X.

After confirming that varying the feed rate led to a change in fiber diameter, the nanoparticle-incorporated fibers were analyzed using confocal microscopy. The results of these experiments can be seen in Figure 1.6. These results show that fiber diameter does have an effect on the relationship between pH and FITC/TRITC dye intensity. The fibers spun at the slowest feed rate, those with the smallest average fiber diameter, were the most responsive to pH change. While the fibers spun at the fastest feed rate, those with the largest average fiber diameter, were the least responsive to pH change. These results can be explained by changes in surface area. Generally, as fibers decrease in diameter, a greater proportion of nanoparticles can be found on the polymer surface. This means that the buffer solutions can interact with more pH-sensitive nanoparticles on thinner fibers, as opposed to thicker fibers. Due to this result, the rest of the experiments will be carried out using fibers spun at 0.03 mL/hr.

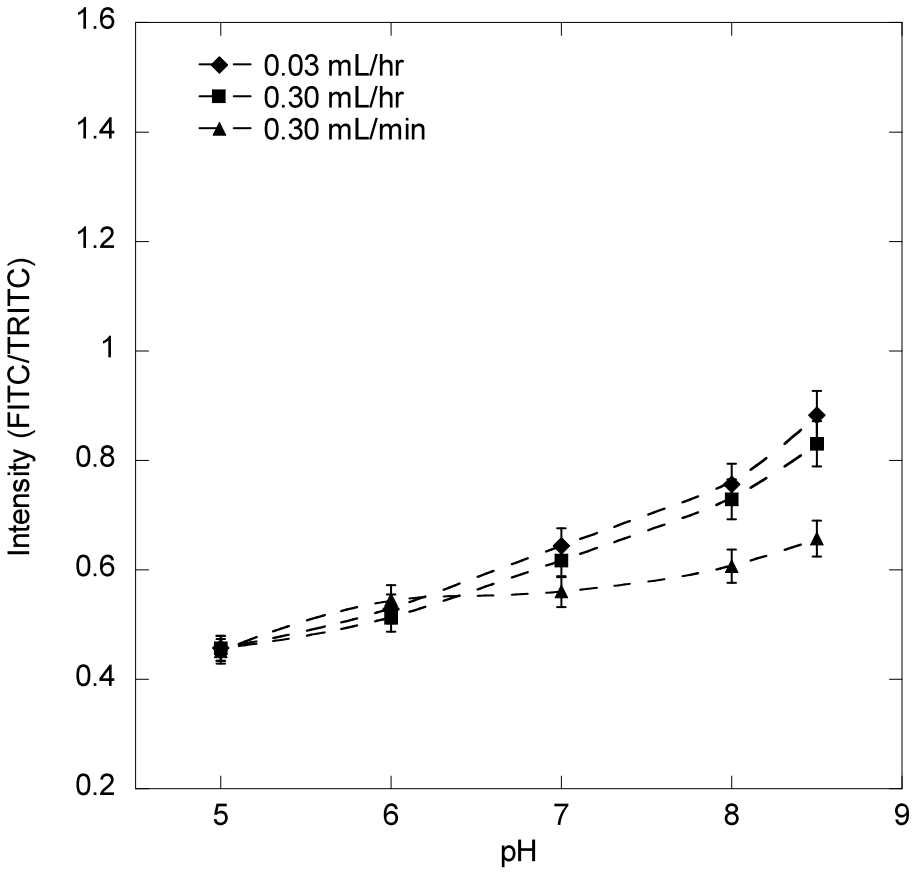

FIGURE 1.6. Average relationship over ten trials between fiber diameter, pH and dye intensity for CA fibers spun on a glass substrate.

1.4.2 Substrate

Next, it was important to understand how the chemistry and structure inherent to certain substrates can influence the pH-sensitive electrospun fibers. Therefore, the nanoparticle-incorporated CA fibers were electrospun onto four different substrates: optical glass slides, cotton, nylon/spandex, and cotton/polyester (Table 1.4). The results in Figure 1.7 indicate that substrate does have an effect on the pH vs. dye intensity measurements.

TABLE 1.4. Basic properties of the substrates used in this study

Substrate	Basic Description	Fluorescence Properties	Fabric Structure	Fabric Color
Optical Glass	Uniform Surface Properties	None	N/A	N/A
Cotton	Cellulosic fiber	440-470 nm	Twill weave	Black
Nylon/Spandex (85:15)	Synthetic fiber	400-460 nm	Interlock knit	Black
Cotton/Polyester (65:35)	Cellulosic/synthetic blend	400-470 nm	Interlock knit	Black

The fibers spun onto optical glass and cotton/polyester exhibit the results one would expect: the intensity of the FITC/TRITC ratio increased with pH. However, the fibers spun onto cotton and nylon/spandex showed some different results. The fibers spun onto cotton underwent a general increase in dye intensity with pH, but the results are more complicated when analyzed further. The FITC/TRITC dye intensity increases with pH until around 8, where a decrease is observed, followed by an increase in dye intensity at a pH of 8.5. This unusual behavior is most likely related to one of cotton's most well known characteristics, moisture absorption. Cotton is a carbohydrate with available hydroxyl groups that can undergo behavioral changes when exposed to different pH buffers [54]. At pH values above 7, where many hydroxyl groups exist in the buffer solutions, the hydrogen ions at the ends of the cellulose chains interact readily with the hydroxyls. This interaction can cause the cotton fibers to swell, invisible to the naked eye, moving the buffer solution closely in contact with the pH-sensitive fibers. At pH levels below 7, the cellulose chains are more stable in the presence of the buffer solutions. There are fewer hydroxyl groups in the buffer solution, so the hydrogen ions are less likely to detach from the cellulose chains. The buffer solution still has some contact with the pH-sensitive fibers, though it is more limited. Therefore, the increase in dye

intensity at a pH of 8.5 is not completely accurate. The C dot-incorporated fibers are not brighter at this pH; it is only that more nanoparticles have an opportunity to come into contact with the buffer solutions.

Conversely, the fibers spun on nylon/spandex show almost a constant relationship between dye intensity and pH. Though it is not pH-sensitive, the chemical structure of nylon/spandex includes several places where water molecules can form bonds, so it can only absorb ~10% of its weight [54]. In addition to its low moisture absorption, nylon/spandex is also a well-known wicking fabric. The results in Figure 1.7 show that the buffer solution is wicked away from the pH-sensitive fibers so quickly that it is nearly impossible to measure any change in the fluorescence intensity of the fibers. These results also explain why the samples spun onto optical glass are more responsive to pH change than those spun onto cotton/polyester fabric. The polyester in the fabric wicks away some of the buffer solution, inhibiting the measurements.

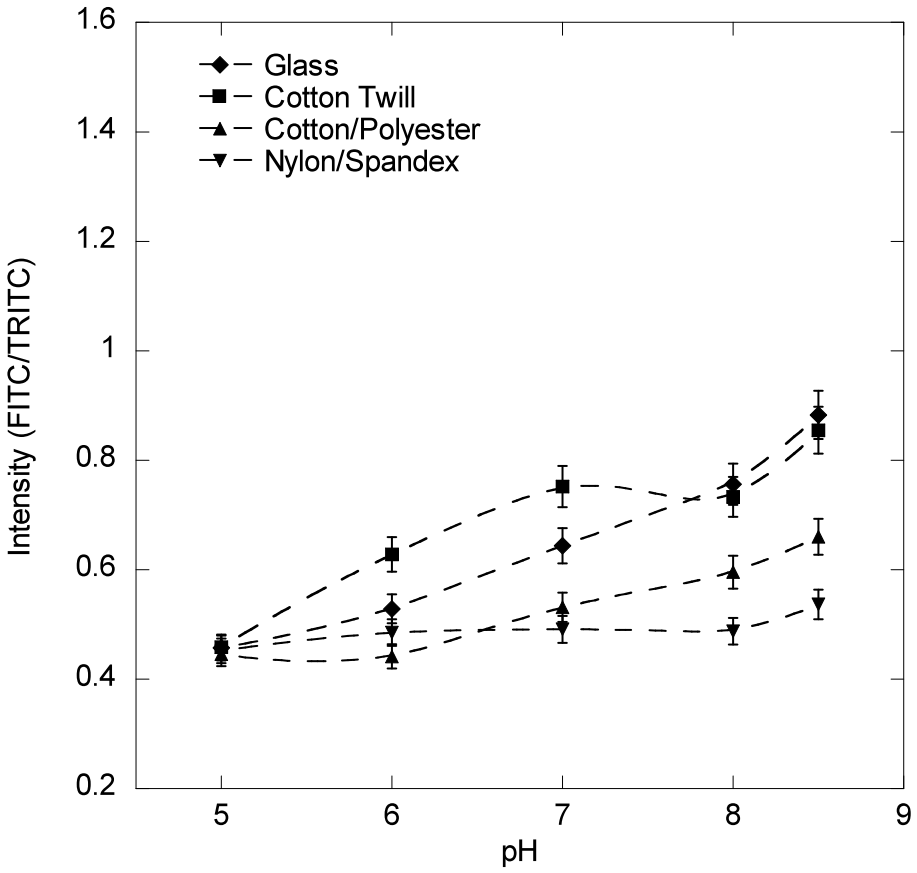

FIGURE 1.7. Average relationship over ten trials between pH and dye intensity for electrospun fibers spun onto various substrates.

Due to these interesting results, the cotton and nylon/spandex fabrics required further study. In order to accomplish this, the pH-sensitive C dots were applied directly to the cotton and nylon/spandex fabrics using a pad-dry-cure process, and then observed under confocal microscopy. The pad-dry-cure process was accomplished by padding the fabric with an 85:15 mixture of acetone: C dots in DI water. The same confocal microscopy setup was used, followed by image analysis. The purpose of this experiment was to determine how substrate affected the relationship between pH and dye intensity, both with and without the electrospun fibers. The results show that applying the nanoparticles to the surface of the substrates

illustrates a different relationship between pH and dye intensity than when the nanoparticles are incorporated into the fibers (Figures 1.8 and 1.9). For the cotton samples, it appears that the electrospun fibers hold the buffer solution in contact with the C dots more efficiently than the nanoparticles alone. Whereas in the nylon/spandex samples, only the applied C dots have sufficient access to the buffer solution to show any response to pH change.

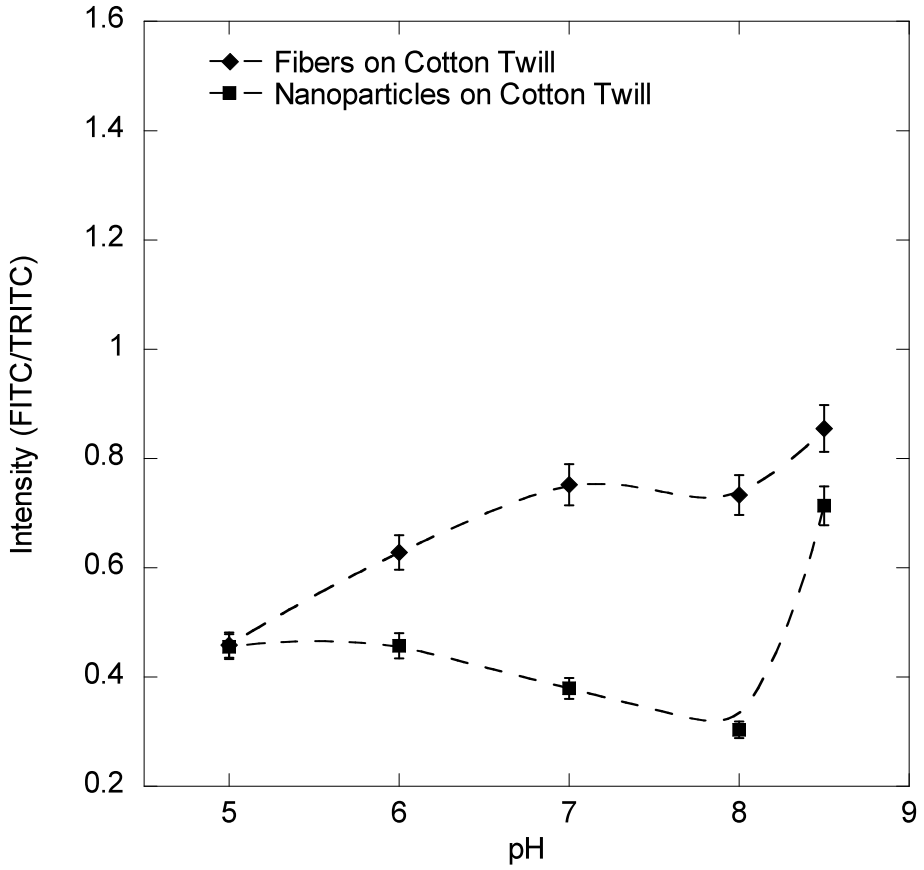

FIGURE 1.8. Average relationship over ten trials between pH and dye intensity for C dots applied to the surface of cotton substrates.

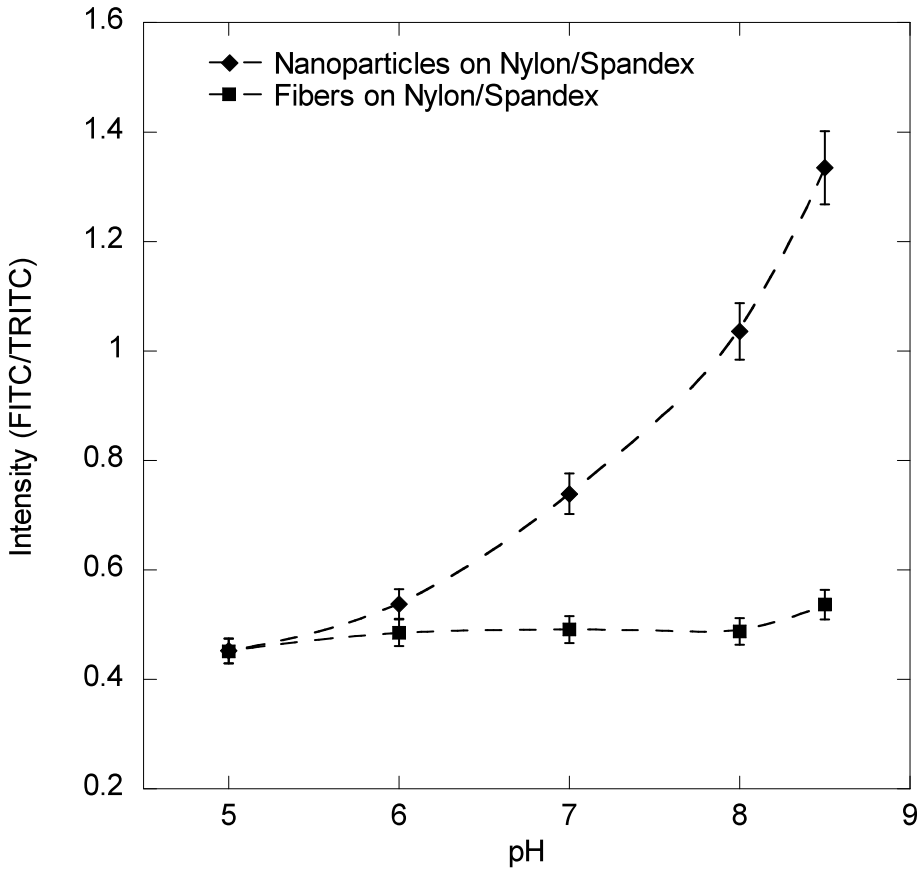

FIGURE 1.9. Average relationship over ten trials between pH and dye intensity for C dots applied to the surface of nylon/spandex substrates.

1.5 CONCLUSIONS

Fluorescent core-shell silica nanoparticles were successfully incorporated into CA fibers for use as a pH-sensing device. Confocal microscopy confirmed that the nanoparticles fluoresce within the fibers at a specific wavelength of light, and can be used to measure pH change. Additionally, through the use of confocal microscopy, the signaling effectiveness of these fibers was studied by varying fiber diameter and substrate. Electrospinning was performed at varying rates to produce fibers with average diameters of 1.1 μm, 1.8 μm and 9.5 μm, respectively. Fibers with greater surface area had a greater sensitivity to pH change than fibers with less surface area (i.e. larger fiber diameters). The response of the pH-sensitive

fibers also varied when the CA fibers were electrospun onto glass slides, cotton, cotton/polyester, or a nylon/spandex fabric. While the fibers spun onto glass and cotton/polyester exhibited a direct relationship between dye intensity and pH, the cotton and nylon/spandex fabrics produced different results. The cotton fabric exhibited an increase in dye intensity at pH values above 7, and nylon/spandex appeared to inhibit the measurements. Even though the measurements were clearly affected by varying substrate, the results are not yet reproducible.

1.6 REFERENCES

[1] J. R. Allan and C. G. Wilson, Influence of acclimatization on sweat sodium concentration, Journal of Applied Physiology, 30 (1971) 708—712.

[2] B. Falk, O. Bar-Or, J. D. MacDougall, L. McGillis, R. Calvert and F. Meyer, Sweat lactate in exercising children and adolescents of varying physical maturity, Journal of Applied Physiology, 71 (1991) 1735—1740.

[3] D. Kaiser, R. Songo-Williams and E. Drack, Hydrogen ion and electrolyte excretion of the single human sweat gland, Pflugers Archiv, 349 (1974) 63—72.

[4] K. Sato and R. L. Dobson, Regional and individual variationsin the function of the human eccrine sweat gland, Journal of Investigative Dermatology, 54 (1970) 443—449.

[5] G. Yosipovitch, J. Reis, E. Tur, H. Blau, D. Harell, G. Moduchowicz and G. Boner, Sweat electrolytes in patients with advanced renal failure, Journal of Laboratory and Clinical Medicine, 124 (1994) 808—812.

[6] M. J. Buono, K. D. Ball and F. W. Kolkhurst, Sodium ion concentration vs. sweat rate relationship in humans, Journal of Applied Physiology, 103 (2007) 990–994.

[7] F. Brouns, Heat—sweat—dehydration—rehydration: a praxis oriented approach, Journal of Sports Science, 9 (1991) 143-152.

[8] S. Robinson and A. H. Robinson, Chemical composition of sweat, Physiological Reviews, 34 (1954) 202-220.

[9] G. W. Mack and E. R. Nadel, Body fluid balance during heat stress in humans, Oxford University Press, New York, 1996.

[10] M. N. Sawka, Body fluid responses and hypohydration during exercise heat stress, Cooper Publishing Group, Indianapolis, 1988.

[11] M. N. Sawka and S. J. Montain, Fluid and electrolyte supplementation for exercise heat stress, American Journal of Clinical Nutrition, 72 (2000) 564-572.

[12] S. W. Coyle, L. King-Tong, S. Brady, G. Wallace and D. Diamond, Bio-sensing textiles – wearable chemical biosensors for health monitoring, in: 4th International Workshop on Wearable and Implantable Body Sensor Networks, Aachen University, 2007.

[13] E. Yan, C. Wang, Z. Huang, Y. Xin and Y. Tong, Synthesis and Characterization of 1D Tris(8-Quinilinolato) Aluminum Fluorescent Fibers by Electrospinning, Materials Science and Engineering, 464 (2007) 59-62.

[14] G. Moreda, F. J. Arregui, M. Achaerandio and I. R. Matias, Study of Indicators for the Development of Fluorescence Based Optical Fiber Temperature Sensors, Sensors and Actuators B: Chemical, 118 (2006) 425-432.

[15] H. Yu, A. Argyros, G. Barton, M. Van Eijkelenborg, C. Barbe, K. Finnie, L. Kong, F. Ladoucer and S. McNiven, Quantum Dot and Silica Nanoparticle Doped Polymer Optical Fibers, Optics Express, 47 (2007) 9989-9994.

[16] V. N. Radojevic, D. Talijan, N. Trifunovic and R. Aleksic, Optical fibers with composite magnetic coating for magnetic field sensing, Journal of Magnetism and Magnetic Materials, 5 (2004) 272-276.

[17] X. Lu, Y. Zhao and C. Wang, Fabrication of PbS nanoparticles in polymer-fiber matrices by electrospinning, Advanced Materials, 17 (2005) 2485-2488.

[18] M. Bayindar, A. Abouraddy, J. Arnold, J. Joannopoulos and Y. Fink, Thermal-Sensing Fiber Devices by Multimaterial Codrawing, Advanced Materials, 18 (2006) 845-849.

[19] A. F. Garito, Y. L. Hsiao and R. Gao, Thermal Polymer Nanocomposites, in: U. S. P. Office (Ed.), United States of America, 2003.

[20] D. W. House, Electrically conducting polymers, in: U. S. P. Office (Ed.), 1985.

[21] A. Dhawan, A. Seyam, T. Ghosh and J. Muth, Woven fabric-based electrical circuits: Part I: Evaluating interconnect methods, Textile Research Journal, 74 (2004) 913-919.

[22] B. Boen, Not-so-Heavy Metal: Electrical Conductivity in Textiles, in: Nasa Spinoff, 2007.

[23] D. M. Jordan and D. R. Walt, Physiological pH fiber-optic chemical sensor based on energy transfer, Analytical Chemistry, 59 (1987) 437-439.

[24] C. Munkholm and D. R. Walt, Polymer modification of fiber optic chemical sensors as a method of enhancing fluorescence signal for pH measurement, Analytical Chemistry, 58 (1986) 1427-1430.

[25] C. H. Lee and J.-M. Kim, Fabrication of patterned fluorescence images in electrospun microfibers, Bulletin of the Korean Chemical Society, 29 (2008) 1657-1658.

[26] T. Abitbol, J. T. Wilson and D. G. Gray, Electrospun fluorescent cellulose triacetate fibers containing quantum dots, in: ACS National Meeting, Salt Lake City, UT, United States, 2009.

[27] I. Cucchi, F. Spano, U. Giovanella, M. Catellani, A. Varesano and C. Calzaferri, Fluorescent electrospun naofibers embedding dye-loaded zeolite crystals, Small, 3 (2007) 305-309.

[28] K. P. Koo and G. H. Sigel, Jr, Characteristics of fiber-optic magnetic-field sensors employing metallic glasses, Optics Letters, 7 (1982) 334-336.

[29] B. Kim, V. Koncar, E. Devaux, C. Dufour and P. Viallier, Electrical and morphological properties of PP and PET conductive polymer fibers, Synthetic Metals, 146 (2004) 167-174.

[30] X. Wang, C. Drew, S.-H. Lee, K. J. Senecal, J. Kumar and L. A. Samuelson, Explosive detection by fluorescent electrospun polymer membrane sensor, in: A. C. Society (Ed.) Chromagenic Phenomena in Polymers, 2005, pp. 388-399.

[31] C. Barrera, K. Hyde, J. P. Hinestroza, T. Gould, G. Montero and C. Rinaldi, Electrospun magnetic nanofibers with anti-counterfeiting applications, in: American Society of Mechanical Engineers, American Society of Mechanical Engineers, 2005, pp. 467-473.

[32] M. K. Tiwari, A. L. Yarin and C. M. Megaridis, Electrospun fibrous nanocomposites as permeable, flexible strain sensors, Journal of Applied Physics, 103 (2008) 044305/044301-044305/044310.

[33] K. J. Senecal, D. P. Ziegler, J. He, R. Mosurkal, H. Schreuder-Gibson and L. A. Samuelson, Photoelectric response from nanofibrous membranes, in: Materials Research Society Symposium Proceedings, Organic Optoelectronic Materials, Processing and Devices, 2002, pp. 285-289.

[34] J. Memisevic, L. Riley and S. A. Grant, Electrospun sol-gel fibers for fluorescence-based sensing, in: SPIE, Smart Biomedical and Physiolofical Sensor Technology VI, 2009, pp. 731301/731301-773130I/731308.

[35] C. Barrera, C. Rinaldi, M. Satcher and J. P. Hinestroza, Electrospun nanofibers with magnetic domains for smart tagging of textile products, in: W. A. Goddard, III (Ed.) Handbook of Nanoscience, Engineering, and Technology, 2007, pp. 17-26.

[36] Y. Long, H. Chen, Y. Yang, H. Wang, Y. Yang, N. Li, K. Li, J. Pei and F. Liu, Electrospun nanofibrous film doped with a conjugated polymer for DNT fluorescence sensor, Macromolecules, 42 (2009) 6501-6509.

[37] A. Camposeo, F. Di Benedetto, R. Stabile, R. Cingolani and D. Pisignano, Electrospun dye-doped polymer nanofibers emitting in the near infrared, Applied Physics Letters`, 90 (2007) 143115/143111-143115/143113.

[38] T. M. Fulghum, A. Marruffo, V. Subramanian, W. Kaul, S. Baldelli, P. Taranekar, J. Macossay-Torres and R. Advincula, Electrospinning of precursor and electroactive polymers, Polymer Preprints, 47 (2006) 562-563.

[39] S. Lee, Multifunctionality of layered fabric systems based on electrospun polyurethane/zinc oxide nanocomposite fibers, Journal of Applied Polymer Science, 114 (2009) 3652-3658.

[40] F. A. Sheikh, N. A. M. Barakat, M. A. Kanjwal, A. A. Chaudhari, I.-H. Jung, J. H. Lee and H. Y. Kim, Electrospun antimicrobial polyurethane nanofibers containing silver nanoparticles for biotechnological applications, Macromolecular Research, 17 (2009) 688-696.

[41] X. Xu, Q. Yang, J. Bai, T. Lu, Y. Li and X. Jing, Fabrication of biodegradable electrospun poly(L-lactide-co-glycolide) fibers with antimicrobial nanosilver particles, Journal of Nanoscience and Nanotechnology, 8 (2008) 5066-5070.

[42] B. Ding, M. Wang, J. Yu and G. Sun, Gas sensors based on electrospun nanofibers, Sensors, 9 (2009) 1609-1624.

[43] S. Yoon, A. A. Prabu, S. Ramasundaram and K. J. Kim, PVDF nanoweb touch sensors prepared using electro-spinning process for smart apparels applications, Advances in Science and Technology, 60 (2008) 52-57.

[44] H. Ow, D. R. Larson, M. Srivastava, B. Baird, W. W. Webb and U. Wiesner, Bright and stable core-shell fluorescent silica nanoparticles, Nano Letters, 5 (2004) 113-117.

[45] A. Burns, Sengupta, P., Zedayko, T., Baird, B., Wiesner, U., Core-shell fluorescnet silica nanoparticles for chemical sensing: towards single particle laboratories, Small, 2 (2006) 723-726.

[46] E. Herz, Burns, A., Lee, S., Sengupta, P., Bonner, D., Ow, H., Lidell, C., Wiesner, U. , Fluorescent core-shell silica nanoparticle: an alternative radiative materials platform,

Proceedings of the SPIE: Colloidal Quantum dors for Biomedical Applications, 6096 (2006) 1-12.

[47] A. Burns, H. Ow and U. Wiesner, Fluorescent core–shell silica nanoparticles: towards Lab on a Particle architectures for nanobiotechnology, Chemical Society Reviews, 35 (2006) 1028-1042.

[48] D. R. Larson, H. Ow, H. D. Vishwasrao, A. A. Heikal, U. Wiesner and W. W. Webb, Silica nanoparticle architecture determines radiative properties of encapsulated fluorophores, Chemistry of Materials, 20 (2008) 2677–2684.

[49] W.-C. Sun, K. R. Gee, D. H. Klaubert and R. P. Haugland, Synthesis of Fluorinated Fluoresceins, Journal of Organic Chemistry, 62 (1997) 6469-6475.

[50] T. N. Maeda, Tetsuhiko; Aida, Misako; Ishibashi, Taka-aki, Identification of chemical species of fluorescein isothiocyanate isomer-I (FITC) monolayers on platinum by doubly resonant sum-frequency generation spectroscopy, Journal of Raman Spectroscopy, 39 (2008) 1694-1702.

[51] C. K. Kim, D. S. Kim, S. Y. Kang, M. Marquez and Y. L. Joo, Structural Studies of Electrospun Cellulose Nanofibers, Polymer, 47 (2006) 5097-5107.

[52] E. S. Hendrick, Cellulose acetate fibers with fluorescing nanoparticles for anti-counterfeiting purposes, in: Fiber Science & Apparel Design, Cornell University, Ithaca, 2008.

[53] E. Hendrick, M. Frey, E. Herz and U. Wiesner, Cellulose acetate fibers with fluoresceing nanoparticles for anti-counterfeiting and pH-sensing applications, Journal of Engineered Fibers and Fabrics, 5 (2010) 21-30.

[54] S. Kadolf and A. Langford, Textiles, Macmillan Publishing Co., New York, 1993.

CHAPTER 2

MODIFICATION OF SURFACE HYDROPHILICITY IN POLY(LACTIC ACID) ELECTROSPUN FIBERS

2.1 ABSTRACT

Poly(lactic acid) – b – poly(ethylene glycol) (PLA-b-PEG) copolymers with block lengths of 1000-750, 5000-1000 and 1000-5000 and bulk PEG were added to PLA electrospinning dopes to create hydrophilic but non-water soluble nanofibers. PLA-b-PEG block lengths strongly affected the total amount of PEG that could be incorporated, spinnability and fiber morphology. Solutions containing >1% w/w of the lowest molecular weight copolymer PLA (1000) – b – PEG (750) formed an unspinnable, cloudy gel. Addition of the PLA (5000) – b – PEG (1000) to the base spinning solution influenced fiber diameters and spinnability in the same manner as simply increasing PLA concentration in the spinning dope. Addition of PLA (1000) – b – PEG (5000) resulted in decreased fiber diameters, and allowed for the highest overall copolymer loading. In final fiber formulations, maximums of 0.9, 2.9 and 9.3 wt% PEG could be added to the fibers using the PLA-b-PEG 1000-750, 5000-1000 and 1000-5000 respectively. PEG (M_W = 3350 g/mol) homopolymer was added to the spinning dopes to result in 1.0 and 5.0 wt% PEG in the final fibers. These spinning dopes were electrospun with more non-uniform and variable morphology and diameter size than occurred with the addition of PEG in block copolymer form. Water absorbance by electrospun nonwoven fabrics increased by four times over the control PLA with the addition of 1.0 wt% PEG, and by eighteen times with the addition of 9.3 wt% PEG with the block copolymers. At similar overall PEG loadings, the addition of PLA-b-PEG resulted in a two to four fold increase in water wicking over the addition of PEG homopolymer.

2.2 INTRODUCTION

Increasing the hydrophilicity of nanofibers can improve their performance in applications involving aqueous media, including biomedical devices, tissue engineering scaffolds, and biosensors [1-14]. Improving surface wetting is advantageous as it leads to a significant improvement in material biocompatibility and functionality [15-16]. Biosensors are an application that often involves the use of nanometer-scale structures. Nanoscale materials provide increased surface area over bulk materials, enabling more effective capture and detection of aqueous media. Therefore, when using nanoscale materials it is important to maximize their surface functionality. In previous studies, monitoring changes in contact angle and wettability have proven to be an effective technique for measuring improvements in surface hydrophilicity [15-16].

When using nanofibers to construct a biosensor, there are necessary components that must be considered. Both the surface and bulk polymer properties can influence the strength of the sensor signal, so they must be chosen carefully [17-18]. For example, the polymer matrix must be suitably hydrophilic to allow the aqueous media to wet, and then penetrate the material. Additionally, the polymer matrix cannot be so water soluble as to dissolve in the presence of any aqueous media.

Poly(lactic acid) (PLA) is an easily spinnable, biocompatible, and biodegradable polymer often used in biomedical devices [19]. The surface of PLA is strongly hydrophobic, but in order to improve its biocompatibility, surface modifications can be performed [20]. One successful strategy for increasing surface hydrophilicity of PLA films and particles is to blend it with biocompatible and hydrophilic poly(ethylene glycol) (PEG). Both Ouyang and Bhattarai et al. showed that the surface hydrophobicity of PLA films could be decreased through the addition of < 10 wt% PEG [21-25]. In these studies, pure PLA films had contact

angles on the order of 80°, and adding ~10 wt% PEG caused the contact angle of these films to decrease to 68°. Additionally, Luu et al. showed that adding more than 10 wt% PEG from a PLA-b-PEG copolymer into poly(lactide-co-glycolide) (PLGA) affected the structural morphology of the electrospun fibers [26]. Therefore, in this study, the surface wettability of electrospun PLA was modified through the addition of varying amounts of both PEG homopolymer, and PLA-b-PEG block copolymers. It is expected that using a diblock copolymer should be more effective in tailoring surface properties without changing fiber structure over adding PEG in bulk [27-29]. Theoretically, the PLA block of the copolymer should be miscible with the bulk PLA chains during the spinning process, allowing the hydrophilic PEG block to phase separate towards the fiber surface (Figure 2.1) [30]. This phase separation is caused by both a difference in surface energies, as well as a repulsive interaction between the chemically different copolymer blocks [31]. In this way, the morphology of the fibers should remain relatively constant, while the wetting properties of the fiber should be improved.

Electrospinning is a unique method for fabricating submicron scale fibers using electrostatic forces. When an electrical force is applied at the interface of a liquid polymer, a charged jet is ejected. The jet initially extends in a straight line, then moves into a whipping motion caused by the electro-hydrodynamic instability at the tip. As the solvent evaporates, the polymer is collected, e.g. onto a grounded piece of copper as a nonwoven mat [14]. Solution parameters such as concentration, viscosity, surface tension and solution conductivity can all affect fiber and nonwoven fabric properties [32]. In this study, PLA fibers were electrospun with several different PEG weight percent concentrations, and three different PLA-b-PEG copolymers. These diblock copolymers contained three different copolymer chain lengths, and

ratios: PLA (1000) – b – PEG (750), PLA (5000) – b – PEG (1000), and PLA (1000) – b – PEG (5000).

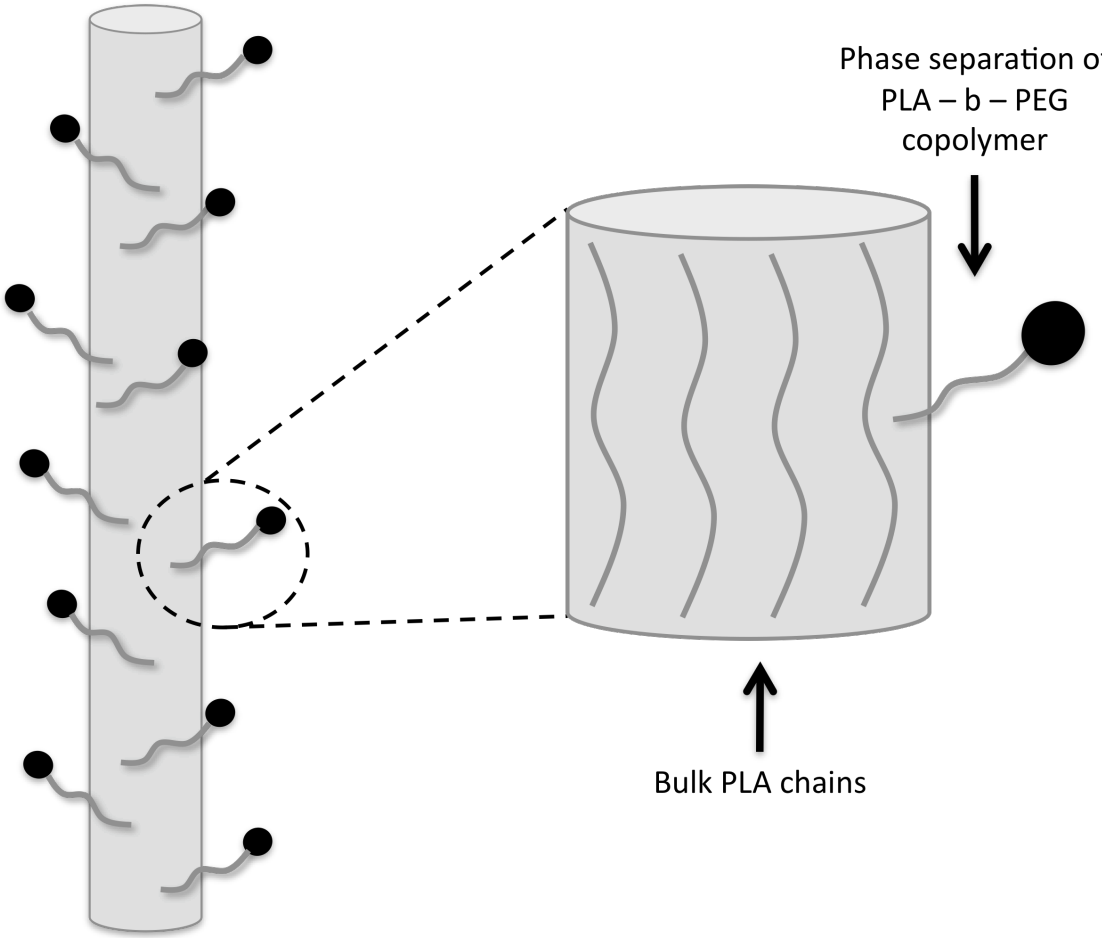

FIGURE 2.1. Schematic illustrating PLA-b-PEG copolymer electrospun into bulk PLA.

2.3 MATERIALS AND METHODS

2.3.1 Materials

PLA (M_w = 211,332 g/mol) was supplied by Cargill Dow (Minnetonka, MN). PEG (M_w = 3350 g/mol) was supplied by Fisher Scientific (Pittsburgh, PA). The PLA (1000) – b – PEG (750) (M_w = 1000 g/mol, 750 g/mol) and dimethylformamide (DMF) were supplied by

Sigma Aldrich (St. Louis, MO). The PLA (5000) – b – PEG (1000) (M_w = 5000 g/mol, 1000 g/mol) and PLA (1000) – b – PEG (5000) (M_w = 1000 g/mol, 5000 g/mol) block copolymers were purchased from Advanced Polymer Materials (Montreal, QC).

2.3.2 Preparation of electrospun solutions

The electrospun fabrics were formed using 25 wt% PLA with varied amounts of bulk PEG and PLA-b-PEG dissolved in DMF at 70ºC. The PLA/PEG and PLA/PLA-b-PEG copolymer concentrations in solution are detailed in Tables 2.1 and 2.2.

TABLE 2.1. Weight percent concentrations of PEG homopolymer added to 25 wt% PLA solutions.

25 wt% PLA, 0.3 wt% PEG
25 wt% PLA, 1.3 wt% PEG
25 wt% PLA, 2.7 wt% PEG

TABLE 2.2. Weight percent concentrations of PLA – b – PEG added to 25 wt% PLA solutions.

25 wt% PLA
25 wt% PLA, 0.2 wt% PLA (1000) – b – PEG (750)
25 wt% PLA, 0.4 wt% PLA (1000) – b – PEG (750)
25 wt% PLA, 0.6 wt% PLA (1000) – b – PEG (750)
25 wt% PLA, 0.6 wt% PLA (5000) – b – PEG (1000)
25 wt% PLA, 1.6 wt% PLA (5000) – b – PEG (1000)
25 wt% PLA, 5.0 wt% PLA (5000) – b – PEG (1000)
25 wt% PLA, 0.3 wt% PLA (1000) – b – PEG (5000)
25 wt% PLA, 3.0 wt% PLA (1000) – b – PEG (5000)

2.3.3 Electrospinning

The electrospinning apparatus consisted of a programmable syringe pump (Harvard Apparatus, MA) and a high-voltage supply (Gamma High Voltage Research Inc., FL). Electrospinning of the PLA/PEG and PLA/PLA-b-PEG solutions was carried out at 70ºC with a feed rate of 20 µl/min, and an applied voltage of 15 kV. Table 2.3 details the weight percent

polymer in solution, and in the final fibers. The nonwoven fibers were spun onto grounded sheets of copper approximately 15 cm from the spinneret tip (Figure 2.2).

TABLE 2.3. Weight percent polymer in solution, and in the final fibers

Weight percent concentrations of PLA/PLA-b-PEG in solution	**Total weight percent concentrations of PLA/PEG/DMF in solution**	**Total weight percent PLA/PEG in the final fibers**
25 wt% PLA	25 / 0 / 75	100 / 0
25 wt% PLA, 0.3 wt% PEG	25.1 / 0.3 / 74.6	99.0 / 1.0
25 wt% PLA, 1.3 wt% PEG	24.9 / 1.3 / 73.8	95.0 / 5.0
25 wt% PLA, 2.7 wt% PEG	24.5 / 2.7 / 72.8	90.0 / 10.0
25 wt% PLA, 0.2 wt% PLA (1000) – b – PEG (750)	25.3 / 0.1 / 74.6	99.6 / 0.4
25 wt% PLA, 0.4 wt% PLA (1000) – b – PEG (750)	25.3 / 0.2 / 74.5	99.3 / 0.7
25 wt% PLA, 0.6 wt% PLA (1000) – b – PEG (750)	25.4 / 0.2 / 74.4	99.1 / 0.9
25 wt% PLA, 0.6 wt% PLA (5000) – b – PEG (1000)	25.5 / 0.1 / 74.4	99.6 / 0.4
25 wt% PLA, 1.6 wt% PLA (5000) – b – PEG (1000)	26.1 / 0.3 / 73.6	99.0 / 1.0
25 wt% PLA, 5.0 wt% PLA (5000) – b – PEG (1000)	28.1 / 0.9 / 71.0	97.1 / 2.9
25 wt% PLA, 0.3 wt% PLA (1000) – b – PEG (5000)	25.1 / 0.2 / 74.7	99.1 / 0.9
25 wt% PLA, 3.0 wt% PLA (1000) – b – PEG (5000)	25.6 / 2.6 / 71.8	90.7 / 9.3

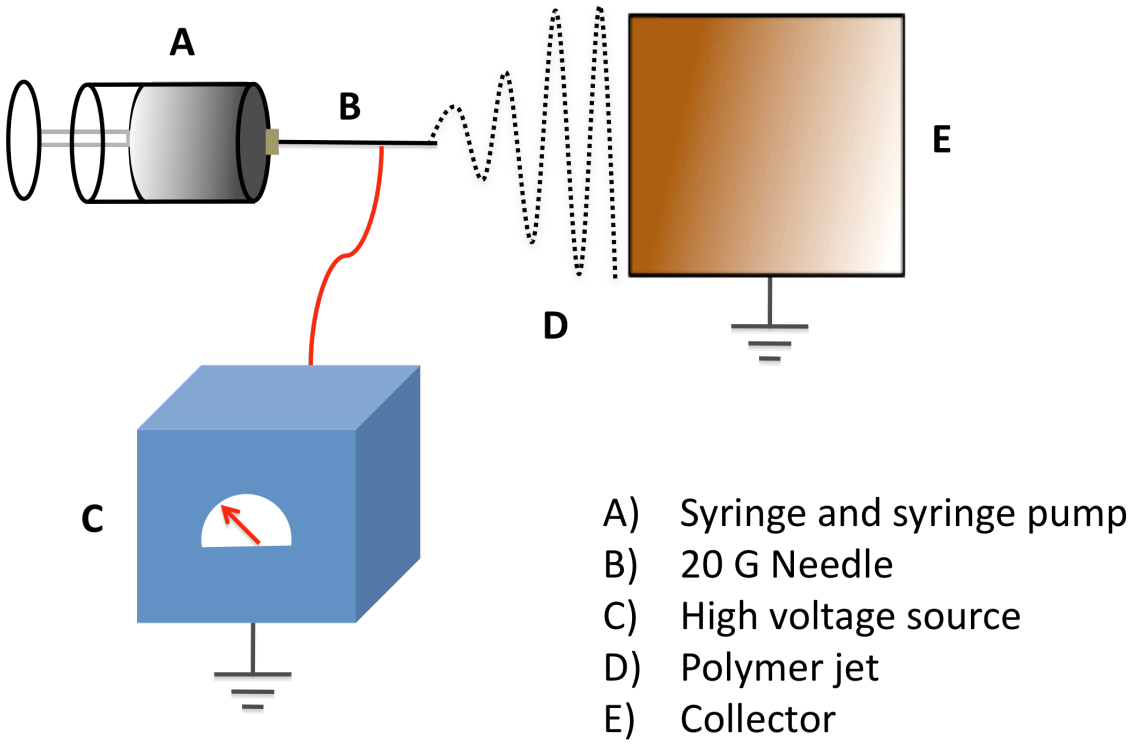

FIGURE 2.2. Schematic of the electrospinning process.

2.3.4 Scanning Electron Microscopy

Examination of the morphology and fiber geometry of the electrospun mats was performed using a Leica 440 scanning electron microscope (SEM) at 25 kV. Samples were coated for 30 seconds with 10 nm Au–Pd prior to imaging in order to prevent charging. The average fiber diameters and pore sizes of the nonwoven samples were analyzed from the SEM images using ImageJ software. Histogram data of the pore size distributions were fit using the Levenburg-Marquardt algorithm (Kaleidagraph 4.0, Synergy Software).

2.3.5 Water Wettability

Wettability testing was performed using a KSV Sigma wetting balance. Samples were cut into 3 cm by 0.5 cm rectangles, glued to wire hooks, and allowed to dry. To test, the

nonwoven sample was suspended above a dish of water, and the dish was raised to meet the sample until contact was made. The sample was weighed every 0.6 seconds for 10 minutes to determine the amount of water absorbed by the nonwoven mat.

2.4 RESULTS AND DISCUSSION

2.4.1 Morphology of PLA-PEG Blended Fibers and Nonwoven Fabrics

Fiber and nonwoven fabric morphology, average fiber diameters and pore size distributions of the electrospun samples were assessed using SEM images. Samples spun with PEG homopolymer as control samples, and those spun with the three PLA-b-PEG copolymers at various loadings, showed significant differences in morphology resulting more from the mode of PEG addition than the total weight percent of PEG incorporated. Both the addition of PEG via a block copolymer or homopolymer, and the actual diblock co-polymer structure, significantly influenced the spinnability and final morphology of electrospun fibers and nonwoven fabrics. These observed physical characteristics play a role in the transport of aqueous media in nonwoven fabrics. Both the fibers, and the pore spacings between them, affect the capillary action of the samples, influencing the amount of media absorbed.

2.4.1.1 Addition of PEG Homopolymer

Incorporating PEG homopolymer into PLA resulted in a significant decrease in fiber uniformity, which can be seen in both SEM images (Figure 2.3) and in the standard deviations of the fiber diameters (Table 2.4). Solutions containing greater than 5.0 wt% PEG homopolymer were not spinnable. Images showing the control PLA, and fibers spun with 1.0 and 5.0 wt% PEG homopolymer can be seen in Figure 2.3. These images show the electrospun

fibers spun with PLA and 1.0 wt% PEG to be characteristically smooth and round, while the samples spun with 5.0 wt% PEG have a mixture of round and non-uniformly shaped fibers. Additionally, the average fiber diameters for the PLA and PLA/PEG fibers are detailed in Table 2.4. The sample spun with 1.0 wt% of the bulk PEG produced average fiber diameters that were not significantly different from the control PLA. However, the fibers spun with 5.0 wt% PEG had variable diameter sizes, and were significantly larger than the control PLA samples. Similar results confirming the poor compatibility between PEG and PLA have been reported previously [24-25, 33].

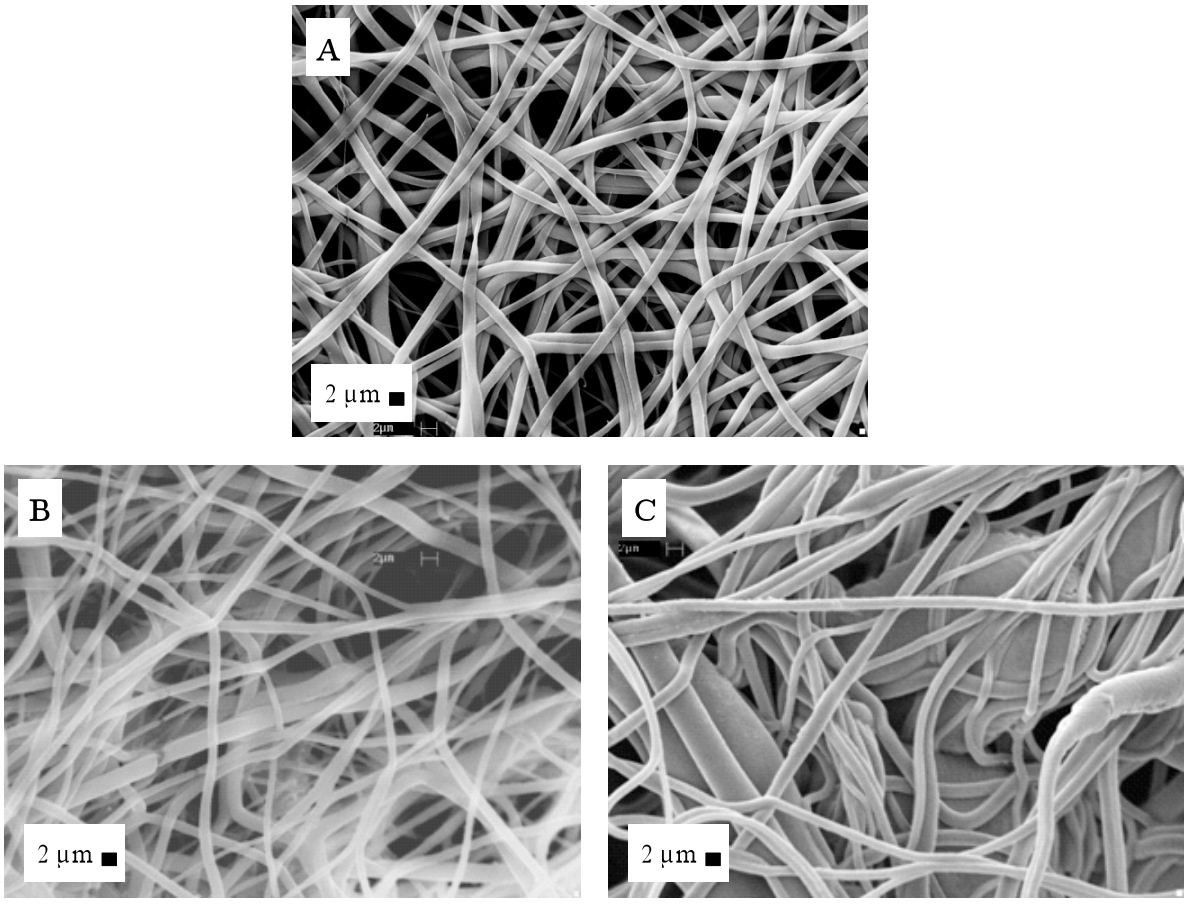

FIGURE 2.3. SEM images of electrospun A) 100 wt% PLA B) 99 wt% PLA, 1.0 wt% PEG C) 95 wt% PLA, 5.0 wt% PEG.

TABLE 2.4. Average fiber diameters for samples spun with PLA and PEG homopolymer.

Sample	Average Fiber Diameter (μm)
PLA	1.3 ± 0.2
99 wt% PLA, 1.0 wt% PEG	1.3 ± 0.6
95 wt% PLA, 5.0 wt% PEG	1.5 ± 0.6

2.4.1.2 Addition of PLA-b-PEG copolymer

In comparison to the addition of PEG homopolymer, incorporation of PEG as part of a diblock copolymer improved fiber morphology. The specific composition of the diblock copolymer, however, significantly influenced both the quantity of copolymer that could be added to the spinning dope, as well as the final fiber properties. To describe these results, each copolymer will be discussed separately in order of increasing PEG block length.

PLA (1000) – b – PEG (750) was added to the base spinning dope as described in Table 2.3. Images showing the fibers spun with varying concentrations of PLA (1000) – b – PEG (750) are presented in Figure 2.4. These images show the electrospun fibers to be consistent with the control PLA fibers, characteristically smooth and round. Additionally, the average fiber diameters of the PLA/PLA (1000) – b – PEG (750) were all relatively consistent with the control PLA fibers (Table 2.5). Unlike the PEG homopolymer experiments, samples spun with 0.9 wt% PEG from PLA (1000) – b – PEG (750) produced fibers with general morphology and average diameter sizes that were more consistent with the control PLA. Even though the ratio of PLA: DMF increased slightly within the polymer solution, from 25 wt% PLA to 25.4 wt% PLA, the final fiber properties were not affected.

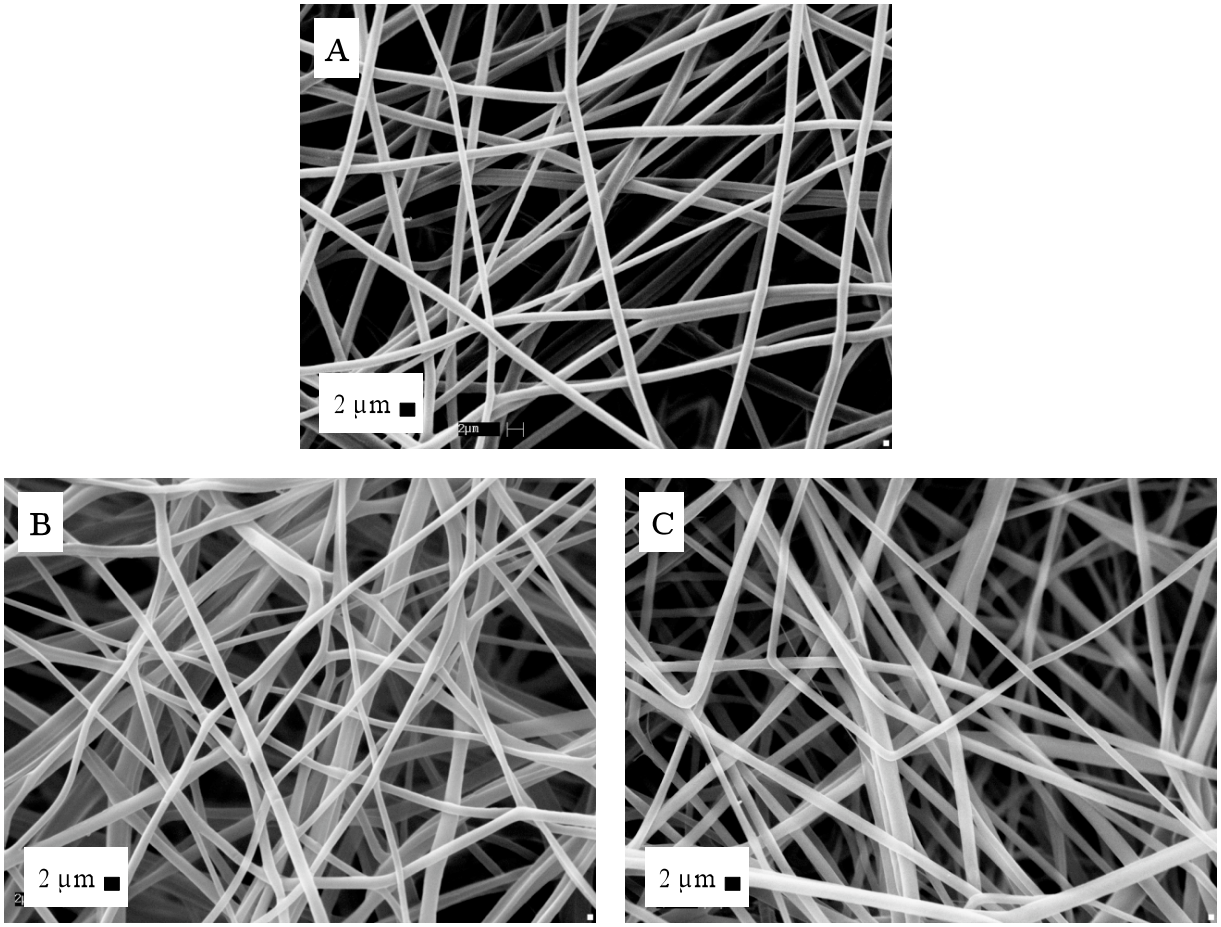

FIGURE 2.4. SEM images of A) PLA B) 99.6 wt% PLA, 0.4 PEG wt% C) 99.3 PLA wt%, 0.7 PEG wt% and D) 99.0 PLA wt%, 0.9 PEG wt% electrospun fibers.

TABLE 2.5. Average fiber diameters for samples spun with varying concentrations of PLA (1000) – b – PEG (750).

Sample	Average Fiber Diameter (µm)
99.6 wt% PLA, 0.4 wt% PEG	1.2 ± 0.2
99.3 wt% PLA, 0.7 wt% PEG	1.3 ± 0.3
99.0 wt% PLA, 0.9 wt% PEG	1.3 ± 0.3

Interestingly, it was only possible to add concentrations of the PLA (1000) – b – PEG (750) copolymer to the PLA solutions up to 0.8 wt% of the block copolymer in the spinning dope. At higher concentrations of the copolymer, the system formed a stiff and slightly cloudy

gel (Figure 2.6). Previous authors have reported that the relatively short PLA (1000) – b – PEG (750) chains can aggregate to form micelles within the solution [34-37]. PLA-b-PEG is an example of an amphiphilic molecule, meaning that it contains both a polar "head", and a non-polar "tail". Typically, at the critical micelle concentration in polar DMF, these molecules aggregate, causing the hydrophobic "tails" to cluster together [38]. This phenomenon can be observed in bulk, and is characterized by an observed cloudiness in the solution [39-41]. In this case, the formation of a gel phase indicates that the micelles form with PLA at the exterior, where it can interact with the PLA homopolymer in solution and form cross links (Figure 2.5) [42].

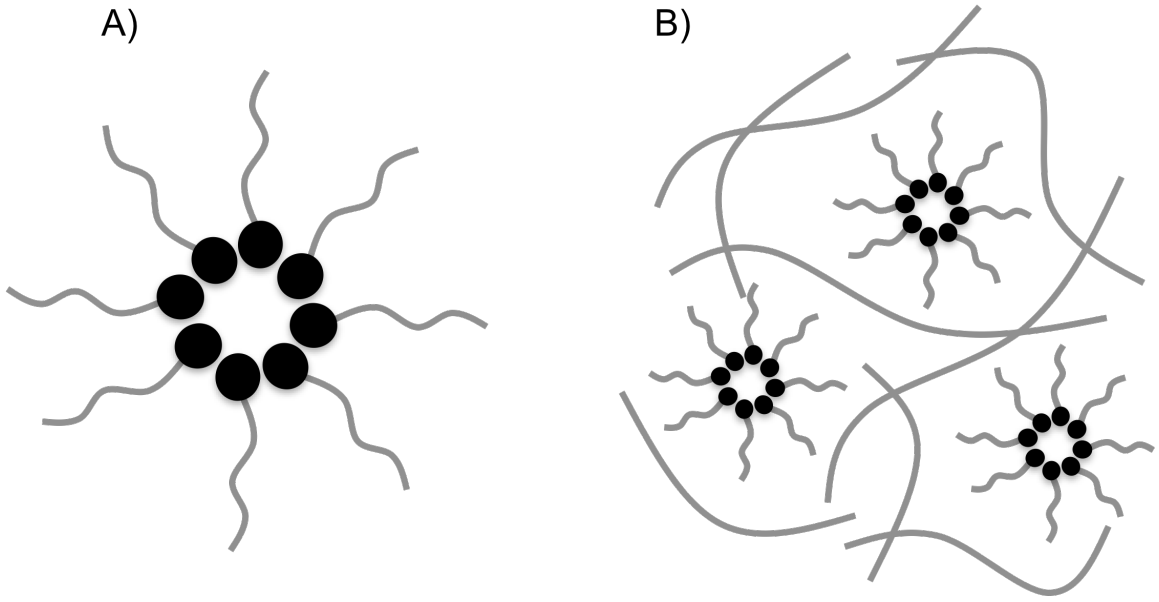

FIGURE 2.5. Schematic illustrating A) Micelle formation of PLA-b-PEG at the critical micelle concentration and B) Gel structure formed at 0.8 wt% PLA (1000) – b – PEG (750).

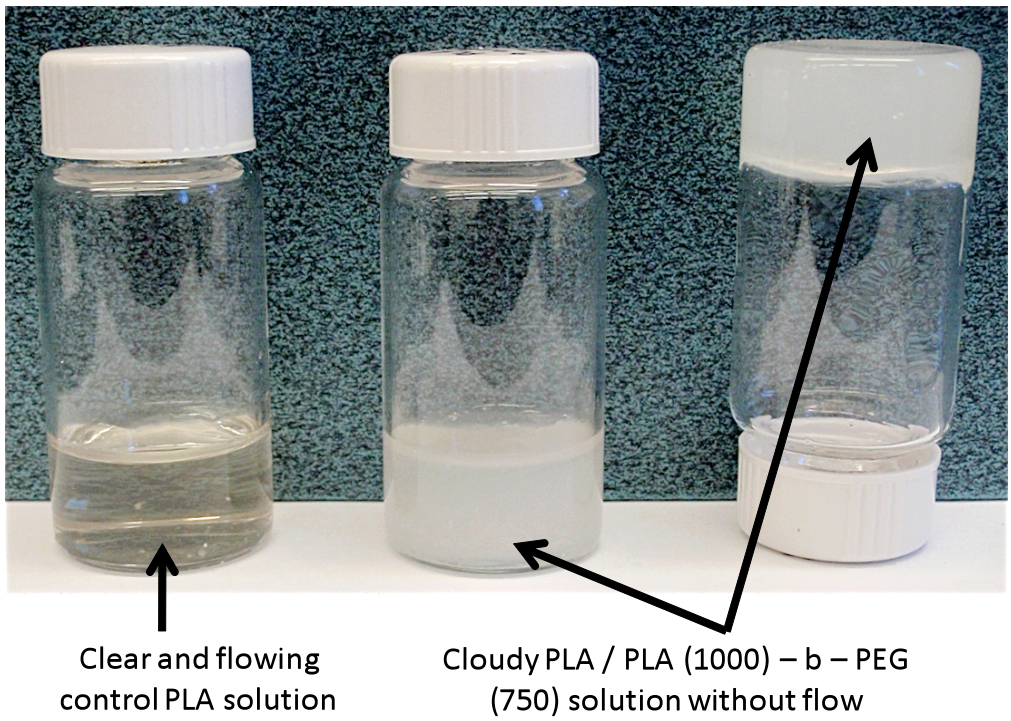

FIGURE 2.6. Observed cloudiness and increase in solution viscosity at higher concentrations of PLA/PLA (1000) – b – PEG (750).

A second PLA-b-PEG chain length copolymer was selected to continue the experiments, using block lengths of PLA (5000) – b – PEG (1000). Table 2.3 details the polymer concentrations in solution, as well as the final fiber compositions. During the experiments using the PLA-weighted chain length copolymer, PLA (5000) – b – PEG (1000), three different concentrations of PEG were added to the PLA fibers: 0.4, 1.0, and 2.9 wt% PEG. The 0.4 wt% PEG samples had morphology and average fiber diameters consistent with the control PLA sample (Figure 2.7 and Table 2.6). However, fibers spun with the higher concentrations of PLA-b-PEG copolymer had fiber diameters that were significantly larger than the PLA fibers. Fibers spun with 1.0 wt% and 2.9 wt% PEG had average diameters that were significantly higher than the control PLA samples. Unlike the fibers spun with PEG homopolymer these fibers were much more uniform, illustrating that the use of PLA-b-PEG

copolymers helped to retain smooth, uniform fiber morphology, even though fiber diameter increases.

The long PLA block in this copolymer results in a significant increase in total PLA concentration, leading to an incremental increase in the PEG concentration (5:1). Table 2.3 shows that the total weight percent of PLA within the DMF solutions increased gradually with the PLA (5000) – b – PEG (1000) loadings, from 25 wt% PLA to 28.1 wt% PLA. The results are consistent with previous studies that showed an increase in the concentration of PLA in a DMF solution causes an increase in fiber diameter [43-45]. Increasing the polymer to solvent ratio has been attributed to increases in electrospinning parameters, including dope viscosity and surface tension, which have been correlated to increased final fiber diameter [46-47]. Previous studies by He, Sunthornvarabhas, and Deitzel et al. showed that increasing the concentration of PLA led to an increase in solution viscosity, which corresponded to electrospun fibers with larger average fiber diameters [43-45]. Further confirmation of this result can be seen in Figure 2.8, which shows an SEM image of fibers spun with 29 wt% PLA homopolymer in DMF. The SEM image shows the fibers to be bulky and non-uniform, with an average diameter size significantly larger than fibers spun with 25 wt% PLA.

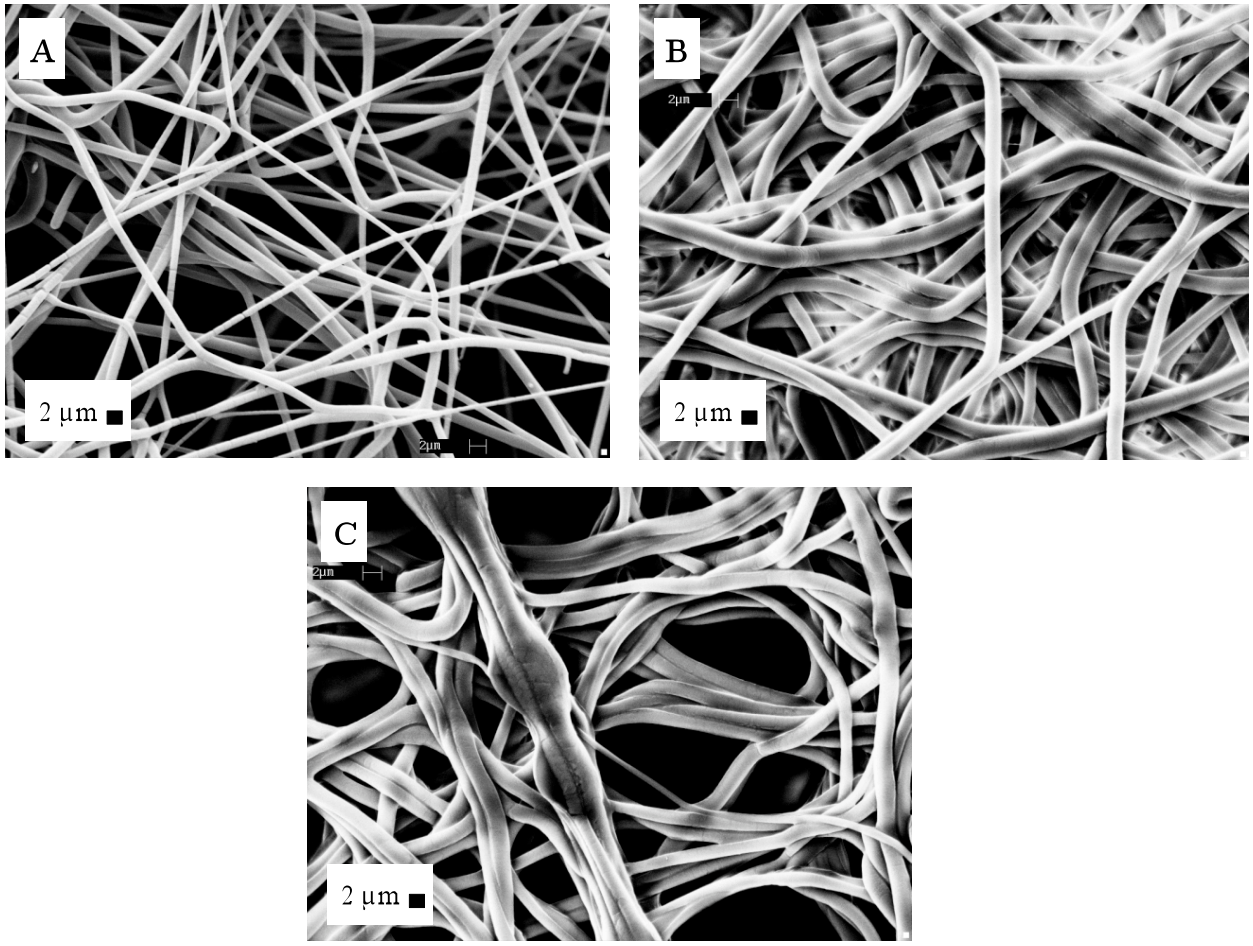

FIGURE 2.7. SEM images of A) 99.6 wt% PLA, 0.4 wt% PEG B) 99.0 wt% PLA, 1.0 wt% PEG D) 97.1 wt% PLA, 2.9 wt% PEG electrospun fibers.

TABLE 2.6. Average fiber diameters for electrospun samples with different concentrations of PLA (5000) – PEG (1000) copolymer.

Sample	Average Fiber Diameter (µm)
100% PLA	1.3 ± 0.2
99.6 wt% PLA, 0.4 wt% PEG	1.3 ± 0.3
99.0 wt% PLA, 1.0 wt% PEG	1.6 ± 1.3
97.1 wt% PLA, 2.9 wt% PEG	1.7 ± 0.7

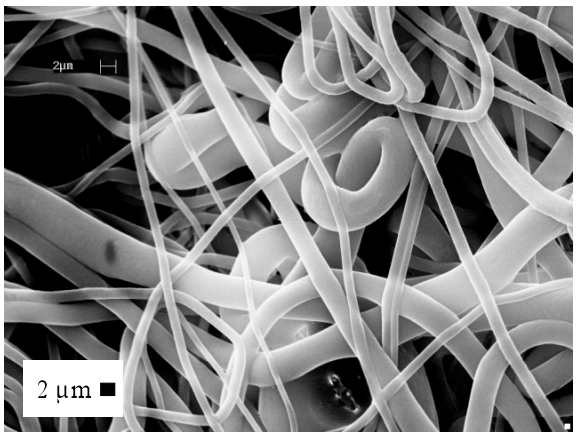

FIGURE 2.8. SEM image showing 29 wt% PLA electrospun fibers. The diameters of these fibers are variable, 1.9 ± 1.3 µm.

A third block copolymer, PLA (1000) – b – PEG (5000), was used in order to add more PEG to the spinning dope without significantly increasing PLA concentration. PLA (1000) – b – PEG (5000) was added to the base PLA solutions at concentrations resulting in PEG content within the final fibers at 0.9, and 9.3 wt% (Table 2.3). The polymer solution that contained 9.3 wt% PEG took approximately 5 extra minutes to fully dissolve into solution, which corresponded to previous studies that identified the maximum PEG loading to be ~10 wt%. Although fibers spun with 1.0 or 5.0 wt% PEG homopolymer were non-uniform and no fibers were formed from solutions with >5 wt% PEG homopolymer, fine, uniform fibers were formed when the PEG was incorporated as a block copolymer. SEM images show that the fiber mats had smooth, uniform morphology, but with average fiber diameters that were significantly lower than the control PLA (Table 2.7 and Figure 2.9). The PEG-weighted copolymer allowed for more PEG to be incorporated into the fiber without significantly increasing the concentration of PLA in the spinning solution. The results are also consistent with previous studies which reported that adding higher concentrations of PEG into a PLA/PEG solution resulted in a decrease in solution viscosity, resulting in thinner fibers [47-51]. These results are interesting considering that the experiments performed in the previous section showed lumpy

and non-uniform fibers produced using 5.0 wt% of PEG homopolymer. Both Cui and Spasova et al. showed that relatively smooth and uniform PLA/PEG fibers with approximately 10 wt% PEG could be electrospun successfully [48-49]. However, the molecular weights (MW of PLA = 78,000 – 152,000 g/mol, MW of PEG = 2000 g/mol), and overall concentration of polymer used (10 wt% polymer in solution) was much lower than in the presented study. The molecular weight of PLA used in this study was 211,332 g/mol, the molecular weight of PEG homopolymer = 3350 g/mol, while the total polymer concentration in DMF was around 26 wt%. The results of this experiment show that under these spinning conditions, the most productive method of increasing PEG content is to use a diblock copolymer.

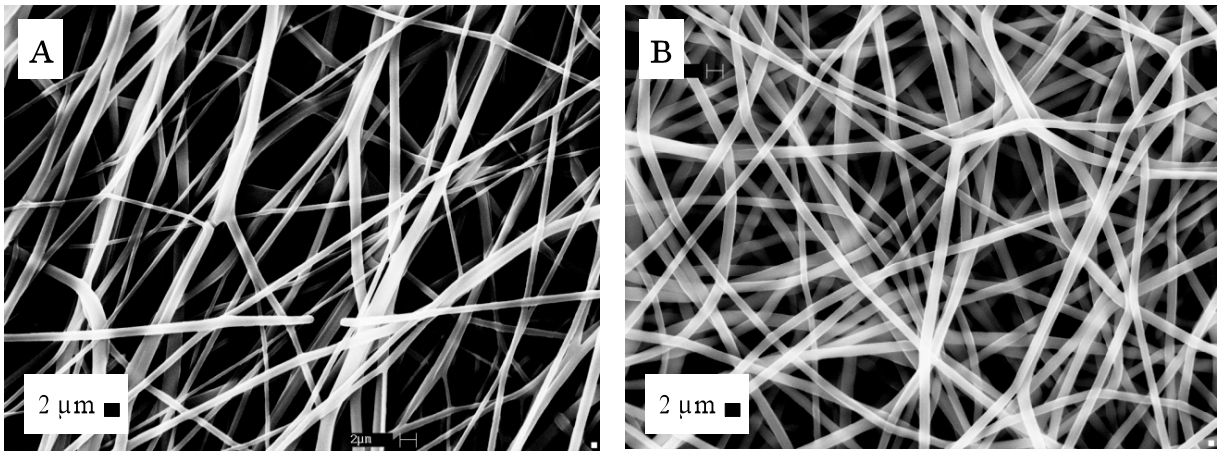

FIGURE 2.9. SEM images of A) 99.1 wt% PLA, 0.9 wt% PEG B) 90.7 wt% PLA, 9.3 wt% PEG electrospun fibers.

TABLE 2.7. Average fiber diameters for electrospun samples with different concentrations of PLA (5000) – b – PEG (1000) copolymer.

Sample	Average Fiber Diameter (µm)
100% PLA	1.3 ± 0.2
99.1 wt% PLA, 0.9 wt% PEG	1.1 ± 0.4
90.7 wt% PLA, 9.3 wt% PEG	1.1 ± 0.2

2.4.1.3 Pore Size and Pore Size Distribution of PLA-b-PEG Electrospun Nonwoven fabrics

Moisture transport in nonwoven fabrics depends on the pore spacing between fibers, as well as the individual fiber surface properties [52]. Variations in spacing between fibers were evident in the SEM images presented above, and were quantified from these images. Table 2.8 provides a comparison of the average pore sizes and distributions of these samples with the average fiber diameters that were previously measured. For electrospun nonwoven fabrics, and PLA specifically, pore size and pore size distribution have been correlated with individual fiber diameter [55]. These results hold true for this sample set as well.

The results show that pore size and distribution are consistent with fiber diameter. Increases and decreases in fiber diameter are accompanied by an increase or decrease in pore size/pore size distribution [53]. For the samples spun with PLA and PLA (1000) – b – PEG (750), average fiber diameters were consistent, as well as pore size and distribution (Figure 2.10). The fiber diameter, pore size, and pore size distribution measurements for samples spun with 0.4 wt% PEG from PLA (5000) – b – PEG (1000) were also consistent with the control PLA (Figure 2.11).

For the samples spun with 1.0 and 2.9 wt% PEG from PLA (5000) – b – PEG (1000), the results were slightly different. For both samples, the average fiber diameters were significantly larger than PLA. However, the pore sizes for the 1.0 wt% PEG were comparable to PLA, though the distribution was much larger. For the 2.9 wt% PEG samples, both the pore sizes and pore size distribution were much larger than PLA (Figure 2.11). These results correspond with the data for the samples spun with 1.0 and 5.0 wt% of the PEG homopolymer. Both of these samples showed an increase in fiber diameter and pore size and distribution. Conversely, the samples spun with PLA (1000) – b – PEG (5000) had both average fiber

diameters and pore sizes that were lower than PLA. Interestingly enough, the pore size distributions of these samples were slightly broader than PLA (Figure 2.12).

TABLE 2.8. Summarization of the average pore sizes and fiber diameters for the nonwoven samples spun with PLA/PEG and PLA / PLA-b-PEG.

Samples	Average Pore Size (μm^2)	Average Fiber Diameter (μm)
PLA	3.3 ± 1.9	1.3 ± 0.2
0.4 wt% PEG from PLA (1000) – b – PEG (750)	3.3 ± 3.1	1.2 ± 0.2
0.7 wt% PEG from PLA (1000) – b – PEG (750)	4.0 ± 3.3	1.3 ± 0.3
0.9 wt% PEG from PLA (1000) – b – PEG (750)	3.3 ± 2.6	1.3 ± 0.3
0.4 wt% PEG from PLA (5000) – b – PEG (1000)	4.5 ± 2.9	1.3 ± 0.3
1.0 wt% PEG from PLA (5000) – b – PEG (1000)	4.1 ± 2.7	1.6 ± 1.3
2.9 wt% PEG from PLA (5000) – b – PEG (1000)	6.8 ± 1.9	1.7 ± 0.7
0.9 wt% PEG from PLA (1000) – b – PEG (5000)	5.0 ± 2.9	1.1 ± 0.4
9.3 wt% PEG from PLA (1000) – b – PEG (5000)	2.9 ± 2.2	1.1 ± 0.2
1.0 wt% PEG Homopolymer	4.8 ± 4.5	1.4 ± 0.6
5.0 wt% PEG Homopolymer	7.1 ± 6.2	1.5 ± 0.6

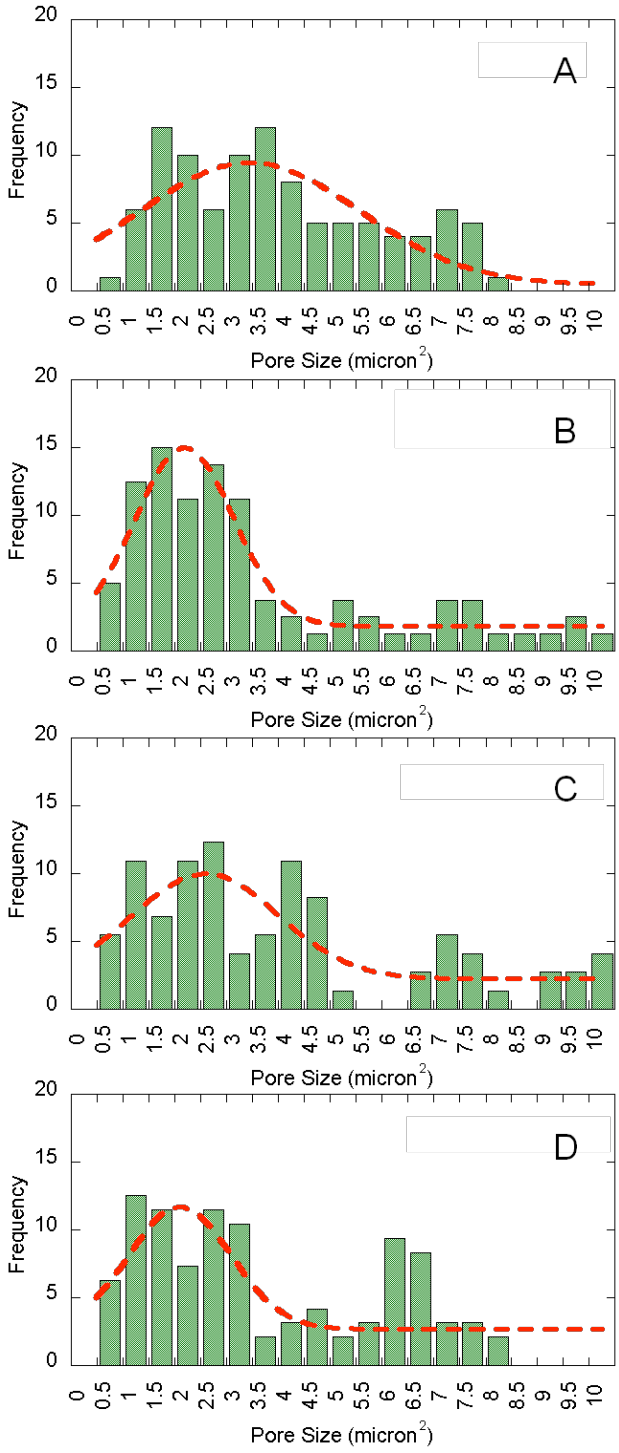

FIGURE 2.10. Histograms illustrating pore size and pore size distribution for nonwoven samples spun with A) PLA B) 0.4 wt% PEG D) 0.7 wt% PEG D) 0.9 wt% PEG from PLA (1000) – b – PEG (750).

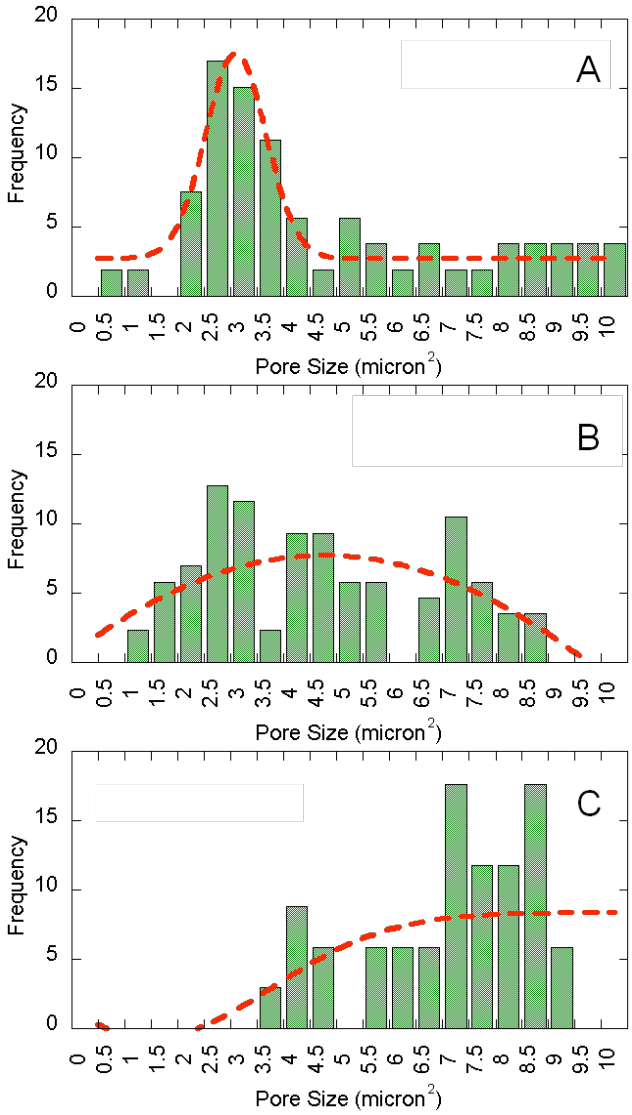

FIGURE 2.11. Histograms illustrating pore size and pore size distribution for nonwoven samples spun with A) 0.4 wt% PEG B) 1.0 wt% PEG and C) 2.9 wt% PEG from PLA (5000) – b – PEG (1000).

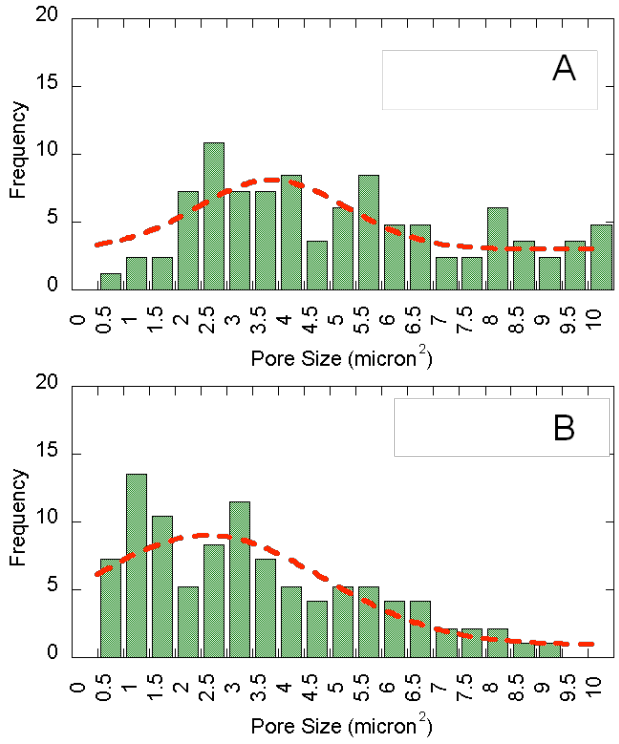

FIGURE 2.12. Histograms illustrating pore size and pore size distribution for nonwoven samples spun with A) 0.9 wt% PEG and B) 9.3 wt% PEG from PLA (1000) – b – PEG (5000).

2.4.2 Water Wettability

Increased hydrophilicity of PLA/PEG nonwoven fabrics was assessed using water wettability testing. The transport of liquid in a nonwoven fabric is governed by liquid properties, interactions between the liquid and nonwoven, and fiber geometry (i.e. fiber diameter, pore size and distribution). The affinity of the liquid and nonwoven, as well as the spacing between the fibers, influence the transport of liquid in the porous medium. For example, Xiang et al. found that hydrophobic PLA absorbed 4.4 g of mineral oil/g of sample, and only absorbed 0.3 g of water/g of sample [54]. Additionally, Rebovich et al. showed that nonwoven samples with smaller pore sizes and distributions were more wettable than those possessing large pore sizes and distributions, as a result of capillary action [52]. Given that

wettability testing is influenced by both liquid/surface contact angle and liquid uptake, it is a suitable method for measuring changes in the surface hydrophilicity of nonwoven samples.

The results in Figure 2.13 illustrate the influence of PEG homopolymer and PLA-b-PEG diblock copolymers on the wettability of PLA nonwoven fabrics. The data shows that, as expected, the PLA samples took up only a small amount of water. For the samples spun with PLA (1000) – b – PEG (750), wettability increased with weight percent PEG. Given that fiber diameter, pore size, and pore size distribution were constant among these samples, the improvement in wettability can be attributed to the addition of PEG to the fibers.

The improvement in wettability continued for the samples spun with 0.4 wt% PEG from PLA (5000) – b – PEG (1000). Fiber diameter, pore size and pore size distribution remained constant for this sample, so the improvement in wettability was a factor of PEG concentration and copolymer chain length. The samples spun with 0.4 wt% PEG from PLA (5000) – b – PEG (1000) were more wettable than the samples spun with 0.4 wt% PEG from PLA (1000) – b – PEG (750). The result suggests that using a longer chain length copolymer assists in driving more PEG to the fiber surface. This theory can be further confirmed by the samples spun with 1.0 wt% PEG from PLA (5000) – b – PEG (1000). It has already been discussed that these samples underwent both an increase in fiber diameter and pore size distribution, yet the wettability improved. Even though the changes in fiber diameter and pore size distribution should lower capillary action in the nonwoven, increased PEG on the fiber surface helped to overcome this. However, a decrease in wettability was observed for samples spun with 2.9 wt% PEG from PLA (5000) – b – PEG (1000). In these samples, the continued increase of fiber diameter, pore size and pore size distribution countered the increased concentration of PEG.

Nonwoven samples spun with 0.9 and 9.3 wt% PEG from PLA (1000) – b – PEG (5000) showed an improvement in wettability, which can be attributed to the increased PEG loading from the longer PEG block, as well as a decrease in fiber diameter and pore size. The samples spun with 0.9 wt% PEG from PLA (1000) – b – PEG (5000) were more wettable than the samples spun with 0.9 wt% PEG from PLA (1000) – b – PEG (750) and 1.0 wt% PEG from PLA (5000) – b – PEG (1000). Samples spun with 9.3 wt% PEG showed the highest wettability of the PLA/PEG nonwoven fabrics.

Regardless of the differences between the chain length copolymers, the results showed very clearly that using a diblock copolymer provided improved wettability over adding PEG homopolymer. Samples spun with 1.0 and 5.0 wt% PEG homopolymer were considerably less wettable than those spun with comparable PEG loadings from the diblock copolymers.

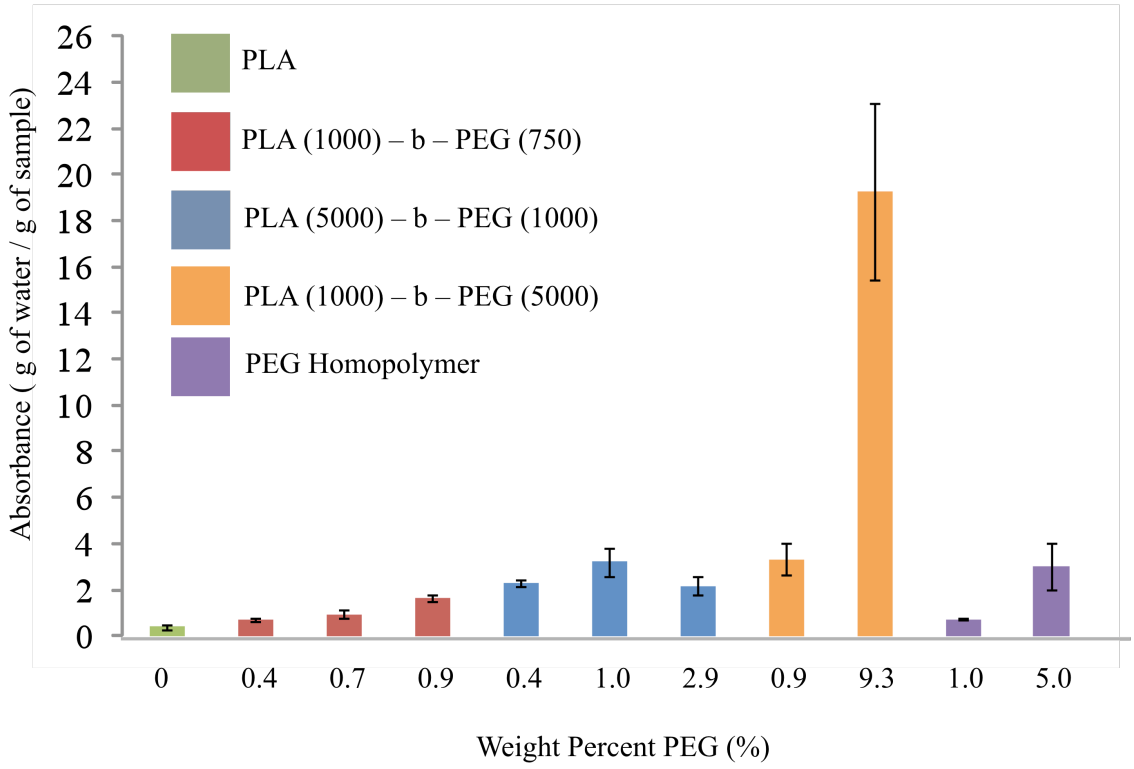

FIGURE 2.13. Wettability data for PLA, and PLA/PLA-b-PEG electrospun samples.

2.5 CONCLUSIONS

The hydrophilicity of PLA electrospun fibers was modified through the incorporation of PEG homopolymer and PLA-b-PEG copolymers of different block lengths. The lengths of the blocks were found to influence the maximum amount of PEG that could be incorporated, as well as spinnability and morphology. With the shorter chain length copolymer, PLA (1000) – b – PEG (750), micelle formation was found to impede the electrospinning process at concentrations greater than 0.8 wt% copolymer. Adding PLA (5000) – b – PEG (1000) to the spinning dope led to an increase in fiber diameter consistent with increasing the concentration of PLA in the solution. The maximum copolymer loading was achieved using PLA (1000) – b – PEG (5000), which was also accompanied by a decrease in fiber diameter. In contrast to the addition of the block copolymer, adding PEG homopolymer to the spinning dope produced fibers with highly variable morphology. Water wettability improved significantly with the addition of PEG to the electrospinning dopes, with PLA-b-PEG copolymers providing a greater increase than the PEG homopolymer.

2.6 REFERENCES

[1] E. Balaur, J. M. Macak, L. Taveira and P. Schmuki, Tailoring the wettability of TiO2 nanotube layers, Electrochemistry Communications, 7 (2005) 1066–1070.

[2] T. Sun, L. Feng, X. Gao and L. Jiang, Bioinspired Surfaces with Special Wettability, Accounts of Chemical Research, 38 (2005) 644-652.

[3] T. Zhang, D. Hu, J. Jin, S. Yang, G. Li and J. Jiang, Improvement of surface wettability and interfacial adhesion ability of poly(p-phenylene benzobisoxazole) (PBO) fiber by incorporation of 2,5-dihydroxyterephthalic acid (DHTA), European Polymer Journal, 45 (2009) 302-307.

[4] N. Encinas, M. Pantoja, J. Abenojar, Mart and M. A. nez, Control of Wettability of Polymers by Surface Roughness Modification, Journal of Adhesion Science and Technology, 24 (2010) 1869-1883.

[5] K. S. Teh and Y. W. Lu, Surface nanostructuring of biocompatible polymer for wettability control in MEMS, in: Micro Electro Mechanical Systems, 2008. MEMS 2008. IEEE 21st International Conference on, 2008, pp. 363-366.

[6] W. Lee, M.-K. Jin, W.-C. Yoo and J.-K. Lee, Nanostructuring of a Polymeric Substrate with Well-Defined Nanometer-Scale Topography and Tailored Surface Wettability, Langmuir, 20 (2004) 7665-7669.

[7] T. P. Russell, Surface-Responsive Materials, Science, 297 (2002) 964-967.

[8] D. Hegemann, M. M. Hossain and D. J. Balazs, Nanostructured plasma coatings to obtain multifunctional textile surfaces, Progress in Organic Coatings, 58 (2007) 237-240.

[9] V. Sorna Gowri, L. Almeida, M. de Amorim, N. Pacheco, A. Souto, M. Esteves and S. Sanghi, Functional finishing of polyamide fabrics using ZnO–PMMA nanocomposites, Journal of Materials Science, 45 (2010) 2427-2435.

[10] J. Nadeau, Nanotechnological Advances in Biosensors, Sensors, 9 (2009) 8907-8910.

[11] V. Ilic´, Z. Šaponjic´, V. Vodnik, S. a. Lazovic´, S. Dimitrijevic´, P. Jovančic´, J. M. Nedeljkovic´ and M. Radetic´, Bactericidal Efficiency of Silver Nanoparticles Deposited onto Radio Frequency Plasma Pretreated Polyester Fabrics, Industrial & Engineering Chemistry Research, 49 (2010) 7287-7293.

[12] Y. Arima and H. Iwata, Effect of wettability and surface functional groups on protein adsorption and cell adhesion using well-defined mixed self-assembled monolayers, Biomaterials, 28 (2007) 3074-3082.

[13] H. S. Yoo, T. G. Kim and T. G. Park, Surface-functionalized electrospun nanofibers for tissue engineering and drug delivery, Advanced Drug Delivery Reviews, 61 (2009) 1033-1042.

[14] T. G. Kim and T. G. Park, Biomimicking Extracellular Matrix: Cell Adhesive RGD Peptide Modified Electrospun Poly(D,L-lactic-co-glycolic acid) Nanofiber Mesh, Tissue Engineering, 12 (2006) 221-233.

[15] K. L. Menzies and L. Jones, The Impact of Contact Angle on the Biocompatibility of Biomaterials, Optometry & Vision Science, 87 (2010) 387-399 310.1097/OPX.1090b1013e3181da1863e.

[16] A. M. Rossi, L. Wang, V. Reipa and T. E. Murphy, Porous silicon biosensor for detection of viruses, Biosensors and Bioelectronics, 23 (2007) 741-745.

[17] W. K. Son, J. H. Youk, T. S. Lee and W. H. Park, Preparation of Antimicrobial Ultrafine Cellulose Acetate Fibers with Silver Nanoparticles, Macromolecular Rapid Communications, 25 (2004) 1632-1637.

[18] P. Dayal, J. Liu, S. Kumar and T. Kyu, Experimental and Theoretical Investigations of Porous Structure Formation in Electrospun Fibers, Macromolecules, 40 (2007) 7689-7694.

[19] Y. Ikada and H. Tsuji, Biodegradable polyesters for medical and ecological applications, Macromolecular Rapid Communications, 21 (2000) 117-132.

[20] É. Kiss, I. Bertóti and E. I. Vargha-Butler, XPS and Wettability Characterization of Modified Poly(lactic acid) and Poly(lactic/glycolic acid) Films, Journal of Colloid and Interface Science, 245 (2002) 91-98.

[21] P. Ouyang, Y.-q. Kang, G.-f. Yin, Z.-b. Huang, Y.-d. Yao and X.-m. Liap, Fabrication of hydrophilic paclitaxel-loaded PLA-PEG-PLA microparticles via SEDS process, Frontiers of Materials Science in China, 3 (2009) 15-24.

[22] M. Zhang, X. H. Li, Y. D. Gong, N. M. Zhao and X. F. Zhang, Properties and biocompatibility of chitosan films modified by blending with PEG, Biomaterials, 23 (2002) 2641-2648.

[23] S. R. Bhattarai, N. Bhattarai, P. Viswanathamurthi, H. K. Yi, P. H. Hwang and H. Y. Kim, Hydrophilic nanofibrous structure of polylactide; fabrication and cell affinity, Journal of Biomedical Materials Research Part A, 78A (2006) 247-257.

[24] H. Otsuka, Y. Nagasaki and K. Kataoka, Surface Characterization of Functionalized Polylactide through the Coating with Heterobifunctional Poly(ethylene glycol)/Polylactide Block Copolymers, Biomacromolecules, 1 (2000) 39-48.

[25] H. Otsuka, Y. Nagasaki, T. Okano and K. Kataoka, Functionalization of polylactide(PLA) surface using heterobifunctional PEG/PLA block copolymers for the control of cell behavior at surfaces, in: EMBS International Conference, Chicago, IL, 2000.

[26] Y. K. Luu, K. Kim, B. S. Hsiao, B. Chu and M. Hadjiargyrou, Development of a nanostructured DNA delivery scaffold via electrospinning of PLGA and PLA-PEG block copolymers, Journal of Controlled Release, 89 (2003) 341-353.

[27] M. K. Ma, Vahik; Yu, Jian; Thomas, Edwin; Rutledge, Gregory Electrospun polymer nanofibers with internal periodic structure obtained by microphase separation of cylindrically confined block copolymers, Nano Letters, 6 (2006) 2969-2972.

[28] F.-C. C. Chen, Shang-Chieh Nanoscale functional interlayers formed through spontaneous vertical phase separation in polymer photovoltaic devices, Journal of Materials Chemistry, 19 (2009) 6865–6869.

[29] R. A. Quirk, M. C. Davies, S. J. B. Tendler and K. M. Shakesheff, Surface Engineering of Poly(lactic acid) by Entrapment of Modifying Species, Macromolecules, 33 (2000) 258-260.

[30] X. Xu, L. Yang, X. Xu, X. Wang, X. Chen, Q. Liang, J. Zeng and X. Jing, Ultrafine medicated fibers electrospun from W/O emulsions, Journal of Controlled Release, 108 (2005) 33-42.

[31] M. W. Matsen, The standard Gaussian model for block copolymer melts, Journal of Physics Condensed Matter, 14 (2002) R21-R47.

[32] C. Kong, T. Lee, S. Lee and H. Kim, Nano-web formation by the electrospinning at various electric fields, Journal of Materials Science, 42 (2007) 8106-8112.

[33] G. Yu, J. Ji, H. Zhu and J. Shen, Poly(D,L-lactic acid)-block-(ligand-tethered poly(ethylene glycol)) copolymers as surface additives for promoting chondrocyte attachment and growth, Journal of Biomedical Materials Research Part B: Applied Biomaterials, 76B (2006) 64-75.

[34] L. Chen, Z. Xie, J. Hu, X. Chen and X. Jing, Enantiomeric PLA–PEG block copolymers and their stereocomplex micelles used as rifampin delivery, Journal of Nanoparticle Research, 9 (2007) 777-785.

[35] Y. Q. Li, Xian Rong; Maitani, Yoshie; Nagai, Tsuneji PEG–PLA diblock copolymer micelle-like nanoparticles as all-trans-retinoic acid carrier: in vitro and in vivo characterizations, Nanotechnology, 20 (2009) 055106.

[36] E. Pierri and K. Avgoustakis, Poly(lactide)-poly(ethylene glycol) micelles as a carrier for griseofulvin, Journal of Biomedical Materials Research Part A, 75A (2005) 639-647.

[37] T. Riley, S. Stolnik, C. R. Heald, C. D. Xiong, M. C. Garnett, L. Illum, S. S. Davis, S. C. Purkiss, R. J. Barlow and P. R. Gellert, Physicochemical Evaluation of Nanoparticles Assembled from Poly(lactic acid)–Poly(ethylene glycol) (PLA–PEG) Block Copolymers as Drug Delivery Vehicles, Langmuir, 17 (2001) 3168-3174.

[38] D. Brizzolara, H. J. Cantow, R. Mülhaupt and A. J. Domb, Novel materials through stereocomplexation, Journal of Computer-Aided Materials Design, 3 (1996) 341-350.

[39] Z. Wang, F. Zhao and D. Li, Determination of solubilization of phenol at coacervate phase of cloud point extraction, Colloids and Surfaces A: Physicochemical and Engineering Aspects, 216 (2003) 207-214.

[40] L. Zhang, H. Shen and A. Eisenberg, Phase Separation Behavior and Crew-Cut Micelle Formation of Polystyrene-b-poly(acrylic acid) Copolymers in Solutions, Macromolecules, 30 (1997) 1001-1011.

[41] X.-M. Liu, K. P. Pramoda, Y.-Y. Yang, S. Y. Chow and C. He, Cholesteryl-grafted functional amphiphilic poly(N-isopropylacrylamide-co-N-hydroxylmethylacrylamide): synthesis, temperature-sensitivity, self-assembly and encapsulation of a hydrophobic agent, Biomaterials, 25 (2004) 2619-2628.

[42] D. Gersappe, Modelling micelle formation in confined geometries, High Performance Polymers, 12 (2000) 573-579.

[43] J.-H. W. He, Yu-Qin; Yu, Jian-Yong Effect of concentration on electrospun polyacrylonitrile (PAN) nanofibers, Fibers and Polymers, 9 (2008) 140-142.

[44] J. Sunthornvarabhas, P. Chatakanonda, K. Piyachomkwan and K. Sriroth, Electrospun polylactic acid and cassava starch fiber by conjugated solvent technique, Materials Letters, 65 (2011) 985-987.

[45] J. M. Deitzel, J. Kleinmeyer, D. Harris and N. C. Beck Tan, The effect of processing variables on the morphology of electrospun nanofibers and textiles, Polymer, 42 (2001) 261-272.

[46] E. D. Boland, K. J. Pawlowski, C. P. Barnes, D. G. Simpson, G. E. Wnek and G. L. Bowlin, Electrospinning of Bioresorbable Polymers for Tissue Engineering Scaffolds, in: Polymeric Nanofibers, American Chemical Society, 2006, pp. 188-204.

[47] A. Vega-Gonzalez, P. Subra-Paternault, F. Nudda and B. Marongiu, Viscosity measurements of various polymer/solvent solutions and their relation with a dimensional numbers involved in the antisolvent techniques, in: Supercritical Fluids: Reactions, Materials and Natural Products Processing, Strasbourg/Colmar, France, 2005.

[48] W. Cui, X. Zhu, Y. Yang, X. Li and Y. Jin, Evaluation of electrospun fibrous scaffolds of poly(dl-lactide) and poly(ethylene glycol) for skin tissue engineering, Materials Science and Engineering: C, 29 (2009) 1869-1876.

[49] M. Spasova, O. Stoilova, N. Manolova, I. Rashkov and G. Altankov, Preparation of PLLA/PEG Nanofibers by Electrospinning and Potential Applications, Journal of Bioactive and Compatible Polymers, 22 (2007) 62-76.

[50] A. Moriya, T. Maruyama, Y. Ohmukai, T. Sotani and H. Matsuyama, Preparation of poly(lactic acid) hollow fiber membranes via phase separation methods, Journal of Membrane Science, 342 (2009) 307-312.

[51] M. Mazandarani, A. Eliassi and M. Fazlollahnejada, Experimental data and correlation of surface tension of binary polymer solutions at different temperatures and atmospheric pressure, in: European Congress of Chemical Engineering, Copenhagen, 2007.

[52] M. E. Rebovich, D. Vynias and M. W. Frey, Formation and functions of high-surface-area fabrics, International Journal of Fashion Design, Technology and Education, 3 (2010) 129 - 134.

[53] D. Li, M. W. Frey and Y. L. Joo, Characterization of nanofibrous membranes with capillary flow porometry, Journal of Membrane Science, 286 (2006) 104-114.

[54] C. Xiang, M. W. Frey, A. G. Taylor and M. Rebovich, Selective chemical absorbance in electrospun nonwovens, Journal of Applied Polymer Science, 106 (2007) 2363-2370.

CHAPTER 3

STIMULI-RESPONSIVE CELLULOSE ACETATE AND POLY(LACTIC ACID) ELECTROSPUN FIBERS INTEGRATED INTO A PROTOTYPE FLUIDIC DEVICE

3.1 ABSTRACT

By incorporating pH-sensitive nanoparticles into electrospun fibers, stimuli-responsive cellulose acetate (CA) and poly(lactic acid) (PLA) fibers were created, and integrated into a prototype fluidic device. CA fibers are relatively hydrophilic, but the hydrophobic PLA fibers required surface modification to improve interactions with aqueous media. Poly(lactic acid) – b – poly(ethylene glycol) (PLA-b-PEG) copolymers with block lengths of 1000-750, 5000-1000 and 1000-5000 were added to PLA electrospinning dopes to create hydrophilic but non-water soluble nanofibers. The morphology of the CA and PLA fibers were consistent with previous studies, but the addition of the PLA-b-PEG block lengths strongly affected the final fiber properties. Changes in the polymer to solvent interactions caused by the addition of PLA-b-PEG copolymers affected final fiber diameter, pore size and pore size distribution. The changes in fiber geometry also affected the relative surface area of the nonwoven fabrics. Samples containing 2.0 wt% PEG showed an increase in fiber diameter and pore size, which was accompanied by a decrease in surface area and water wicking rate. Samples containing 6.3 wt% PEG observed a decrease in fiber diameter and pore size, as well as an increase in surface area and water wicking rate. Variations in surface area and water wicking rate, as well as nanoparticle distribution, influenced the effectiveness of the pH-sensitive electrospun fibers. pH measurements taken with confocal microscopy and image analysis showed that response to pH change improved with increasing surface area and water wicking rate. The stimuli-

responsive fibers were shown to take relatively consistent pH measurements both on glass slides, and within a prototype fluidic device.

3.2 INTRODUCTION

The current trend in analytical devices is for the creation of smaller, simpler, and smarter methods of analysis [1]. For this reason, microfluidic systems have the potential to become a popular platform for laboratory analysis and diagnostics. Microfluidics is an interdisciplinary field that deals with the flow and reaction of small amounts of fluid [2]. The great potential in these devices lies in the ability to integrate a laboratory's worth of instrumentation to produce "lab on a chip" systems [3]. Some practical examples include microfluidic platforms designed to perform rapid diagnostics on saliva, sweat, and water. Currently, a significant amount of research is being devoted to the exploration of various microfluidic systems for biomedical and environmental monitoring [2, 4-19].

One successful way to use microfluidic technology for sensor applications is by integrating stimuli-responsive nanofibers into microfluidic chips [20-24]. Sensor nanoparticles can be incorporated into the nanofibers, and patterned at specific locations and orientations within the microfluidic channels [25-26]. The response of the nanoparticles to the samples (i.e. saliva, sweat, water, blood) flowing through the microfluidic channels can be maximized by engineering the fiber surface properties. For example, studies have shown that engineering the surface hydrophilicity of nanofibers can improve their performance in such applications [27-40].

When using nanofibers to construct a sensor, there are necessary components that must be considered. Both the surface and bulk polymer properties can influence the strength of the sensor signal, so they must be chosen carefully [41-42]. For example, the polymer matrix must

be suitably hydrophilic to allow the aqueous media to wet, and then penetrate, the material. Additionally, the polymer matrix cannot be so water soluble as to dissolve in the presence of any aqueous media. These requirements present an interesting challenge when choosing materials in which to incorporate sensor nanoparticles.

In the present work, cellulose acetate (CA) and poly(lactic acid) (PLA) fibers were studied. CA is a relatively hydrophilic material, so it was expected to be very responsive to pH change in aqueous media [43]. PLA is an easily spinnable, biocompatible, and biodegradable polymer often used in biomedical devices [44]. The surface of PLA is strongly hydrophobic, but in order to improve its biocompatibility, surface modifications can be performed [45]. One successful strategy for increasing surface hydrophilicity of PLA films and particles is to blend it with biocompatible and hydrophilic poly(ethylene glycol) (PEG). Previous work has shown that the wettability of PLA can be improved by the addition of < 10 wt% of PEG [46-48]. Both Ouyang and Otsuka et al. showed that the surface hydrophobicity of PLA films could be decreased through the addition of increasing amounts of PEG. In these studies, pure PLA films had contact angles on the order of 80°, and adding ~10 wt% PEG caused the contact angle of these films to decrease to 68°. In this study, the hydrophilicity of PLA electrospun fibers was modified through the incorporation of several different PEG weight percent concentrations, and three different PLA-b-PEG copolymers. The PLA block of the copolymer should be miscible with the bulk PLA chains during the spinning process, allowing the hydrophilic PEG block to phase separate towards the fiber surface [50]. These diblock copolymers contained three different copolymer chain lengths, and ratios: PLA (1000) – b – PEG (750), PLA (5000) – b – PEG (1000), and PLA (1000) – b – PEG (5000). Previous work showed that the lengths of the blocks influenced the maximum amount of PEG that could be incorporated, as well as

spinnability and morphology [49]. With the shorter chain length copolymer, PLA (1000) – b – PEG (750), micelle formation was found to impede the electrospinning process at concentrations greater than 0.8 wt% copolymer. Adding PLA (5000) – b- PEG (1000) to the spinning dope led to an increase in fiber diameter consistent with increasing the concentration of PLA in the solution. The maximum copolymer loading was achieved using PLA (1000) – b – PEG (5000), which was also accompanied by a decrease in fiber diameter. Water wettability improved significantly with the addition of PEG to the electrospinning dopes, with longer PEG blocks in the PLA-b-PEG copolymers providing a greater increase [46, 51-52]. By incorporating stimuli-responsive nanoparticles into these fibers, and integrating them into a prototype fluidic chip, a functional sensing device can be created.

Several different methods have previously been described for the fabrication of fluidic devices, but soft lithography is one on the most popular [53-56]. Soft lithography is a method that allows for the reproduction of complex microstructures using moldable "soft" materials. This technique is relatively inexpensive, and can quickly produce many structures from a master (Figure 3.1).

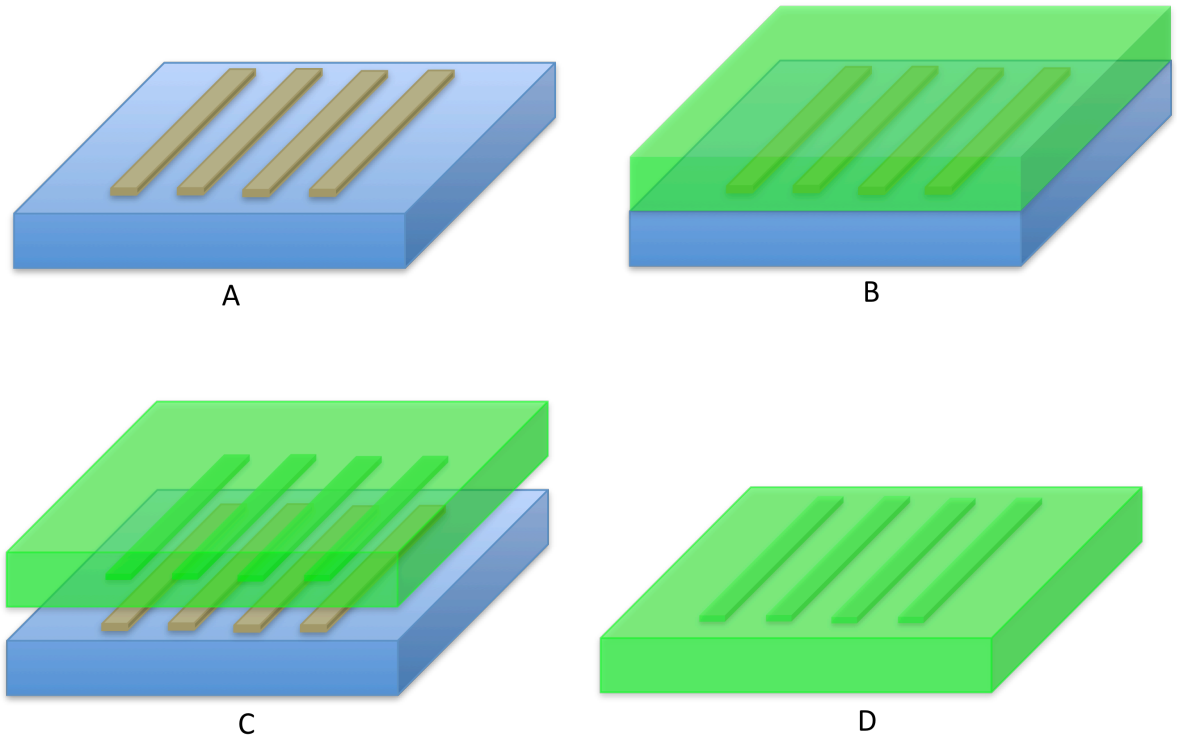

FIGURE 3.1. Schematic for producing gelatin chips using soft lithography A) Master mold is made with desired features B) Gelatin mixture is poured into the mold, and cured C) The solidified chip is peeled off the mold D) Final chip ready for use.

The following study uses a modified version of work done by Yang et al. to fabricate fluidic chips from petri dish molds and gelatin [57]. The simplicity of this method provides a fast and inexpensive method to perform preliminary experiments. The accessibility of the starting materials should provide research groups without immediate access to clean room facilities with a method to perform proof of concept experiments. One of the barriers to further expansion of microfluidic technology into the mainstream is the high cost of chip production [58]. For this reason, many different low-cost, and even DIY methods have been published. Researchers have used wax [53], paper [59], thread [60], 3D printers [61], and even Shrinky Dinks™ [62], to create microfluidic devices. Gelatin is water soluble, easily moldable, and can be made relatively robust and thermally stable in higher concentrations. The gelatin chips can

mold over time, approximately three days while refrigerated, but they provide an incredibly accessible platform for introductory experiments.

In this study, gelatin chips were used to create a prototype pH-sensing fluidic device. This device is composed of pH-sensing nanoparticles electrospun into fibers, and incorporated into channels formed in gelatin. The fluorescence response of the nanoparticles within the nanofibers was measured by changes in florescence intensity, while solutions with varying pH flowed through the channels. These pH-sensing nanoparticles are composed of two different fluorescent dyes; one with intensity response proportional to pH, and the second with constant intensity to serve as an internal standard.

The pH-sensitive nanoparticles used here, C dots, were developed in the Wiesner group in the Materials Science and Engineering department at Cornell University [63]. These nanoparticles are composed of a dye rich core surrounded by a silica shell, which exhibits fluorescent emission when excited by an external light source at a specific wavelength. The 30 nm C dots are 20-30 times brighter than single fluorescent dye molecules, resistant to quenching, and exhibit greater resistance to photo bleaching [64]. These nanoparticles can be dispersed in many different polar solvents, including water and acetone, without degradation. Additionally, the dye encapsulated within the nanoparticles can resist degradation at temperatures up to 150°C, depending on dye structure and heat duration [65-68]. In addition to these structural benefits, the unique core–shell architecture of the C dots is ideal for the development of ratiometric nanoscale fluorescent sensors [69].

The nanoparticles use a tetramethylrhodamine (TRITC) dye core as an internal reference, allowing for quantitative concentration measurements. By placing a fluorescein isothiocyanate (FITC) sensor dye on the surface of the silica shell, the maximum amount of surface area can be exposed to the environment.

FITC was chosen as a pH sensor because, with a pK_a of 6.4, it has excellent pH response in the biologically relevant range from pH 5–8.5 [70]. In aqueous solutions, FITC can exist in cationic, neutral, anionic, and dianionic forms. These molecular structures have different requirements for photon absorption, making the fluorescence properties strongly dependent on pH. The anionic form of FITC has a quantum yield of 36%, while the dianionic form yields 93% (Table 3.1) [71]. This means that the intensity of the FITC dye changes with its molecular state, which can be varied in the presence of aqueous buffer solutions. TRITC was chosen as the internal standard because its quantum yield is unaffected by pH changes in this range [64]. Therefore, by taking a ratio between these two dyes, a ratiometric sensor can be created.

TABLE 3.1. Quantum yields of FITC and TRITC dyes at pH values of 5 and 8.5.

Dye	Quantum Yield at pH 5 (%)	Quantum Yield at pH 8.5 (%)
FITC	36	93
TRITC	35	35

Electrospinning was used to incorporate the C dots into CA and PLA/PLA-b-PEG fibers to ensure that the C dots were well-dispersed in the nonwoven mat [26]. Electrospinning is a unique method for fabricating submicron scale fibers using electrostatic forces. When an electrical force is applied at the interface of a liquid polymer, a charged jet is ejected. The jet initially extends in a straight line, then moves into a whipping motion caused by the electro-hydrodynamic instability at the tip. As the solvent evaporates, the polymer is collected, e.g. onto a grounded piece of aluminum foil as a nonwoven mat [72]. Solution parameters such as concentration, viscosity, surface tension and solution conductivity can all affect nonwoven fiber properties [73].

Previous research has already shown that it is possible to successfully incorporate C dots into fibers by electrospinning [26, 74]. Therefore, the focus of this study was on the creation of unique pH-sensitive CA and PLA/PLA-b-PEG fibers. The response of the pH-sensitive fibers was observed first on glass slides, and then within a prototype fluidic device. By engineering the surface properties of these fibers, we hope to improve their response in aqueous media.

3.3 MATERIALS AND METHODS

3.3.1 Materials

Poly(lactic acid) (M_w = 211,332 g/mol) was supplied by Cargill Dow (Minnetonka, MN). The shorter chain length PLA (1000) – b – PEG (750) copolymer (M_w = 1000 g/mol, 750 g/mol), dimethylformamide (DMF) and cellulose acetate (M_w = 30,000 g/mol) were supplied by Sigma Aldrich (St. Louis, MO). The longer chain length PLA-b-PEG copolymers, PLA (5000) – b – PEG (1000) (M_w = 5000 g/mol, 1000 g/mol) and PLA (1000) – b – PEG (5000) (M_w = 1000 g/mol, 5000 g/mol) were purchased from Advanced Polymer Materials (Montreal, QC). Plastic petri dishes were purchased from VWR Scientific (West Chester, PA). Monobasic sodium phosphate (M_w = 137.99 g/mol), dibasic sodium phosphate (M_w = 141.96 g/mol), and sodium chloride (M_w = 58.44 g/mol) were supplied by Aldrich Chemical Co Ltd (St. Louis, MO). The C dots were made by the Wiesner lab in the Materials Science and Engineering department at Cornell University using previously described techniques [63, 68]. Lemon-flavored Jell-O® powder, unflavored Knox® gelatin, wooden coffee stirrers, transparency sheets, and double sided tape were obtained from local convenience stores.

3.3.2 Mold Fabrication

The prototype fluidic chips were fabricated using a soft lithography technique designed by the Lagally group at the University of British Columbia [75]. Molds with the desired features were made using the bottoms of plastic petri dishes, coffee stirrers, and double-sided tape. To make the chips, two pouches of Jell-O® powder were dissolved in 120 mL of purified water in a beaker. One pouch of Knox® gelatin powder was dissolved in the same amount of water in a second beaker. The beaker containing the Jell-O® solution was placed on a hot plate, and heated to a boil. This beaker was removed from the heat, and the gelatin solution was added to it. The mixture of Jell-O® and gelatin solution was again heated to a boil, and removed from the heat. The gelatin mixture was poured into the molds, and was then transferred to a refrigerator for curing. After curing overnight, the Jell-O® chips were peeled off of the petri dish bottom, and transferred to the petri dish top (Figure 3.2). The molds produced channels with the following dimensions: 50 mm in length, 4.5 mm in width, and 1 mm in depth.

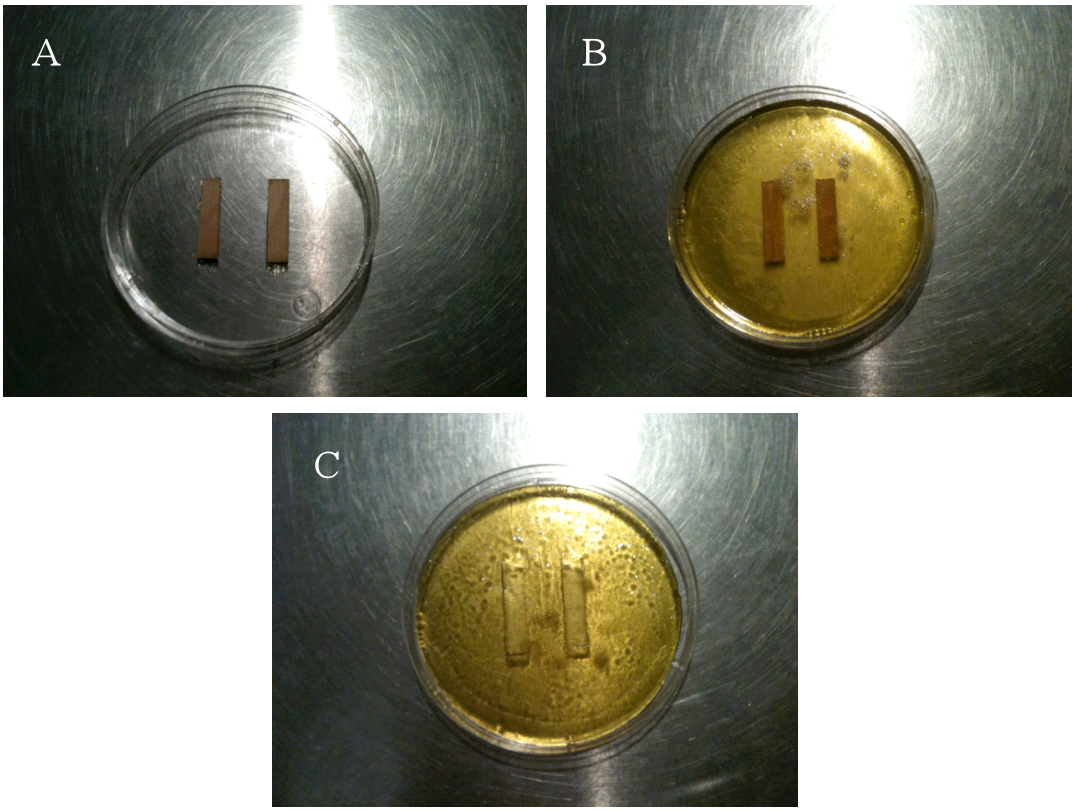

FIGURE 3.2. Schematic for prototype chip fabrication A) Molds with the desired features made using the bottoms of plastic petri dishes, coffee stirrers, and double sided tape B) Gelatin mixture in petri dish mold C) Prototype chip removed from the mold.

3.3.3 Preparation of electrospun solutions

The electrospun fabrics were manufactured using 25 wt% PLA dissolved in DMF at 70ºC, and 17 wt% cellulose acetate dissolved in a 3:1 v/v acetone: water solution. The C dots were suspended in DMF or acetone, respectively, and were added to the solutions in 15 vol%. PLA-b-PEG copolymers of different chain lengths were added to PLA in different concentrations.

3.3.4 Electrospinning

The electrospinning apparatus consisted of a programmable syringe pump (Harvard Apparatus, MA) and a high-voltage supply (Gamma High Voltage Research Inc., FL). For the PLA solutions, electrospinning was carried out at 70ºC with a feed rate of 20 µl/min, and an

applied voltage of 15 kV. For the CA solutions, electrospinning was carried at 0.3 ml/hr with an applied voltage of 14 kV. Table 3.2 details the weight percent concentrations of PLA/PEG within the final fibers. All of the polymer samples were electrospun onto glass slides, and transparency sheets with inlet and outlet holes punctured. The glass slides were imaged under confocal microscopy as formed, but the transparency sheets required integration into the gelatin fluidic devices.

TABLE 3.2. Weight percent polymer in solution, and in the final fibers

Weight percent concentrations of PLA/PLA-b-PEG and C dots in solution	**Total weight percent concentrations of PLA/PEG/DMF/C dots in solution**	**Total weight percent PLA/PEG/C dots in the final fibers**
25 wt% PLA	22.2 / 0 / 65.9 / 11.9	65 / 0 / 35
25 wt% PLA, 0.24 wt% PLA (1000) – b – PEG (750), 15 wt% C dots	22.3 / 0.09 / 65.7 / 11.9	65.0 / 0.3 / 34.7
25 wt% PLA, 0.40 wt% PLA (1000) – b – PEG (750), 15 wt% C dots	22.3 / 0.15 / 65.7 / 11.9	65.0 / 0.4 / 34.6
25 wt% PLA, 0.56 wt% PLA (1000) – b – PEG (750), 15 wt% C dots	22.4 / 0.2 / 65.6 / 11.9	64.9 / 0.6 / 34.5
25 wt% PLA, 0.56 wt% PLA (5000) – b – PEG (1000), 15 wt% C dots	22.5 / 0.1 / 65.6 / 11.9	65.3 / 0.2 / 34.5
25 wt% PLA, 1.6 wt% PLA (5000) – b – PEG (1000), 15 wt% C dots	23.0 / 0.2 / 65.0 / 11.8	65.8 / 0.7 / 33.6
25 wt% PLA, 5.0 wt% PLA (5000) – b – PEG (1000), 15 wt% C dots	24.9 / 0.8 / 62.9 / 11.4	67.3 / 2.0 / 30.7
25 wt% PLA, 0.28 wt% PLA (1000) – b – PEG (5000)	22.2 / 0.2 / 65.7 / 11.9	64.7 / 0.6 / 34.7
25 wt% PLA, 3.0 wt% PLA (1000) – b – PEG (5000), 15 wt% C dots	22.0 / 2.2 / 64.1 / 11.6	61.4 / 6.3 / 32.3

3.3.5 *Prototype Fluidic Chip Assembly*

The transparency sheets were placed (fiber side down) on top of the gelatin chips, and tubing was attached to create pressure driven flow through the channel (Figure 3.3). The edges of the channels were very sharp and uniform, and the excess of sugars in the gelatin helped to facilitate an excellent seal with the transparency sheets. A syringe pump was used to deliver buffer solutions to the fibers within the channels.

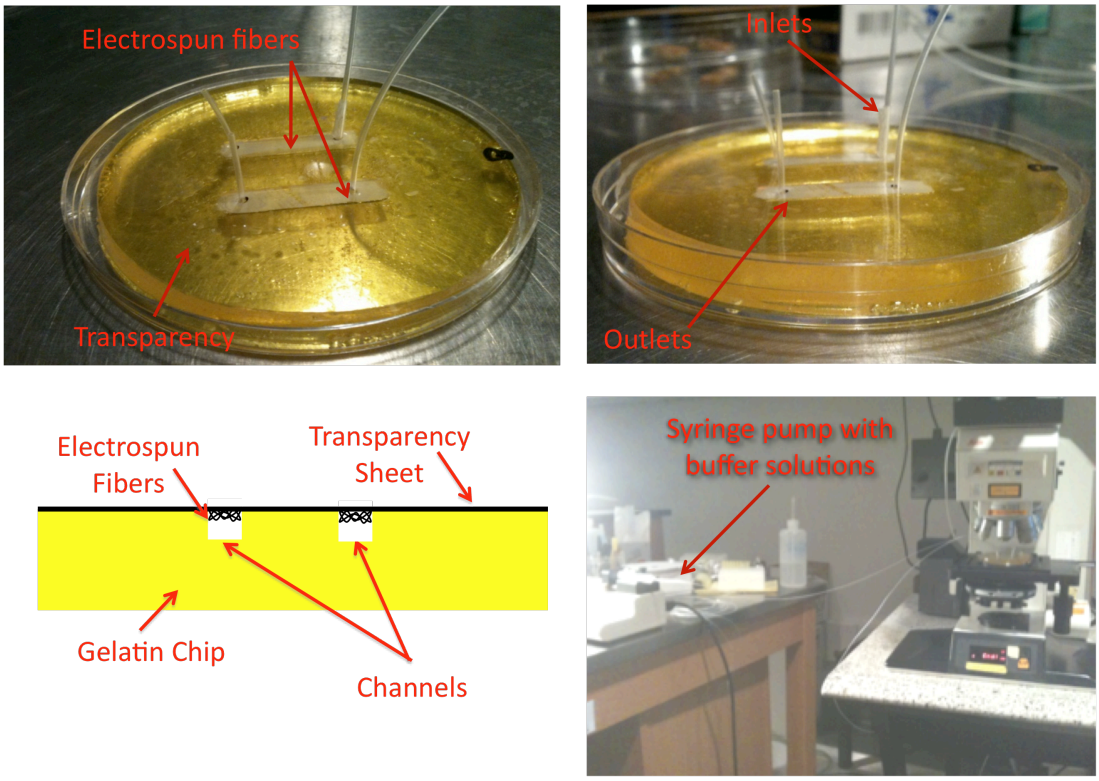

FIGURE 3.3. Experimental setup for nanofiber-incorporated prototype fluidic chips.

3.3.6 *Scanning Electron Microscopy*

Examination of the morphology and fiber diameters of the electrospun mats was performed using a Leica 440 scanning electron microscope (SEM) at 25 kV. Samples were coated for 30 seconds with 10 nm Au–Pd prior to imaging in order to prevent charging. The

average fiber diameter and pore sizes of the nonwoven samples were analyzed from the SEM images using ImageJ software.

3.3.7 Water Wettability and Wicking Rate

Water wettability testing was performed using a KSV Sigma wetting balance. Samples were cut into 3 cm by 0.5 cm rectangles, glued to wire hooks, and allowed to dry. To test, the sample was suspended above a dish of water, and the dish was raised to the sample until contact was made. The sample was weighed every 0.6 seconds for 10 minutes to determine the amount of water absorbed by the nonwoven mat. The wettability profile shows that the amount of water absorbed initially increases linearly with time; the slope of this part of the curve yields the initial wicking rate (Figure 3.4).

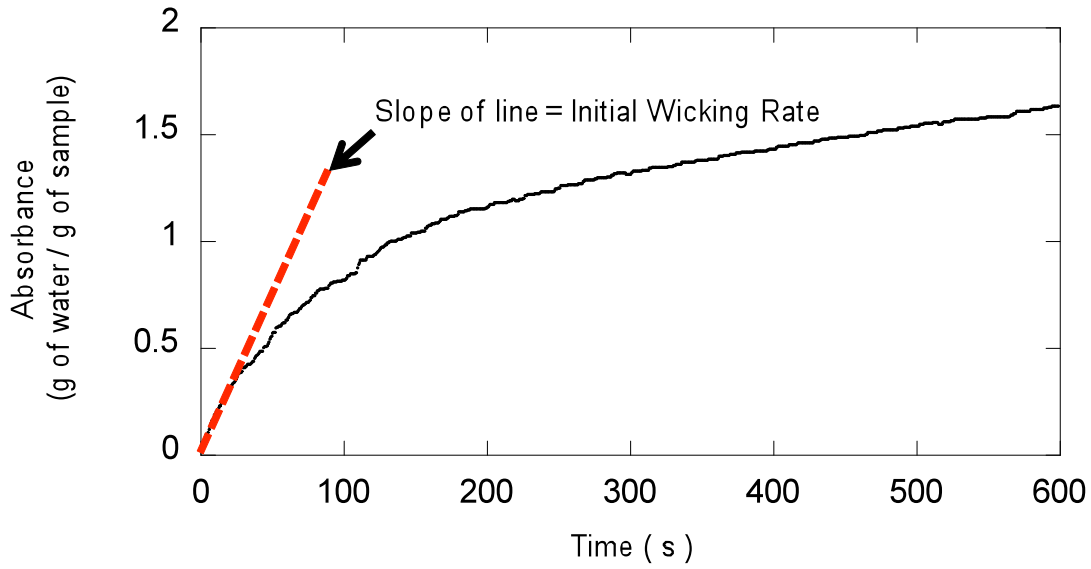

FIGURE 3.4. Calculation of initial wicking rate from wettability profile.

3.3.8 Preparation of Buffer Solutions

Precise pH buffer solutions with pH values ranging from 5 to 8.5 were prepared by mixing 0.15 M monobasic sodium phosphate buffer solution (0.01 M NaH_2PO_4, 0.14 M NaCl), and 0.15 M dibasic sodium phosphate buffer solution (0.01 M Na_2HPO_4, 0.14 M NaCl) in deionized water.

3.3.9 Confocal Microscopy

A Leica TCS SP2 laser confocal scanning microscope was used to examine the fluorescence of the C dots within the fibers. The pH-sensitive electrospun fabrics were imaged at 200 X with both red (460-500 nm) and green (480/40 nm) fluorescence filters. Imaging was performed, and a ratio of the pixel intensity in the green and red filtered images was taken and plotted against pH (Figure 3.5).

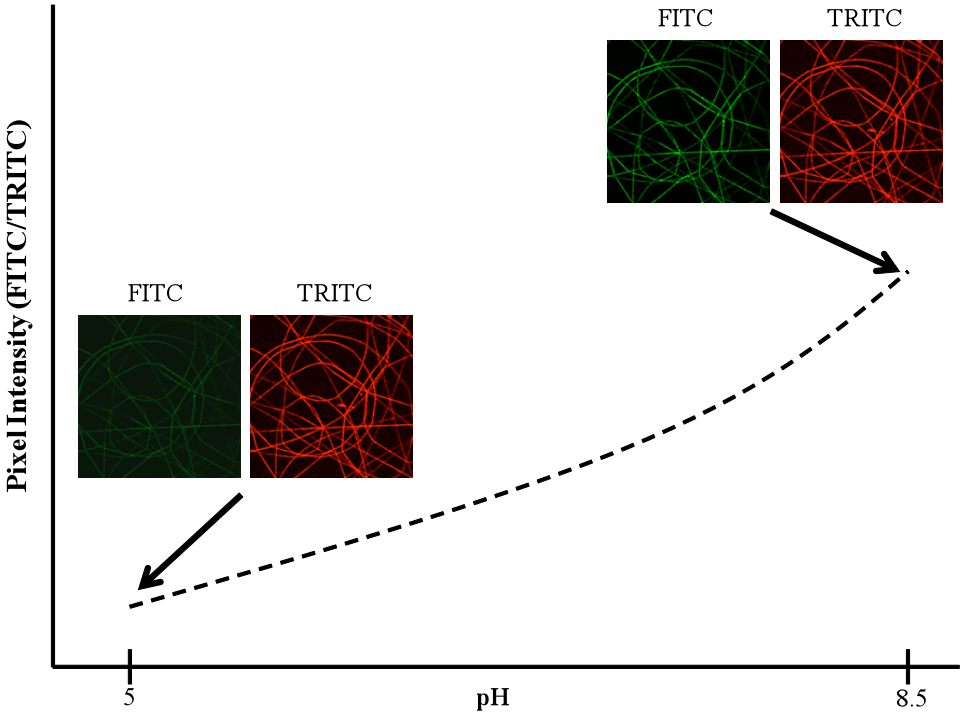

FIGURE 3.5. The relationship between fluorescence intensity and pH for electrospun fabrics containing pH-sensitive core-shell silica nanoparticles.

3.4 RESULTS AND DISCUSSION

3.4.1 SEM Imaging

In order to study fiber morphology, average fiber diameter and pore size distribution, the electrospun samples were imaged using SEM. Figure 3.6 illustrates the average fiber diameters and pore sizes that were measured from the previously compiled images. The average diameters for the CA and PLA samples were consistent with previous results [69, 76]. The changes in the average fiber diameters and pore sizes that were observed in the PLA/PLA-b-PEG fibers were caused by changing polymer to solvent interactions during electrospinning. Increases in the average fiber diameter size was accompanied by an increase in pore size and pore size distribution. Previously reported work by Hendrick et al. discuss these results in great detail [69, 76].

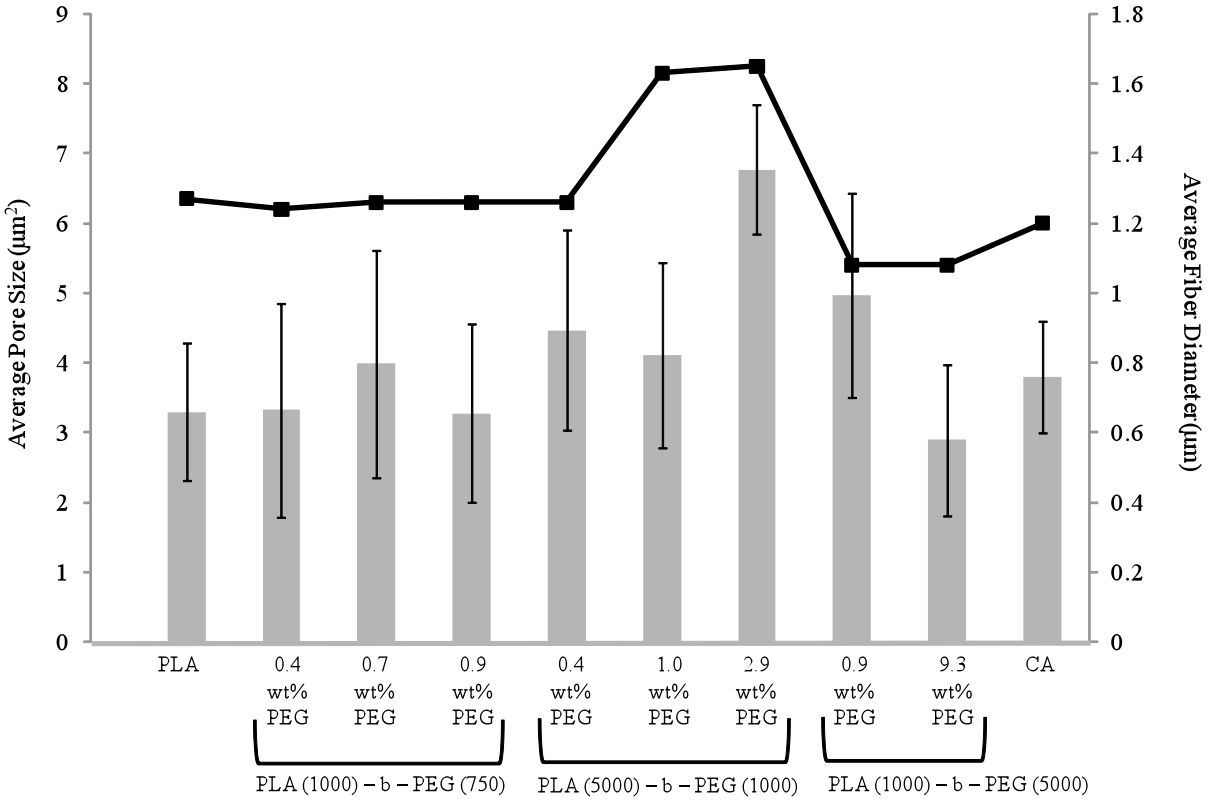

FIGURE 3.6. Average pore size and fiber diameters for electrospun samples.

3.4.2 Water Wettability and Initial Wicking Rate

Increased hydrophilicity of PLA/PEG nonwoven fabrics was assessed by using water wettability testing, and calculating the initial wicking rate. The transport of liquid in a nonwoven fabric is governed by liquid properties, interactions between the liquid and nonwoven, and fiber geometry (i.e. fiber diameter, pore size and distribution). The affinity of the liquid and nonwoven, as well as the spacing between the fibers, influence the transport of liquid in the porous medium [78-80]. The results shown in Table 3.3 describe the initial wicking rates for the electrospun fabrics [76]. These initial wicking rates were governed primarily by PEG content, copolymer chain length, and fiber surface area. Wicking rate increased with PEG content for samples spun with PLA (1000) – b – PEG (750), samples that were shown to have consistent fiber diameter, pore sizes and surface area [76]. The wicking rate for the samples spun with PLA (5000) – b – PEG (1000) were strongly affected by the previously observed increase in fiber diameter, and subsequent decrease in surface area [69]. As surface area decreased, both capillary action and wicking rate decreased. The wicking rate data for the samples spun with PLA (1000) – b – PEG (5000) were influenced by an increase in surface area, as well as a decided increase in PEG loading. Both factors contributed to the increased wicking rate for these samples.

TABLE 3.3. Initial wicking rate data for PLA, CA and PLA/PLA-b-PEG electrospun fabrics.

Sample	PLA – b – PEG Chain Length	Initial Wicking Rate (Water absorbed g / Time s)
PLA	NA	0.003
CA	NA	0.038
0.3 wt% PEG	PLA (1000) – b – PEG (750)	0.008
0.4 wt% PEG	PLA (1000) – b – PEG (750)	0.010
0.6 wt% PEG	PLA (1000) – b – PEG (750)	0.013
0.2 wt% PEG	PLA (5000) – b – PEG (1000)	0.027
0.7 wt% PEG	PLA (5000) – b – PEG (1000)	0.012
2.0 wt% PEG	PLA (5000) – b – PEG (1000)	0.006
0.6 wt% PEG	PLA (1000) – b – PEG (5000)	0.034
6.3 wt% PEG	PLA (1000) – b – PEG (5000)	0.504

3.4.3 Measuring pH Response with Confocal Microscopy

The stimuli response of the modified electrospun fibers was observed using confocal microscopy. Table 3.4 details the calibration curve that was derived for the native C dot sensor particles. Since previous experiments have already shown an improvement in wicking rate with the addition of PLA-b-PEG, it was expected that the pH-sensitivity of the fibers would be similarly improved. The stimuli response of the pH-sensitive CA and PLA/PLA-b-PEG fibers was tested initially on glass slides, followed by select samples within a prototype fluidic device.

TABLE 3.4. Calibration curve showing the relationship between pH and dye intensity for the native C dot sensor nanoparticles.

pH	Intensity (FITC/TRITC)
5	0.45
6	0.47
7	0.60
8	0.70
8.5	0.80

3.4.3.1 Measuring pH-change on glass slides

Representative confocal microscopy images for CA fibers on glass slides can be seen in Figures 3.7. The images illustrate the change in dye intensity within the fibers at a pH of 5 and 8.5. It is clear from these images that the pH-sensitive CA fibers function properly on the glass slides. Additionally, the images show the C dots to be very well dispersed in the fibers, though the fibers themselves are non-uniform. The results of pH-measurements using CA fibers spun onto glass slides has been described in depth in previously reported work by Hendrick et al. [69].

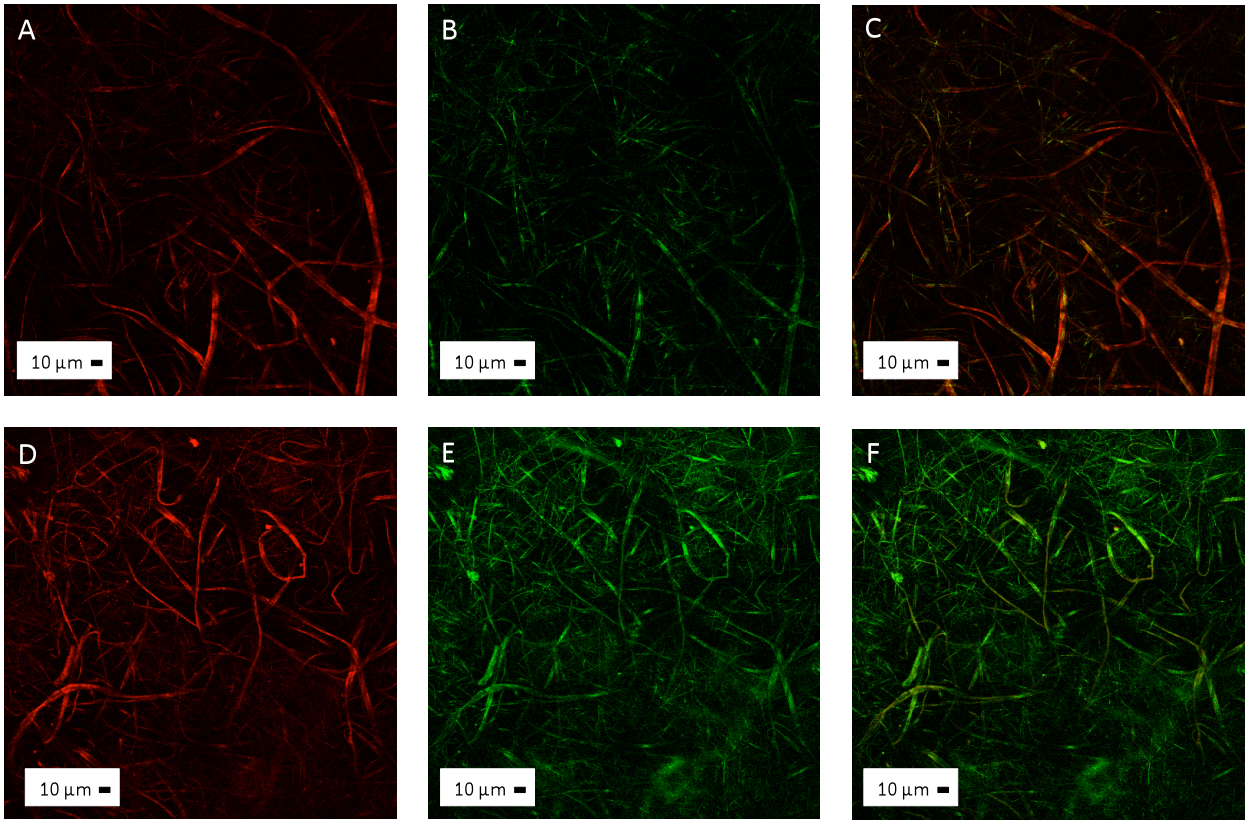

FIGURE 3.7. Confocal microscopy images of CA fibers illustrating A) TRITC at pH 5 B) FITC at pH 5 C) FITC/TRITC overlay at pH 5 D) TRITC at pH 8.5 E) FITC at pH 8.5 F) FITC/TRITC overlay at pH 8.5

The results of the experiments for fibers spun with PLA and PLA (1000) – b – PEG (750) can be seen in Figure 3.8. The results show that even though the C dots were well dispersed within the hydrophobic fibers, PLA was not sensitive to pH change (Figure 3.9). In contrast to the wicking rate data, the samples electrospun with 0.3, 0.4, and 0.6 wt% PEG could not be differentiated from the PLA sample. The results of these experiments were very uniform, but the addition of PLA (1000) – b – PEG (750) did not improve the response of the nanoparticle-containing fibers.

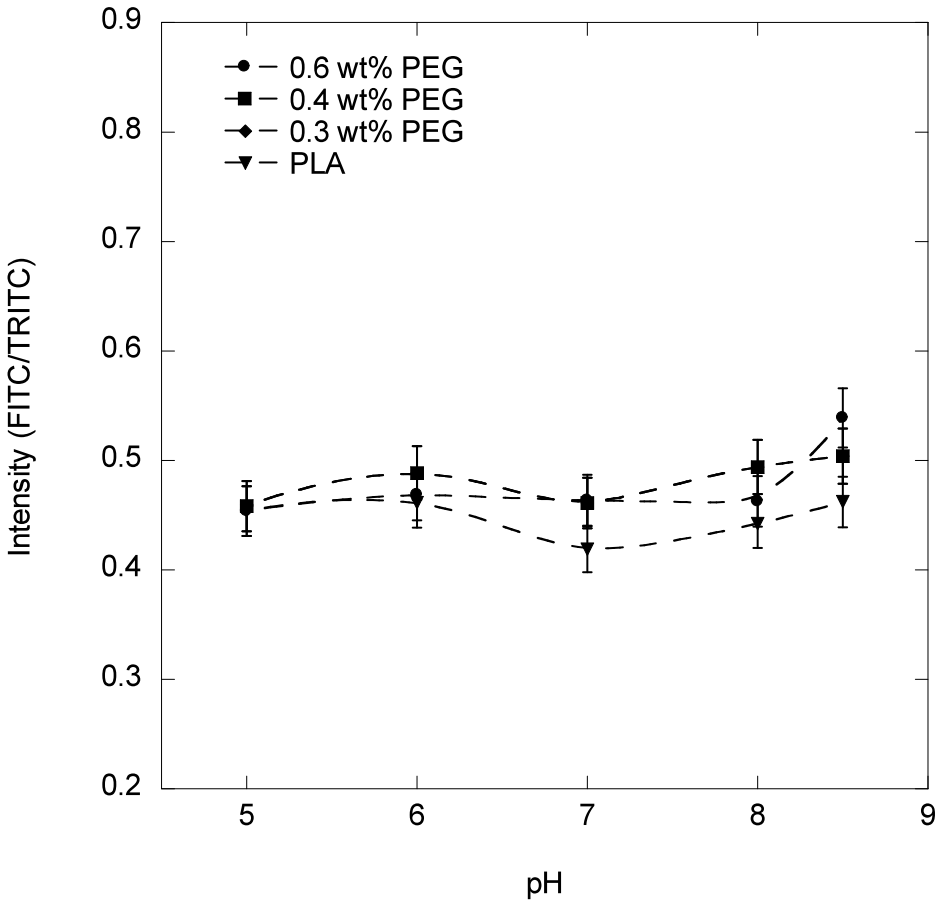

FIGURE 3.8. Confocal data for PLA and PLA / PLA (1000) – b – PEG (750) samples over ten trials.

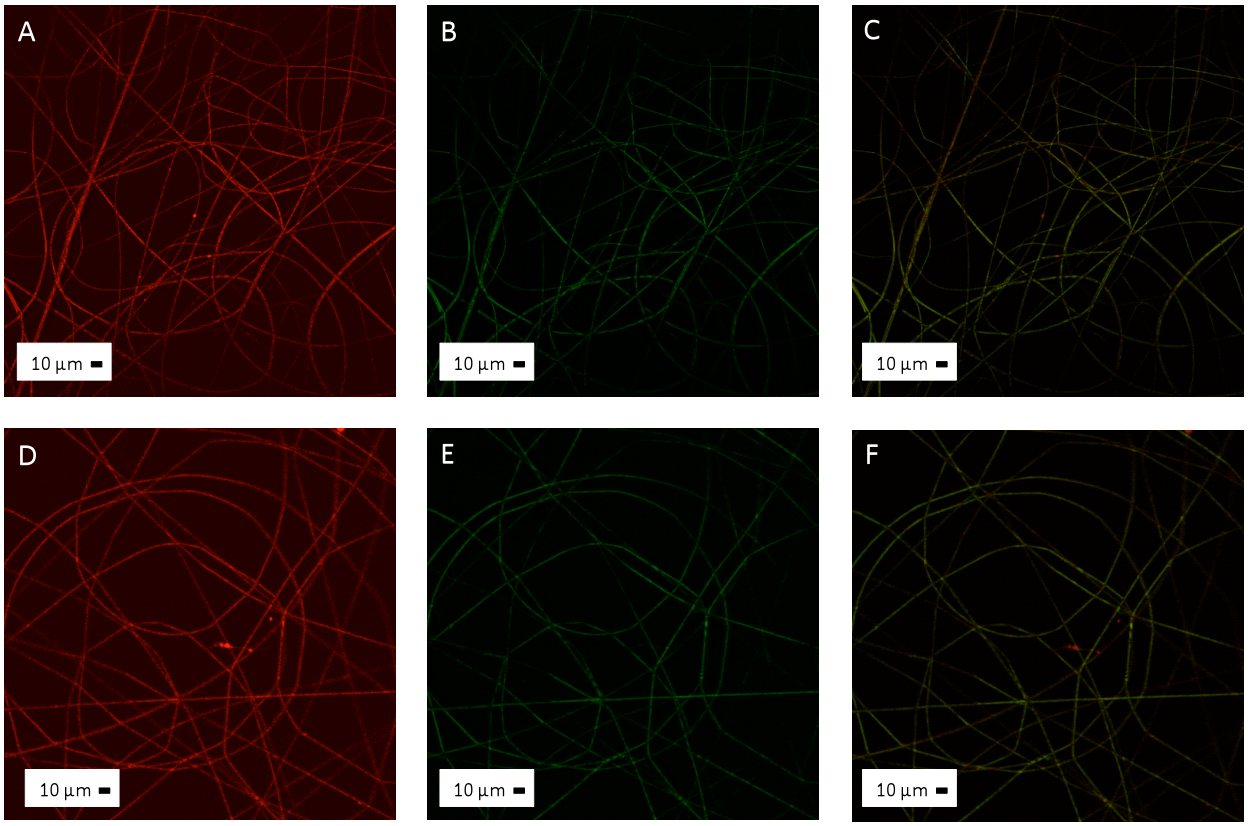

FIGURE 3.9. Confocal microscopy images of PLA fibers illustrating A) TRITC at pH 5 B) FITC at pH 5 C) FITC/TRITC overlay at pH 5 D)TRITC at pH 8.5 E) FITC at pH 8.5 F) FITC/TRITC overlay at pH 8.5.

The results of the pH measurement experiments using fibers spun with PLA (5000) – b – PEG (1000) can be seen in Figure 3.10. Fibers spun with the 0.2 wt% PEG showed an improvement in pH-sensitivity over the PLA fibers. The fibers spun with 0.7 and 2.0 wt% PEG contain higher contents of PEG than the 0.2 wt% PEG sample, yet they are less responsive to the pH change. These results were strongly related to the changes in fiber diameter and pore size caused by differences in the polymer/solvent interactions during electrospinning. The results are logical given that previous studies have shown that fiber diameter can affect the response of the pH-sensitive fibers [76]. Due to surface area effects, smaller fibers are more sensitive to the pH change than larger fibers.

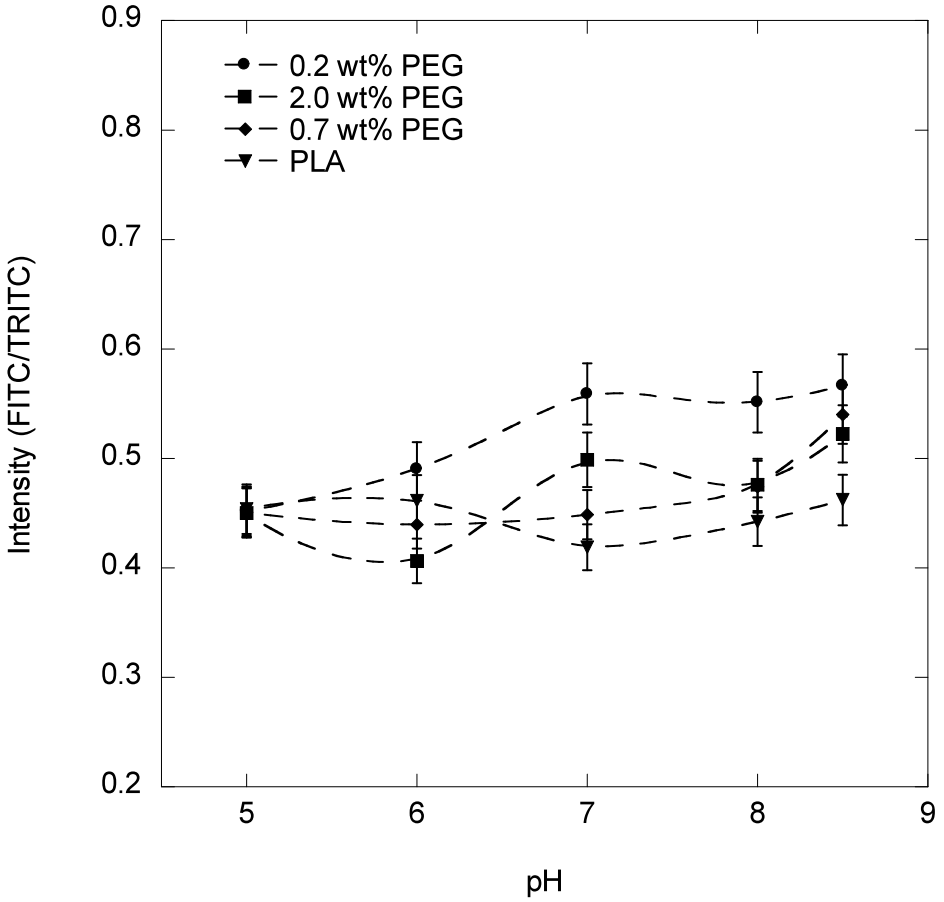

FIGURE 3.10. Confocal data for PLA and PLA / PLA (5000) – b – PEG (1000) samples over ten trials.

The results of the pH measurement experiments for fibers spun with PLA (1000) – b – PEG (5000) can be seen in Figure 3.11. Nonwoven fabrics spun with the 0.6 and 6.3 wt% PEG illustrate an improvement in pH response over PLA. Representative confocal microscopy images for fibers spun with 6.3 wt% PEG can be seen in Figure 3.12. The images show the C dots to be well dispersed within the fibers, and a significant increase in FITC dye intensity with pH. The pH response of these nonwoven samples are influenced by an increase in PEG loading, as well as the previously discussed increase in surface area caused by changes in the viscosity of the spinning solution [49].

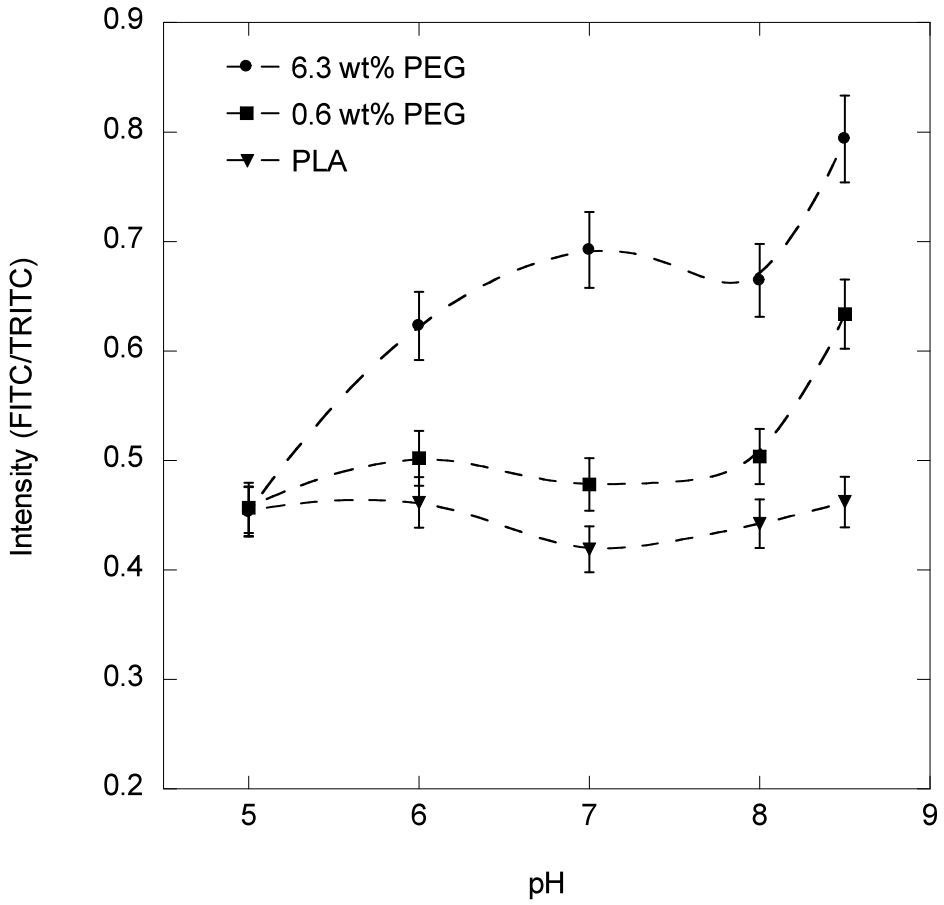

FIGURE 3.11. Confocal data for PLA and PLA / PLA (1000) – b – PEG (5000) samples over ten trials.

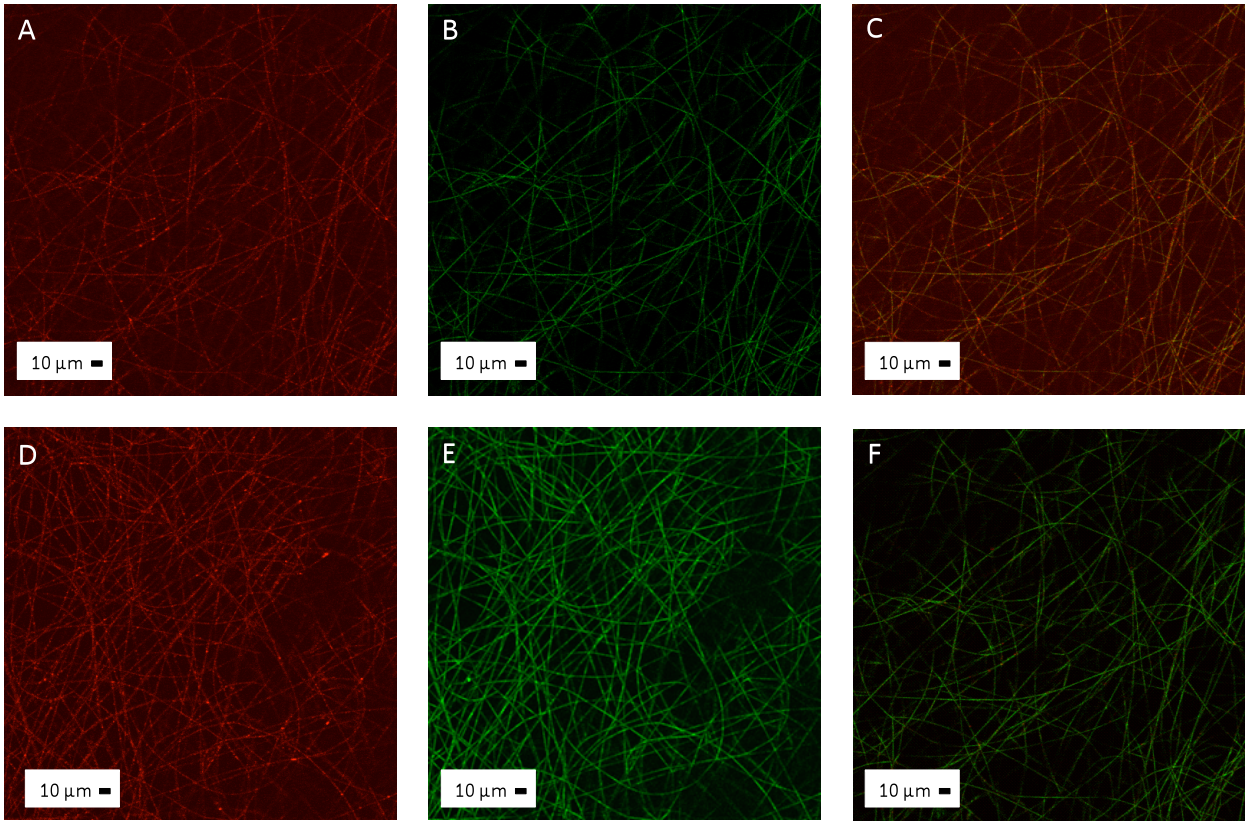

FIGURE 3.12. Confocal microscopy images of 6.3 wt% PEG fibers illustrating A) TRITC at pH 5 B) FITC at pH 8.5 C) TRITC at pH 5 D) FITC at pH 8.5.

The results of the pH measurement experiments for the PLA/PLA-b-PEG electrospun fibers on glass slides followed the same trend as the wicking rate data that was previously compiled. Improvements in wicking rate were accompanied by an improvement in response to pH change. However, even though the general trends were the same, the scale was not. The improvement in response to pH change was not as strong as the improvement in wicking rate. The results of the pH measurement experiments showed that the majority of the samples had a lower response to pH change than the native C dot sensor nanoparticles. Hendrick et al. previously discussed that the results of the wicking rate experiments were a function of copolymer chain length, PEG content, and fiber geometry [49]. Therefore, it was necessary to identify the factors that influence the results of the pH measurement experiments.

The pH measurements were taken by imaging the nonwoven samples with pH buffer solutions, and then taking an average of the FITC/TRITC pixel values. This measurement method gives a general view of the FITC/TRITC pixel values for the image, but it can also have the effect of obscuring some of the brighter pixels in the image. For example, let us consider the raw FITC/TRITC pixel values for the PLA/PLA-b-PEG samples imaged at pH 8.5. The simplest way to look at the data once it is generated is to bin it, and then create a histogram such that it is possible to observe the number of pixels found at each FITC/TRITC pixel value. The calibration curve in Table 3.4 showed that a FITC/TRITC pixel value of 0.8 corresponds to a pH of 8.5. From the histogram data, we can determine the percentage of pixel values at 0.8 (Table 3.5). The results show that a relatively small number of pixels match the values detailed in the calibration curve.

Previous discussion showed that the wicking rate of the nonwoven samples was influenced by a variety of factors. Therefore, it was necessary to determine any trends between copolymer chain length/PEG content, wicking rate, and the percentage of pixels that correspond to a pH of 8.5. Interestingly enough, the percentage of pixels that correspond to a pH of 8.5 had the same general trend as the wicking rate results. Within the copolymer chain lengths, the percentage of matching pixels increased with PEG content, and also varied with fiber geometry (Table 3.5).

TABLE 3.5. Histogram data for PLA/PLA-b-PEG electrospun fibers at pH 8.5.

Sample	% of pixels at pH 8.5
PLA	0.06
0.3 wt% PEG	0.06
0.4 wt% PEG	0.16
0.6 wt% PEG	0.29
0.2 wt% PEG	0.87
0.7 wt% PEG	0.93
2.0 wt% PEG	0.44
0.6 wt% PEG	1.30
6.3 wt% PEG	3.82

The histogram data in Table 3.5 showed that a significant number of pixels corresponded to pH values that were not 8.5. Therefore, the next step was to observe the exact location of these pixels to determine any trends. To accomplish this, single fibers were identified by blowing up the image so that individual pixels could be identified and mapped. The images in Figures 3.13 and 3.14 illustrate examples of this technique using select PLA and 6.3 wt% PEG fiber samples.

The color mapped images show small groupings of pixels that reflect a pH of 8.5. Corresponding to the data in Table 3.6, more pixels corresponding to pH 8.5 can be seen in the color map for the 6.3 wt% PEG fibers than PLA. Once again, both lower and higher intensity pixel values can be seen throughout the fibers. The majority of the higher intensity pixels can be observed towards the center of the fibers, while the lower intensity points are generally closer to the fiber edges. This begs the question, what is the driving force influencing the change in dye intensity within the fibers? It is possible for the dye intensity to be more strongly affected by the location of the nanoparticles within the fibers, meaning that the buffer solution would only be making contact with the nanoparticles on the surface of the fiber. It is also possible that the buffer solution diffuses into the fiber, making contact with nanoparticles at

different points within the fiber. In order to answer this question, it was necessary to consider both SEM and confocal microscopy images.

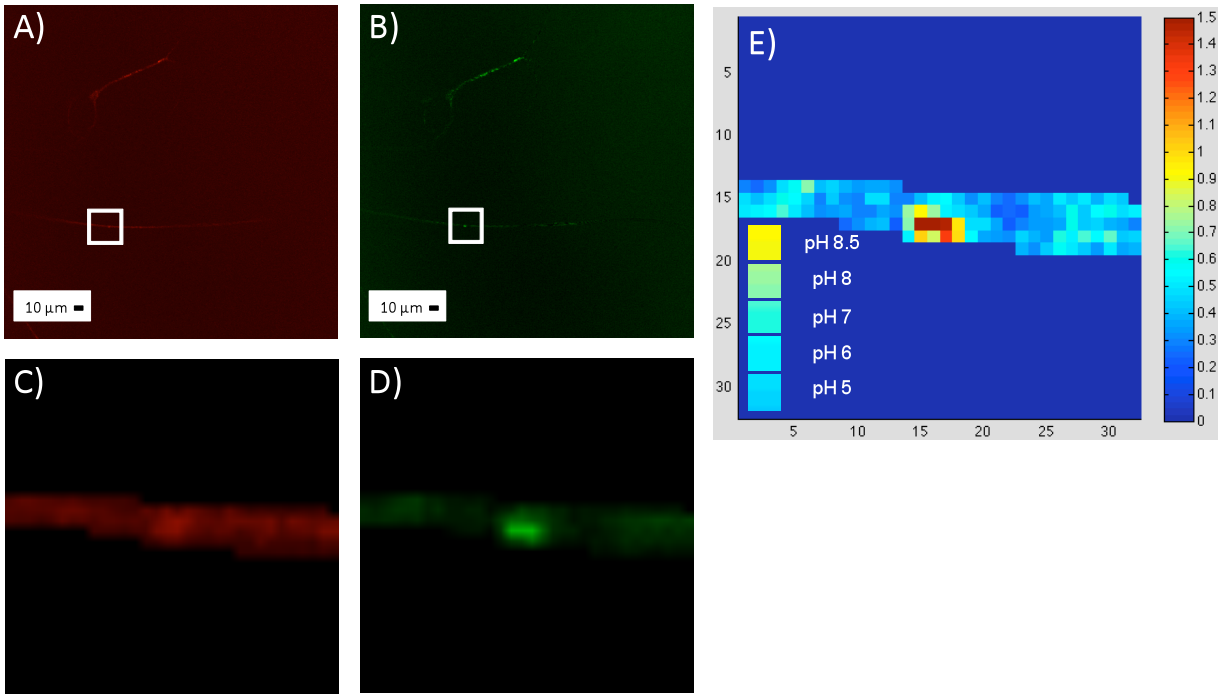

FIGURE 3.13. Images of PLA electrospun fibers illustrating A) TRITC at pH 8.5 B) FITC at pH 8.5 C) Blown-up TRITC at pH 8.5 D) Blown-up FITC at pH 8.5 E) Color mapping of the FITC/TRITC ratio.

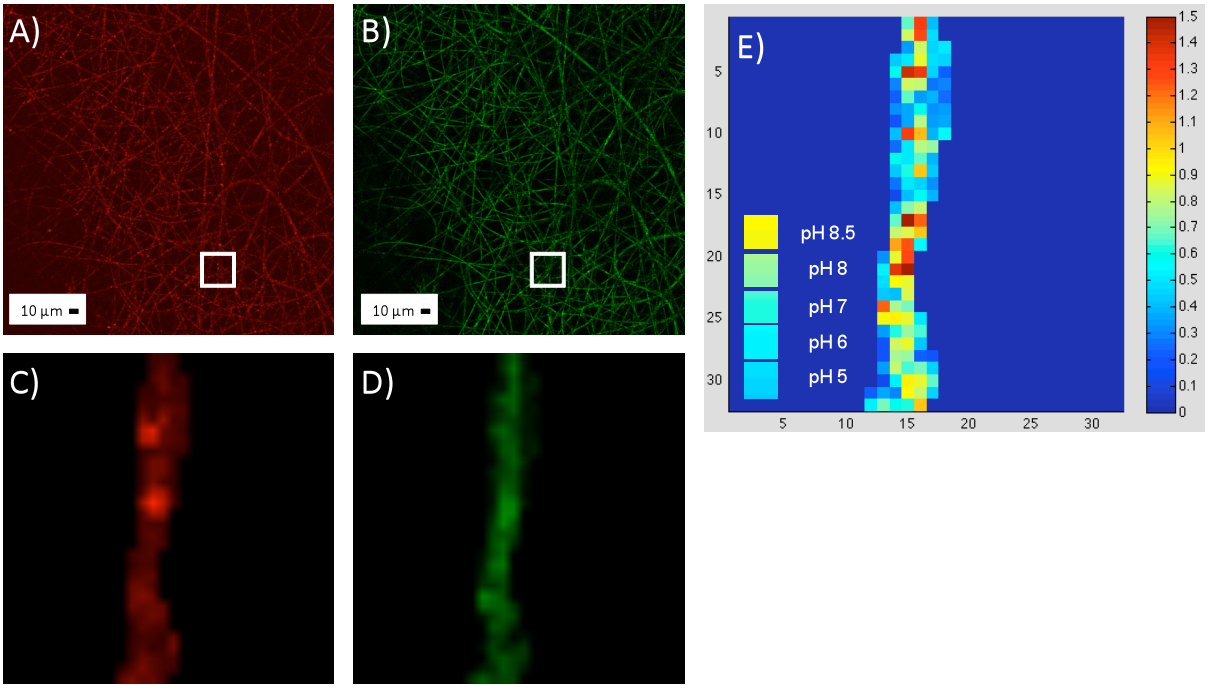

FIGURE 3.14. Images of 6.3 wt% PEG electrospun fibers illustrating A) TRITC at pH 8.5 B) FITC at pH 8.5 C) Blown-up TRITC at pH 8.5 D) Blown-up FITC at pH 8.5 E) Color mapping of the FITC/TRITC ratio.

The confocal microscopy images shown in this study indicate that while there are some nanoparticle agglomerates within the fibers, the nanoparticles are generally well dispersed. The SEM image in Figure 3.15 shows that the fibers are smooth and without visible surface nanoparticles even though 35 wt% of the nonwoven sample contains nanoparticles. If a majority of the nanoparticles were present on the fiber surface, 6% of the FITC/TRITC pixel values would be expected to correspond with pH 8.5. However, the color mapped images show small sections within the fibers that corresponded to pH 8.5, though not spread uniformly across the fiber. By combining this information with the confocal and SEM observations, we can surmise that the buffer solution does not diffuse into the fibers.

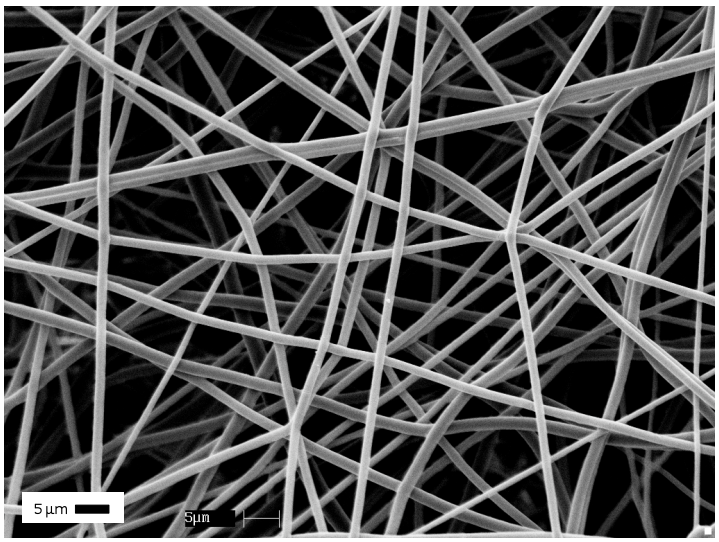

FIGURE 3.15. C dot containing PLA electrospun fibers.

Next, the numerous pixels that correspond to pH values other than 8.5 needed to be addressed. The pixel values that correspond to lower pH values are most likely caused by a lack of nanoparticles close enough to the fiber surface to interact with the buffer solution. The polymers themselves are not pH-sensitive, so the pixels likely represent the natural pH of the polymer. As to the pixel values that correspond to higher pH values, this result is likely related to the additive property of the measurement technique, as well as to small excesses of solvent that can remain within the fiber. The blown-up confocal microscopy images in Figures 3.13 and 3.14 indicate that each pixel represents approximately 200 nm. The C dots used here were approximately 30 nm, so it is possible that seven nanoparticles could be represented in each pixel. This is especially likely for the pixels in the centers of the fibers given that the relatively uniform dispersion of the nanoparticles has already been demonstrated. The analysis method used in this study took a ratio of FITC/TRITC for each pixel, so it is likely that some pixels contain sums of the dye intensity for several different nanoparticles. This would have the effect of producing FITC/TRITC pixel values that are higher than the calibration curve. Additionally,

DMF has a natural pH of 9, so it is also possible that trace amounts of the solvent remain inside the fiber, where it can make contact with the nanoparticles [81].

3.4.3.2 Measuring pH-change in prototype fluidic devices

Representative confocal microscopy images and pH measurements for the select fiber samples integrated into prototype fluidic devices can be seen in Figures 3.16 and 3.17. In general, using the prototype device provided a more controlled method of monitoring pH change in the electrospun fibers. The prototype device provided a more open system than on the glass slides, allowing for improved contact between the buffer solutions and fibers. As opposed to the studies on glass slides, only one set of fibers was imaged for each pH, and three trials were performed for each fiber sample. Unfortunately, the transparency sheets used here did not have the optical clarity of glass coverslips, so viewing very small changes in pixel intensity was a challenge. Given that this is a prototype device, issues with optical clarity should be resolved through use of more traditional coverslips in the finished apparatus.

With the exception of the CA samples, the fiber response was consistent with the results that were previously observed on the glass slides. For the CA samples, the "fluffiness" of the fibers made it very difficult to properly image the pH change. The fibers did not spin flat against the transparency sheets, so maintaining proper focus on the fibers while flushing buffer solutions through was problematic. For the PLA/PLA-b-PEG samples, the average fiber response and standard deviations were consistent with the results that were previously observed on the glass slides. What is most interesting about these results is that virtually the same measurements were taken in three trials using the gelatin channels as were compiled in ten trials on glass slides. This result can be attributed to the fact that only one fiber set was viewed for each pH, and that a larger amount of pH buffer solution remained in the presence of the nonwoven samples throughout imaging. The results showed that using an open system (i.e.

prototype fluidic device) provided a functional and reproducible system for measuring the pH change in the electrospun fibers.

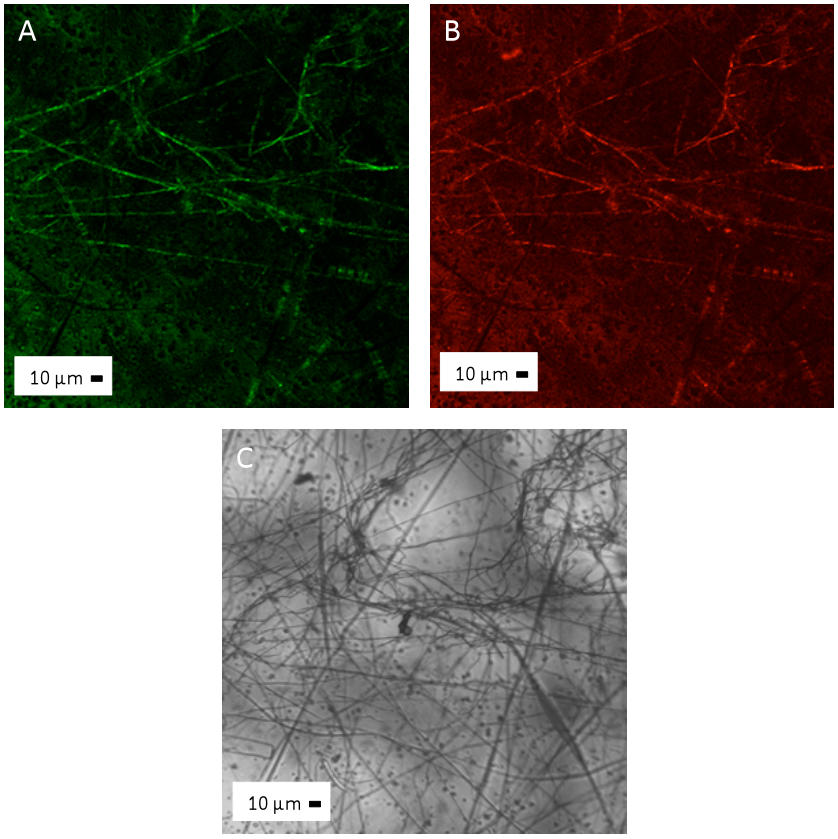

FIGURE 3.16. Confocal microscopy images of 0.2 wt% PEG fibers from PLA (5000) – b – PEG (1000) within a prototype fluidic device. A) Red channel B) Green channel C) Visible light.

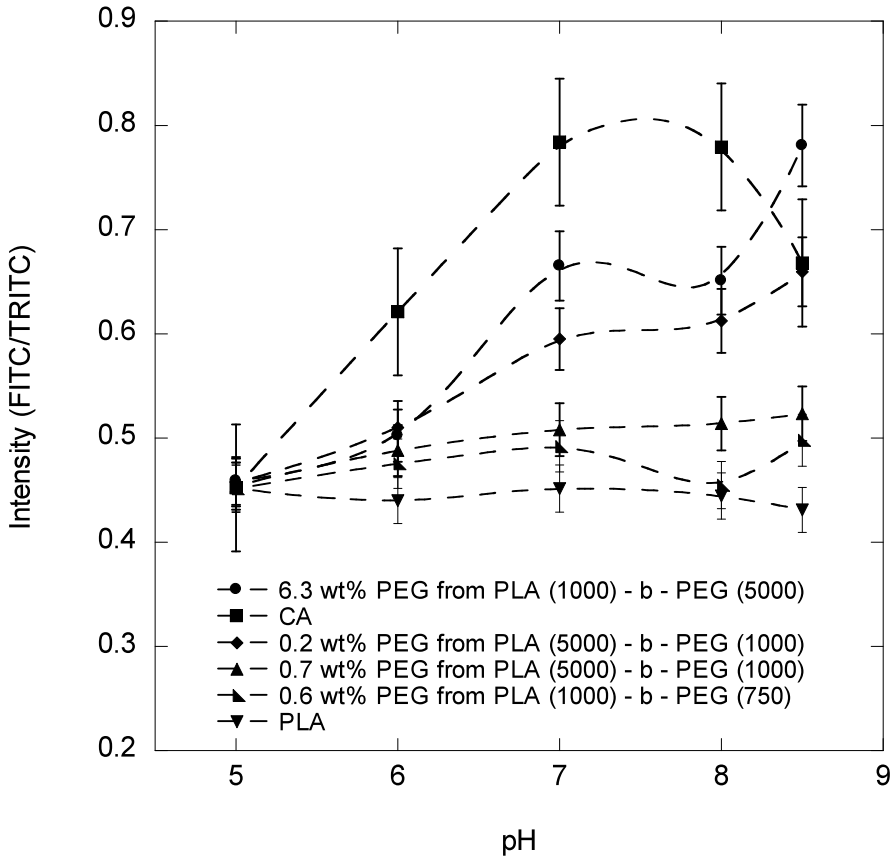

FIGURE 3.17. Confocal microscopy data for electrospun samples in prototype fluidic chips over three trials.

3.5 CONCLUSIONS

A pH-sensing device was created by incorporating pH-sensitive nanoparticles into electrospun fibers, and integrating them into a prototype fluidic device. In order to improve response in aqueous media, the hydrophilicity of PLA electrospun fibers was modified through the incorporation of PLA-b-PEG copolymers of different block lengths. The lengths of the blocks were found to influence the morphology of the fibers due to changes in the polymer to solvent interactions during spinning. Final fiber diameter, pore size and pore size distribution were influenced by changes in solution concentration and viscosity. Samples that underwent a change in fiber geometry also underwent a change in surface area, which affected water

wicking rate. The response of the pH-sensitive fibers on glass slides and within a prototype fluidic device was monitored using confocal microscopy. The response of the fibers was consistent with the increases in surface area and wicking rate, and proved to be a functional method for measuring pH change.

3.6 REFERENCES

[1] T. H. Schulte, R. L. Bardell and B. H. Weigl, Microfluidic technologies in clinical diagnostics, Clinica Chimica Acta, 321 (2002) 1-10.

[2] G. M. Whitesides, The origins and the future of microfluidics, Nature, 442 (2006) 368-373.

[3] J. Nilsson, M. Evander, B. Hammarström and T. Laurell, Review of cell and particle trapping in microfluidic systems, Analytica Chimica Acta, 649 (2009) 141-157.

[4] M. L. Chabinyc, D. T. Chiu, J. C. McDonald, A. Stroock, D.; , J. F. Christian, A. M. Karger and G. M. Whitesides, An integrated fluorescence detection system in poly(dimethylsiloxane) for microfluidic applications, Analytical Chemistry, 73 (2001) 4491-4498.

[5] C.-F. Lin, G.-B. Lee, C.-H. Wang, H.-H. Lee, W.-Y. Liao and T.-C. Choub, Microfluidic pH-sensing chips integrated with pneumatic fluid-control devices, Biosensors and Bioelectronics, 21 (2006) 1468–1475.

[6] J. Hubner, K. B. Mogensen, A. M. Jorgensen, P. Friis, P. Telleman and J. P. Kutter, Integrated optical measurement system for fluorescence spectroscopy in microfluidic channels, Review of Scientific Instruments, 72 (2001) 229-233.

[7] T. Park, S. Lee, G. H. Seoung, J. Choo, E. K. Lee, Y. Kim and W. H. Ji, Highly sensitive signal detection of duplex dye-labelled DNA oligonucleotides in a PDMS microfluidic chip: confocal surface-enhanced Raman spectroscopic study, The Royal Society of Chemistry, 5 (2005) 437–442.

[8] J. G. E. Gardeniers and A. Van den Berg, Lab-on-a-chip systems for biomedical and environmental monitoring, Analytical and Bioanalytical Chemistry, 378 (2004) 1700-1703.

[9] W. Vonau, F. Gerlach and S. Herrmann, Conception of a new technique in cell cultivation using a lab-on-chip aided miniaturised device with calibratable electrochemical sensors, Microchimica Acta, 0026-3672 (2010).

[10] D. Mark, S. Haeberle, G. Roth, F. Von Stettenzab and R. Zengerlez, Microfluidic lab-on-a-chip platforms: requirements, characteristics and applications, Chemical Society Reviews, 39 (2010) 1153–1182.

[11] A. Lymberis, Micro-nano-biosystems: An overview of European research, Minimally Invasive Therapy, 19 (2010) 136–143.

[12] P. Yager, T. Edwards, E. Fu, K. Helton, K. Nelson, M. R. Tam and B. H. Weigl, Microfluidic diagnostic technologies for global public health, Nature, 442 (2006) 412-418.

[13] A. E. Herr, A. V. Hatch, D. J. Throckmorton, H. M. Tran, J. S. Brennan, W. V. Giannobile and A. K. Singh, Microfluidic immunoassays as rapid saliva-based clinical diagnostics, in, 2007, pp. 5268-5273.

[14] J. M. Klostranec, Q. Xiang, G. A. Farcas, J. A. Lee, A. Rhee, E. I. Lafferty, S. D. Perrault, K. C. Kain and W. C. W. Chan, Convergence of Quantum Dot Barcodes with Microfluidics and Signal Processing for Multiplexed High-Throughput Infectious Disease Diagnostics, Nano Letters, 7 (2007) 2812-2818.

[15] Y. Huang, E. Mather, J. Bell and M. Madou, MEMS-based sample preparation for molecular diagnostics, Analytical and Bioanalytical Chemistry, 372 (2002) 49-65.

[16] A. Bhattacharyya and C. M. Klapperich, Thermoplastic Microfluidic Device for On-Chip Purification of Nucleic Acids for Disposable Diagnostics, Analytical Chemistry, 78 (2005) 788-792.

[17] V. Srinivasan, V. K. Pamula and R. B. Fair, An integrated digital microfluidic lab-on-a-chip for clinical diagnostics on human physiological fluid, The Royal Society of Chemistry, 4 (2004) 310-315.

[18] J. Khandurina and A. Guttman, Bioanalysis in microfluidic devices, Journal of Chromatography A, 943 (2002) 159-183.

[19] Z. Du, N. Colls, K. H. Cheng, M. W. Vaughn and L. Gollahon, Microfluidic-based diagnostics for cervical cancer cells, Biosensors and Bioelectronics, 21 (2006) 1991-1995.

[20] D. Yang, X. Niu, Y. Liu, Y. Wang, X. Gu, L. Song, R. Zhao, L. Ma, Y. Shao and X. Jiang, Electrospun Nanofibrous Membranes: A Novel Solid Substrate for Microfluidic Immunoassays for HIV, Advanced Materials, 20 (2008) 4770-4775.

[21] D. Cho, L. Matlock-Colangelo, C. Xiang, P. Asiello, A. Baeumner and M. Frey, Electrospun nanofibers formicrofluidic analytical systems, Polymer, TBA (2011).

[22] K. Sadlej, E. Wajnryb, M. L. Ekiel-Jezewska, D. Lamparska and T. A. Kowalewski, Dynamics of nanofibres conveyed by low Reynolds number flow in a microchannel, International Journal of Heat and Fluid Flow, 31 (2010) 996-1004.

[23] K. Lee, D. Kim, B. Min and S. Lee, Polymeric nanofiber web-based artificial renal microfluidic chip, Biomedical Microdevices, 9 (2007) 435-442.

[24] K. Lee, G. Kwon, S. Shin, J. Baek, D. Han, Y. Park and S. Lee, Hydrophilic electrospun polyurethane nanofiber matrices for hMSC culture in a microfluidic cell chip, Journal of Biomedical Materials Research, 90 (2009) 619-628.

[25] S. Pagliara, A. Camposeo, A. Polini, R. Cingolani and D. Pisignano, Electrospun light-emitting nanofibers as excitation source in microfluidic devices, Lab on a Chip, 9 (2009) 2851-2856.

[26] E. Hendrick, M. Frey, E. Herz and U. Wiesner, Cellulose acetate fibers with fluorescing nanoparticles for anti-counterfeiting and pH-sensing applications, Journal of Engineered Fibers and Fabrics, 5 (2010) 21-30.

[27] E. Balaur, J. M. Macak, L. Taveira and P. Schmuki, Tailoring the wettability of TiO2 nanotube layers, Electrochemistry Communications, 7 (2005) 1066–1070.
[28] T. Sun, L. Feng, X. Gao and L. Jiang, Bioinspired Surfaces with Special Wettability, Accounts of Chemical Research, 38 (2005) 644-652.

[29] T. Zhang, D. Hu, J. Jin, S. Yang, G. Li and J. Jiang, Improvement of surface wettability and interfacial adhesion ability of poly(p-phenylene benzobisoxazole) (PBO) fiber by incorporation of 2,5-dihydroxyterephthalic acid (DHTA), European Polymer Journal, 45 (2009) 302-307.

[30] N. Encinas, M. Pantoja, J. Abenojar, Mart and M. A. nez, Control of Wettability of Polymers by Surface Roughness Modification, Journal of Adhesion Science and Technology, 24 (2010) 1869-1883.

[31] K. S. Teh and Y. W. Lu, Surface nanostructuring of biocompatible polymer for wettability control in MEMS, in: Micro Electro Mechanical Systems, 2008. MEMS 2008. IEEE 21st International Conference on, 2008, pp. 363-366.

[32] W. Lee, M.-K. Jin, W.-C. Yoo and J.-K. Lee, Nanostructuring of a Polymeric Substrate with Well-Defined Nanometer-Scale Topography and Tailored Surface Wettability, Langmuir, 20 (2004) 7665-7669.

[33] T. P. Russell, Surface-Responsive Materials, Science, 297 (2002) 964-967.

[34] D. Hegemann, M. M. Hossain and D. J. Balazs, Nanostructured plasma coatings to obtain multifunctional textile surfaces, Progress in Organic Coatings, 58 (2007) 237-240.

[35] V. Sorna Gowri, L. Almeida, M. de Amorim, N. Pacheco, A. Souto, M. Esteves and S. Sanghi, Functional finishing of polyamide fabrics using ZnO–PMMA nanocomposites, Journal of Materials Science, 45 (2010) 2427-2435.

[36] J. Nadeau, Nanotechnological Advances in Biosensors, Sensors, 9 (2009) 8907-8910.
[37] V. Ilić, Z. Saponjić, V. Vodnik, S. a. Lazović, S. Dimitrijević, P. Jovanc̆ić, J. M. Nedeljković and M. Radetić, Bactericidal Efficiency of Silver Nanoparticles Deposited onto Radio Frequency Plasma Pretreated Polyester Fabrics, Industrial & Engineering Chemistry Research, 49 (2010) 7287-7293.

[38] Y. Arima and H. Iwata, Effect of wettability and surface functional groups on protein adsorption and cell adhesion using well-defined mixed self-assembled monolayers, Biomaterials, 28 (2007) 3074-3082.

[39] H. S. Yoo, T. G. Kim and T. G. Park, Surface-functionalized electrospun nanofibers for tissue engineering and drug delivery, Advanced Drug Delivery Reviews, 61 (2009) 1033-1042.

[40] T. G. Kim and T. G. Park, Biomimicking Extracellular Matrix: Cell Adhesive RGD Peptide Modified Electrospun Poly(D,L-lactic-co-glycolic acid) Nanofiber Mesh, Tissue Engineering, 12 (2006) 221-233.

[41] W. K. Son, J. H. Youk, T. S. Lee and W. H. Park, Preparation of Antimicrobial Ultrafine Cellulose Acetate Fibers with Silver Nanoparticles, Macromolecular Rapid Communications, 25 (2004) 1632-1637.

[42] P. Dayal, J. Liu, S. Kumar and T. Kyu, Experimental and Theoretical Investigations of Porous Structure Formation in Electrospun Fibers, Macromolecules, 40 (2007) 7689-7694.

[43] Z. Ma, M. Kotaki and S. Ramakrishna, Electrospun cellulose nanofiber as affinity membrane, Journal of Membrane Science, 265 (2005) 115-123.

[44] Y. Ikada and H. Tsuji, Biodegradable polyesters for medical and ecological applications, Macromolecular Rapid Communications, 21 (2000) 117-132.

[45] É. Kiss, I. Bertóti and E. I. Vargha-Butler, XPS and Wettability Characterization of Modified Poly(lactic acid) and Poly(lactic/glycolic acid) Films, Journal of Colloid and Interface Science, 245 (2002) 91-98.

[46] P. Ouyang, Y.-q. Kang, G.-f. Yin, Z.-b. Huang, Y.-d. Yao and X.-m. Liap, Fabrication of hydrophilic paclitaxel-loaded PLA-PEG-PLA microparticles via SEDS process, Frontiers of Materials Science in China, 3 (2009) 15-24.

[47] H. Otsuka, Y. Nagasaki and K. Kataoka, Surface Characterization of Functionalized Polylactide through the Coating with Heterobifunctional Poly(ethylene glycol)/Polylactide Block Copolymers, Biomacromolecules, 1 (2000) 39-48.

[48] H. Otsuka, Y. Nagasaki, T. Okano and K. Kataoka, Functionalization of polylactide(PLA) surface using heterobifunctional PEG/PLA block copolymers for the control of cell behavior at surfaces, in: EMBS International Conference, Chicago, IL, 2000.

[49] E. Hendrick, L. Buttaro, A. Naik and M. Frey, Modifying the surface hydrophilicity of poly(lactic acid) electrospun fibers, TBA, (2011).

[50] X. Xu, L. Yang, X. Xu, X. Wang, X. Chen, Q. Liang, J. Zeng and X. Jing, Ultrafine medicated fibers electrospun from W/O emulsions, Journal of Controlled Release, 108 (2005) 33-42.

[51] M. Zhang, X. H. Li, Y. D. Gong, N. M. Zhao and X. F. Zhang, Properties and biocompatibility of chitosan films modified by blending with PEG, Biomaterials, 23 (2002) 2641-2648.

[52] S. R. Bhattarai, N. Bhattarai, P. Viswanathamurthi, H. K. Yi, P. H. Hwang and H. Y. Kim, Hydrophilic nanofibrous structure of polylactide; fabrication and cell affinity, Journal of Biomedical Materials Research Part A, 78A (2006) 247-257.

[53] Y. Lu, W. Shi, J. Qin and B. Lin, Fabrication and Characterization of Paper-Based Microfluidics Prepared in Nitrocellulose Membrane By Wax Printing, Analytical Chemistry, 82 (2009) 329-335.

[54] J. C. McDonald, D. C. Duffy, J. R. Anderson, D. T. Chiu, H. Wu, O. J. A. Schueller and G. M. Whitesides, Fabrication of microfluidic systems in poly(dimethylsiloxane), Electrophoresis, 21 (2000) 27-40.

[55] M. Stjernström and J. Roeraade, Method for fabrication of microfluidic systems in glass, Journal of Micromechanics and Microengineering, 8 (1998) 33.

[56] J. Ma, L. Jiang, X. Pan, H. Ma, B. Lin and J. Qin, A simple photolithography method for microfluidic device fabrication using sunlight as UV source, Microfluidics and Nanofluidics, 9 (2010) 1247-1252.

[57] C. W. T. Yang, E. Ouellet and E. T. Lagally, Using Inexpensive Jell-O Chips for Hands-On Microfluidics Education, Analytical Chemistry, 82 (2010) 5408-5414.

[58] L. J. Lee, M. J. Madou, K. W. Koelling, S. Daunert, S. Lai, C. G. Koh, Y.-J. Juang, Y. Lu and L. Yu, Design and Fabrication of CD-Like Microfluidic Platforms for Diagnostics: Polymer-Based Microfabrication, Biomedical Microdevices, 3 (2001) 339-351.

[59] A. W. Martinez, S. T. Phillips and G. M. Whitesides, Three-dimensional microfluidic devices fabricated in layered paper and tape, Proceedings of the National Academy of Sciences, 105 (2008) 19606-19611.

[60] X. Li, J. Tian and W. Shen, Thread as a Versatile Material for Low-Cost Microfluidic Diagnostics, ACS Applied Materials & Interfaces, 2 (2009) 1-6.

[61] P. K. Yuen and V. N. Goral, Low-cost rapid prototyping of flexible microfluidic devices using a desktop digital craft cutter, Lab on a Chip, 10 (2010) 384-387.

[62] A. Grimes, D. N. Breslauer, M. Long, J. Pegan, L. P. Lee and M. Khine, Shrinky-Dink microfluidics: rapid generation of deep and rounded patterns, Lab on a Chip, 8 (2008) 170-172.
[63] H. Ow, D. R. Larson, M. Srivastava, B. Baird, W. W. Webb and U. Wiesner, Bright and stable core-shell fluorescent silica nanoparticles, Nano Letters, 5 (2004) 113-117.

[64] A. Burns, Sengupta, P., Zedayko, T., Baird, B., Wiesner, U., Core-shell fluorescnet silica nanoparticles for chemical sensing: towards single particle laboratories, Small, 2 (2006) 723-726.

[65] E. Herz, A. Burns, S. Lee, P. Sengupta, D. Bonner, H. Ow, C. Lidell and U. Wiesner, Fluorescent core-shell silica nanoparticle: an alternative radiative materials platform, Proceedings of the SPIE: Colloidal Quantum dors for Biomedical Applications, 6096 (2006) 1-12.

[66] A. Burns, P. Sengupta, T. Zedayko, B. Baird and U. Wiesner, Core-shell fluorescent silica nanoparticles for chemical sensing: towards single particle laboratories, Small, 2 (2006) 723-726.

[67] A. Burns, H. Ow and U. Wiesner, Fluorescent core–shell silica nanoparticles: towards ‘‘Lab on a Particle’’ architectures for nanobiotechnology, Chemical Society Reviews, 35 (2006) 1028–1042.

[68] D. R. Larson, H. Ow, H. D. Vishwasrao, A. A. Heikal, U. Wiesner and W. W. Webb, Silica nanoparticle architecture determines radiative properties of encapsulated fluorophores, Chemistry of Materials, 20 (2008) 2677–2684.

[69] E. Hendrick, L. Buttaro, S. Iyer, U. Wiesner and M. Frey, Stimuli responsive electrospun fibers: the influence of fiber diameter and substrate, (TBA).

[70] D. M. Collier and P. M. Snyder, Extracellular Protons Regulate Human ENaC by Modulating Na+ Self-inhibition, Journal of Biological Chemistry, 284 (2009) 792-798.

[71] W.-C. Sun, K. R. Gee, D. H. Klaubert and R. P. Haugland, Synthesis of Fluorinated Fluoresceins, Journal of Organic Chemistry, 62 (1997) 6469-6475.

[72] C. K. Kim, D. S. Kim;, S. Y. Kang, M. Marquez and Y. L. Joo, Structural Studies of Electrospun Cellulose Nanofibers, Polymer, 47 (2006) 5097-5107.

[73] C. Kong, T. Lee, S. Lee and H. Kim, Nano-web formation by the electrospinning at various electric fields, Journal of Materials Science, 42 (2007) 8106-8112.

[74] E. S. Hendrick, Cellulose acetate fibers with fluorescing nanoparticles for anti-counterfeiting purposes, in: Fiber Science & Apparel Design, Cornell University, Ithaca, 2008.

[75] C. W. O. Yang, Eric; Lagally, Eric T. , Using Inexpensive Jell-O Chips for Hands-On Microfluidics Education, Analytical Chemistry, 82 (2010) 5408–5414.

[76] E. Hendrick, L. Buttaro, A. Naik and M. Frey, Modifying the surface hydrophilicity of electrospun fibers, TBA, (2011).

[77] C. Xiang, M. W. Frey, A. G. Taylor and M. Rebovich, Selective chemical absorbance in electrospun nonwovens, Journal of Applied Polymer Science, 106 (2007) 2363-2370.

[78] C. Nelson and H. Norman, Performance of protective clothing: issues and priorities for the 21st century, ASTM, West Conshohoken, 2000.

[79] Y.-L. Hsieh, Liquid Transport in Fabric Structures, Textile Research Journal, 65 (1995) 299-307.

[80] Y. Zhang, H. P. Wang and Y. H. Chen, Capillary effect of hydrophobic polyester fiber bundles with noncircular cross section, Journal of Applied Polymer Science, 102 (2006) 1405-1412.

[81] F. Inam, H. Yan, M. J. Reece and T. Peijs, Dimethylformamide: an effective dispersant for making ceramic–carbon nanotube composites, Nanotechnology, 19 (2008) 1-5.

CHAPTER 4

CONCLUSIONS AND FUTURE WORK

4.1 CONCLUSION SUMMARY

A comprehensive study of stimuli-responsive electrospun fibers was presented here. Nanoparticles with pH-sensitivity were incorporated into two different polymer fibers, and a variety of fiber parameters were modified in order to achieve the best response to pH change. Cellulose acetate (CA) fibers were electrospun at different feed rates in order to produce fibers with varied diameter sizes. These fibers were also spun onto several different substrates: glass, cotton, cotton/polyester and nylon/spandex. It was found that fibers spun at a slower feed rate produced fibers with increased surface area, which proved to be most effective when monitoring pH change. Additionally, the chemistry inherent to the substrates onto which the fibers were spun was found to affect pH response. Fibers spun onto glass slides and cotton/polyester showed an improvement in sensitivity to pH change, while the cotton and nylon/spandex samples were greatly influenced by the chemistry inherent to these substrates. More hydrophobic substrates impeded the pH measurements, while more hydrophilic substrates enhanced them.

Poly(lactic acid) (PLA) fibers were blended with poly(lactic acid) – b – poly(ethylene glycol) (PLA – b – PEG) diblock copolymers with block lengths of 1000-750, 5000-1000 and 1000-5000 to create hydrophilic but non-water soluble nanofibers. The lengths of the blocks were found to influence the maximum amount of PEG that could be incorporated, as well as spinnability and fiber morphology. Water absorbance by these electrospun nonwoven fabrics increased by four times over the control PLA with the addition of 1.0 wt% PEG, and by

eighteen times with the addition of 9.3 wt% PEG. Variations in surface area and water wicking rate, as well as nanoparticle distribution, influenced the effectiveness of the pH-sensitive electrospun fibers. Confocal microscopy and image analysis were used to take pH measurements, and showed that response to pH change improved with increasing surface area and water wicking rate. The stimuli-responsive fibers were shown to take relatively consistent pH measurements both on glass slides, and within a prototype fluidic device.

4.2 FUTURE WORK

The results show that a number of experiments can be performed to continue and expand on the presented research. This continued work should focus on driving the PEG/nanoparticles to the fiber surface, continued work on incorporating fibers into microfluidic channels, and thermal analysis experiments.

4.2.3 Stimuli Responsive Nanofibers Integrated into Microfluidic Devices

In the continued work for this project, new stimuli-response capabilities and greater surface area for interaction will be incorporated into microfluidic channels. C dot nanoparticles with stimuli response capabilities will be incorporated into nanofibers patterned at specific locations and orientations within microfluidic channels. Response of the C dot particles to samples flowing through the microfluidic channels will be maximized by engineering fiber surface properties, and leveraging the high surface/volume ratio of nanofibers.

Microfluidic devices are capable of precise analyses on small samples. Typically, functionality can be incorporated into channels in the form of pillars or beads. However, nanofibers incorporated into microfluidic devices can provide one hundred times the surface area available for fluid interaction as pillar structures. Nanofibers with a wide variety of properties are simple to produce via electrospinning, and can retain functionality.

Results in this dissertation have shown that the surface properties of C dot containing PLA fibers can be modified by adding <10wt% of PEG. These engineered fibers show a considerable increase in surface wetting, as well as an improvement in sensitivity to pH change. Additionally, preliminary work showed that these fibers can be incorporated into, and function properly, within microfluidic devices.

The current trend in analytical devices is for the creation of smaller, simpler, and smarter methods of analysis [1]. For this reason, microfluidic systems have the potential to become an extremely popular platform for laboratory analysis and diagnostics [2-4]. Several different methods have previously been described for the fabrication of microfluidic devices, but soft lithography is one on the most popular [5]. Soft lithography is a method that uses rapid prototyping to produce microfluidic devices quickly and consistently. By incorporating C dot nanofibers into such devices, a novel microfluidic platform will be created.

To achieve the project goals, the following specific aims are proposed. Fiber surface properties will be engineered to maximize the response of the C dot particles within the fibers. For this purpose, several different blends will be electrospun: such as CA/polyurethane (PU) following previously described methods by Tang, et al [6], and PLA / poly(caprolactone) (PCL) following previously described methods by Liao, et al [7]. Continued work on PLA/PEG will also be performed using a bicomponent spinning system to ensure that the PEG and C dot particles are concentrated on the fiber surface. The presence of PEG on the fiber surface will be verified using x-ray photoelectron spectroscopy (XPS). However, previous studies have shown that PLA has three characteristic peaks at 289, 287, and 285 eV, while PEG has one characteristic peak at 286 eV [8-9] (Figure 4.1). Therefore, given the similarities between the characteristic peaks for PLA and PEG, and the small concentrations being used, a modification must be made. Previous work has shown that it is possible to tag the PEG block

with a more visible end-cap, such as nitrogen, or a fluorescent dye [10-11]. In this way, if the PEG block is present on the fiber surface, characteristic peaks for the end-caps will be seen. Additionally, maximizing the amount of PEG that can be incorporated into the fibers would help improve the accuracy of the XPS analysis.

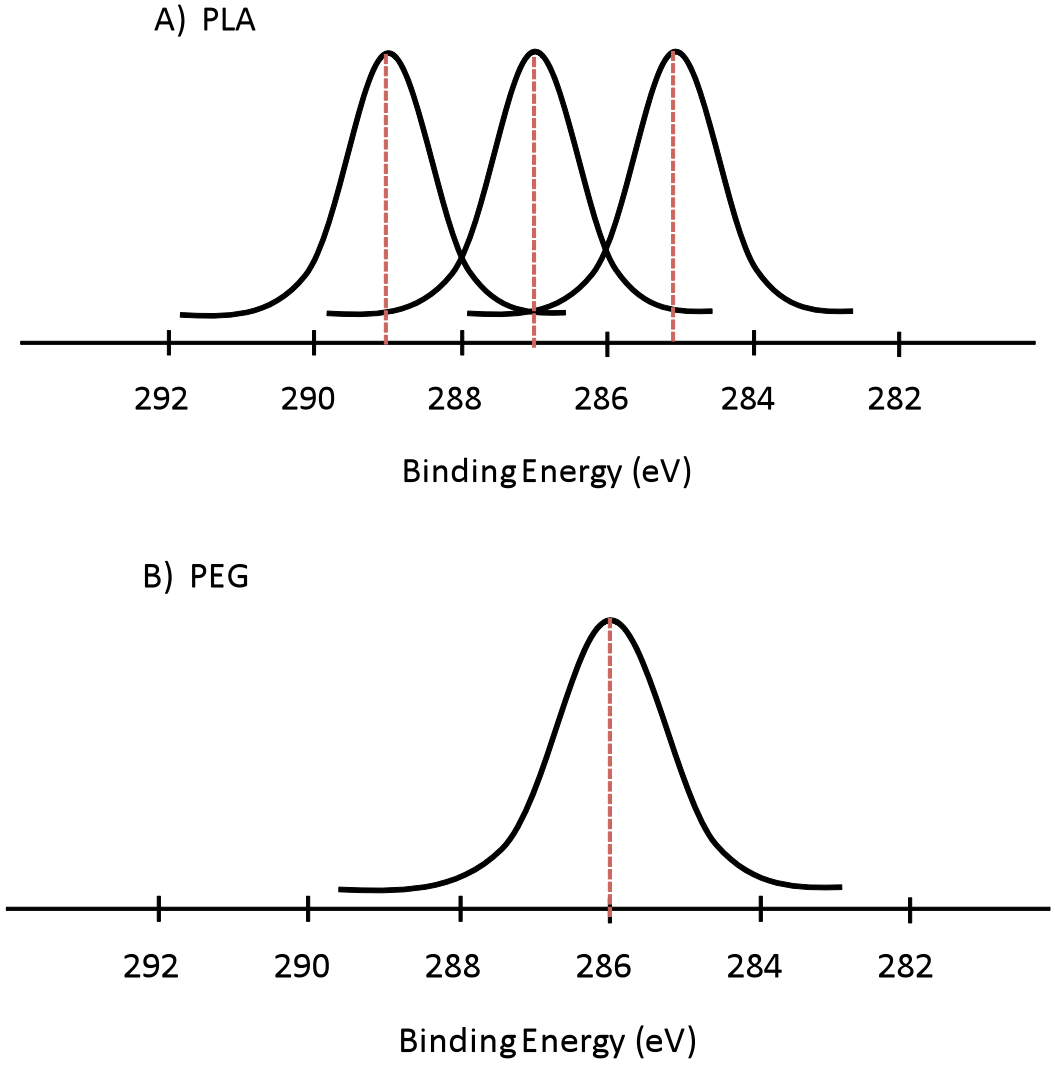

FIGURE 4.1. XPS analysis of bulk A) PLA and B) PEG.

These fibers will be characterized using SEM imaging to determine average fiber diameter and morphology. In order to verify the modification of surface properties, wettability

testing will be performed. Additionally, the engineered nanofibers will be incorporated into microfluidic channels, and their response to stimuli measured with fluorescence microscopy. Fibers will be spun onto glass slides for initial experiments, and then into microfluidic channels (Figure 4.2).

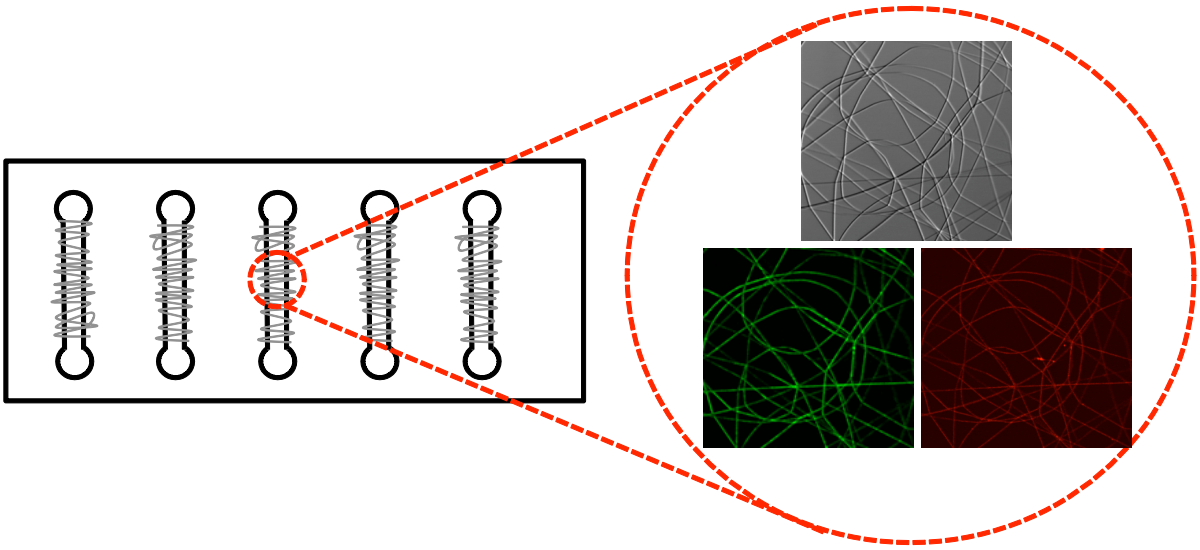

FIGURE 4.2. Engineered nanofibers incorporated into microfluidic channels, and observed under fluorescence microscopy.

4.2.2 Thermal Analysis

Thermal analysis is another experimental procedure of interest because it can determine how much, if at all, the incorporation of PLA-b-PEG copolymers affects the crystallinity of the PLA fibers. The simplest method for measuring fiber crystallinity is to use differential scanning calorimetry (DSC). DSC is a technique that can be used to study what happens to a polymer when it is heated, such as the glass transition temperature (T_g), and the melting temperature (T_m). Some initial studies have been performed on evaluating the T_g and cold crystallization temperatures for the PLA and PLA/PLA-b-PEG fibers (Table 4.1). These results show that the addition of the PLA-b-PEG diblock copolymers lead to a slight increase in the T_g

of the fibers. Additionally, the fact that the cold crystallization temperature decreased for the fibers spun with the longer PLA block copolymer indicates that the crystallinity of the fibers is affected. Hence, a more comprehensive study observing T_m would provide valuable information on this polymer system.

TABLE 4.1. Results of introductory DSC experiments on PLA and PLA/PLA-b-PEG fibers.

Sample	**T_g (°C)**	**Cold Crystallization (°C)**
PLA	57.1	100.7
0.98 wt% PEG from PLA (5000) – b – PEG (1000)	58.1	79.8
0.93 wt% PEG from PLA (1000) – b – PEG (5000)	60.7	82.1

4.3 REFERENCES

[1] M. Spasova, O. Stoilova, N. Manolova, I. Rashkov and G. Altankov, Preparation of PLLA/PEG Nanofibers by Electrospinning and Potential Applications, Journal of Bioactive and Compatible Polymers, 22 (2007) 62-76.

[2] M. L. C. Chabinyc, Daniel T.; McDonald, J.C.; Stroock, Abraham, D.; Christian, James F.; Karger, Arieh M.; Whitesides, George M., An integrated fluorescence detection system in poly(dimethylsiloxane) for microfluidic applications, Analytical Chemistry, 73 (2001) 4491-4498.

[3] C.-F. L. Lin, Gwo-Bin; Wang, Chih-Hao; Lee, Huei-Huang; Liao, Wei-Yin; Choub, Tse-Chuan, Microfluidic pH-sensing chips integrated with pneumatic fluid-control devices, Biosensors and Bioelectronics, 21 (2006) 1468–1475.

[4] J. G. E. V. d. B. Gardeniers, A. , Lab-on-a-chip systems for biomedical and environmental monitoring, Analytical and Bioanalytical Chemistry, 378 (2004) 1700-1703.

[5] J. C. McDonald, D. C. Duffy, J. R. Anderson, D. T. Chiu, H. Wu, O. J. A. Schueller and G. M. Whitesides, Fabrication of microfluidic systems in poly(dimethylsiloxane), ELECTROPHORESIS, 21 (2000) 27-40.

[6] C. Tang, P. Chen and H. Liu, Cocontinuous cellulose acetate/polyurethane composite nanofiber fabricated through electrospinning, Polymer Engineering & Science, 48 (2008) 1296-1303.

[7] G.-Y. Liao, L. Chen, X.-Y. Zeng, X.-P. Zhou, X.-L. Xie, E. J. Peng, Z.-Q. Ye and Y.-W. Mai, Electrospun poly(L-lactide)/poly(ε-caprolactone) blend fibers and their cellular response to adipose-derived stem cells, Journal of Applied Polymer Science, (2010) n/a-n/a.

[8] R. K. Singh, W. S. Kim, M. Ollinger, V. Craciun, I. Coowantwong, G. Hochhaus and N. Koshizaki, Laser based synthesis of nanofunctionalized particulates for pulmonary based controlled drug delivery applications, Applied Surface Science, 197-198 (2002) 610-614.

[9] S. Essa, J. M. Rabanel and P. Hildgen, Effect of polyethylene glycol (PEG) chain organization on the physicochemical properties of poly(d, l-lactide) (PLA) based nanoparticles, European Journal of Pharmaceutics and Biopharmaceutics, 75 (2010) 96-106.

[10] A. Vila, H. Gill, O. McCallion and M. J. Alonso, Transport of PLA-PEG particles across the nasal mucosa: effect of particle size and PEG coating density, Journal of Controlled Release, 98 (2004) 231-244.

[11] Y. Yu, J. Zou, L. Yu, W. Ji, Y. Li, W.-C. Law and C. Cheng, Functional polylactide-g-paclitaxel–poly(ethylene glycol) by azide–alkyne click chemistry, Macromolecules, (2011) null-null.